

Geology and structural controls of lode-gold mineralization around the Navachab Gold Mine in the Pan-African Damara Belt of Namibia

by
Pieter Koenraad Creus

*Thesis presented in partial fulfilment of the requirements for the degree
Master of Science
at the University of Stellenbosch*



Supervisor: Prof. Alex Kisters

Faculty of Science
Department of Earth Sciences

December 2011

Declaration

By submitting this thesis, I declare that the entirety of the work contained therein is my own, original work, that I am the sole author thereof (save to the extent explicitly otherwise stated), that reproduction and publication thereof by Stellenbosch University will not infringe any third party rights and that I have not previously in its entirety or in part submitted it for obtaining any qualification.

December 2011

Copyright © 2011 University of Stellenbosch

All rights reserved

Abstract

Numerous quartz-vein hosted gold prospects in the Karibib district in central Namibia testify to the presence of a large hydrothermal system during Pan-African times in rocks of the Damara Belt and centred around the Navachab Gold Mine. This study presents the results of the regional and detailed mapping of the Navachab synform, a NE-SW trending, regional-scale structure hosting a number of these gold prospects, locally referred to as the “zoo prospects”, in the direct vicinity of the main Navachab Gold Mine.

The zoo prospects are located in the marble-dominated, up to 800 m thick Karibib Formation, which forms the core of the Navachab synform. Regional mapping of the synform identified six main lithological units comprising massive and banded dolomitic and calcareous marbles, intraformational breccias and interlayered calc-silicate felses. Despite characteristic thickness variations, the six units can be correlated throughout the synform, allowing for a lithostratigraphic correlation of units in the otherwise monotonous marble sequence. All of the prospects are spatially closely associated with and adjacent to unit 5, an up to 100 m thick, competent dolomitic marble unit. This suggests a strong lithological control of the mineralisation.

The first-order Navachab synform formed during the regional D_2 phase of deformation. The strongly non-cylindrical, doubly-plunging fold shows open- to close interlimb angles and a pronounced NW vergence in the SW, but is tight- to isoclinal and upright in the NE. Higher fabric intensities and detachment folding are confined to the subvertical limbs of the synform in the north. Here, structures record a subhorizontal, NW-SE directed co-axial shortening strain interpreted to have developed in response to the geometric hardening and layer-normal shortening following the rotation of the fold limbs to subvertical attitudes during progressive D_2 shortening. The mineralisation of the zoo prospects is located where D_2 high-strain zones intersect unit 5. This suggests an additional structural control of the mineralisation.

The detailed mapping of the zoo prospects identified five distinct quartz-vein sets. The geometry, orientation and progressive deformation of the vein sets indicate that veining

occurred during the late stages of the D_2 event and during NW-SE directed, subhorizontal shortening. Areas of increased veining and mineralisation occur preferentially in areas of strain incompatibilities, where the combined effects of D_2 strains and prominent lithological contacts created zones of localized dilatancy. This includes most prominently dilational jog geometries developed between anastomosing D_2 shear zones, where hydrothermal fluid flow has produced pervasive quartz-vein stockworks. This also includes areas of detachment folding, where deformation of the rheological stiffer dolomitic marbles and less competent calcareous marbles has led to detachment surfaces and, locally, dilatancy. Zones of increased permeability are also created where two or more vein sets intersect, which is particularly common within and adjacent to boudin interpartitions of competent dolomite units and along rheologically prominent contacts.

The zoo prospects illustrate the interplay of (1) prominent rheological contrasts between adjacent lithologies, (2) the presence of high-strain zones, and (3) the geometry of host structures for the formation of auriferous quartz veins in the Karibib district.

Uittreksel

Talle goud vooruitsigte, wat kwarts-aar geherberg is, in die Karibib-distrik in Sentraal-Namibië getuig van die teenwoordigheid van 'n groot hidrotermale stelsel tydens die Pan-Afrika-tye in die rotse van die Damara-Belt en is gesentreer rondom die Navachab goudmyn. Hierdie studie stel die resultate van die streeks- en gedetailleerde kartering van die Navachab sinform, 'n NW-SO neiging, streeks-skaal struktuur wat 'n aantal van hierdie goud prospekterplek herberg, plaaslik bekend as die "zoo prospects", in die direkte omgewing van die hoof Navachab goudmyn.

Die "zoo prospects" is geleë in die marmer-gedomineerde, tot 800 m dik Karibib formasie, wat deel vorm van die kern van die Navachab sinform. Streeks kartering van die sinform het ses belangrike litologiese eenhede geïdentifiseer wat uit massiewe en gestreepte dolomitiese kalk marmer, intraformasie breksie en tussengelaagdheid kalksilikaat felses bestaan. Ten spyte van die kenmerkende dikte variasies, kan die ses eenhede gekorreleer word oor die hele sinform, wat toelaat vir 'n litostratigrafiese korrelasie van eenhede in die andersins eentonige marmer opeenvolging. Al die vooruitsigte is ruimtelik verbind met en aangrensend aan Eenheid 5, 'n tot 100 m dik, bevoegde dolomitiese marmer-eenheid. Dit dui op 'n sterk litologiese beheer van die mineralisasie.

Die eerste-orde Navachab sinform het gevorm tydens die plaaslike D_2 fase van deformatsie. Die sterk nie-silindriese, dubbelduikende plooi wys oop- tot noue tussenflankhoeke en 'n uitgespreek NW-vergensie in die SW, maar is styf- tot isoclinaal en regop in die NO. Hoër maaksel sterkte en losmaking plooi is beperk tot die subvertikale flank van die sinform in die noorde. Hierdie strukture is 'n aanduiding van 'n subhorisontale, NW-SO gerigte ko-aksiale verkorting wat geïnterpreteer is as vervorming wat ontwikkel het in reaksie op die geometriese verharding en die laag-normaal verkorting as gevolg van die rotasie van die plooi flanke tot subvertikale houdings tydens die progressiewe D_2 verkorting. Die mineralisasie van die "zoo prospects" is geleë waar D_2 hoë-spanning sones Eenheid 5 sny. Dit dui op 'n addisionele strukturele beheer van die mineralisasie.

Die gedetailleerde kartering van die “zoo prospects” het vyf verskillende kwarts-aar stelle geïdentifiseer. Die geometrie, argitektuur en progressiewe vervorming van die aar-stelle dui daarop dat aar-vorming plaasgevind het gedurende die laat stadium van die D_2 gebeurtenis en tydens die NW-SO gerugte, subhorisontale verkorting. Gebiede van verhoogde aar-vorming en mineralisasie kom verkieslik voor in die gebiede van vervorming verskille, waar die gekombineerde effek van die D_2 vervorming en prominente litologiese kontakte sones van gelokaliseerde dilatansie. Dit sluit die mees prominente uitsettings uitwyking geometrie wat ontwikkel tussen anastomoserend D_2 skuifskursones, waar hidrotermale vloeistof stroming deurdringende kwarts-aar stokwerke geproduseer. Dit sluit ook die gebiede van losmaking plooië, waar die vervorming van die reologiese stywer dolomitiese marmer en minder bevoegde kalk marmer losmaking oppervlaktes gelei het, en plaaslik, dilatansie. Sones van 'n verhoogde deurlaatbaarheid is ook geskep waar twee of meer aar stelle sny, wat is veral algemeen binne en aangrensende boudin tussendeelpartiesies van bevoegde dolomiet-eenhede en langs reologiese prominente kontakte.

Die “zoo prospects” illustreer die wisselwerking tussen (1) prominente reologiese kontraste tussen aangrensende litologie, (2) die teenwoordigheid van hoë-spanning sones, en (3) die geometrie van die geherbergte strukture vir die vorming van goudhoudende kwarts are in die Karibib-distrik.

Acknowledgements

- Professor Alex Kisters for giving me the opportunity to do my MSc and for the constant support and meticulously reviewing every page.
- Frik and Juanita Badenhorst for allowing me to stay at the Barking Gecko and the company during the evenings.
- Many thanks to the staff at Navachab Gold Mine for providing funding and logistics for me to undertake the project.
- All the geologists (Wynand, Katarina, Richard, Nick, Graham) at Navachab for the support while I was in the field.
- Thanks to my fellow post-graduate students at the lab for the conversations while we worked on our respective projects.
- Thanks to my friends and family for your support and motivation.

Table of Contents

Declaration.....	ii
Abstract.....	iii
Uittreksel.....	v
Acknowledgements.....	vii
Appendices.....	xi
List of Figures	xii
List of Tables	xvi
Chapter 1 Introduction	1
1.1. Background and Rationale of Project.....	1
1.2. Aims of the Study	4
1.3. Methodology	5
Chapter 2 Regional Geology and Background	6
2.1. Regional Geological Setting.....	6
2.1.1. Structural Geology	8
2.1.2. Metamorphic Evolution	11
2.2. Lithostratigraphy of the Karibib District.....	11
2.3. Previous Work	16
Chapter 3 Lithostratigraphy of the Navachab Synform.....	19
3.1. Unit 1	19
3.2. Unit 2	20
3.3. Unit 3	21
3.4. Unit 4	21
3.5. Unit 5	22
3.6. Unit 6	22
3.7. Stratigraphic profiles	25

Chapter 4 Structural Geology of the Karibib District	29
4.1. Bedding (S_0)	30
4.2. Planar Tectonic Fabrics (S_1 and S_2)	31
4.2.1. Bedding-Parallel Foliation (S_1)	31
4.2.2. Steep, axial planar foliation (S_2)	32
4.3. High Strain Zones	33
4.4. Linear Fabrics (L_2)	35
4.5. Folds	38
4.5.1. F_1 Folds	38
4.5.2. F_2 Folds	38
Chapter 5 Geology of the Zoo Prospects	45
5.1. Lithological Subdivision of Unit 5	45
5.2. Gecko Prospect	48
5.3. Grid A Open-Pit	52
5.4. Klipspringer Prospect	56
5.5. Steenbok	59
Chapter 6 Quartz Veins in the Zoo Prospects	62
6.1. S_2 Parallel Veins (S_2P)	63
6.2. ac Veins	65
6.3. Shallow, Sheeted Quartz Veins (SSQ)	68
6.4. Shear Veins	68
6.5. Conjugate Set	70
6.6. Vein Stockworks in Dilational Sites	71
6.7. Quantitative Analysis of Quartz Veins in Borehole and Panels	76
6.7.1. Gecko Prospect	78
6.7.2. Grid A Open-Pit	83

6.7.3. Klipspringer Prospect	86
6.7.4. Steenbok	87
Chapter 7 Discussion.....	88
7.1. Karibib Formation.....	88
7.1.1. Depositional Environment	88
7.1.2. Lithological controls on mineralisation.....	89
7.2. Structural Geology of the Navachab Synform.....	90
7.2.1. Structural Geometry of the Navachab synform	90
7.2.2. Strain in the Navachab synform.....	91
7.2.3. High-strain zones	94
7.3. Quartz Veins	95
7.3.1. Progressive Development of Quartz Veins	98
7.4. Fluid-flow in the Navachab Synform.....	102
Chapter 8 Concluding Remarks.....	106
References	108

Appendices

Appendix I: Geological map of the Navachab synform

Appendix IIa: Gecko Pit 1 Panel 1

Appendix IIb: Gecko Pit 1 Panel 2

Appendix IIc: Gecko Pit 2 Panel 1

Appendix IId: Gecko Pit 2 Panel 2

Appendix IIe: Borehole AWD-3

Appendix IIf: Borehole AWD-4

Appendix IIg: Borehole AD-128

Appendix IIh: Borehole AD-129

Appendix Iii: Borehole AD-130

Appendix IIIa: Grid A ML Panel 1

Appendix IIIb: Grid A ML Panel 2

Appendix IIIc: Grid A ML Panel 3

Appendix IIId: Grid A UL Panel 1

Appendix IIIe: Grid A UL Panel 2

Appendix IIIf: Borehole AD-122

Appendix IIIg: Borehole AD-123

Appendix IV: Klipsringer

Appendix V: Steenbok

List of Figures

1.1: Locality map of the study area	3
2.1: Simplified tectonic map of the Damara Belt	6
3.1: Outcrop appearance of the main units of the Karibib Formation	23
3.2: Geological map of the Navachab synform	24
3.3: Lithostratigraphic column (section 1) through the Karibib Formation in the hinge of the Usakos dome	26
3.4: Lithostratigraphic columns (sections 2-6) through the Karibib Formation in the Navachab synform	28
4.1: Photos of the development of S_2 in outcrop	32
4.2: Field sketches illustrating the development and attenuation of S_2 foliation	33
4.3: Transposition and attenuation of bedding	36
4.4: Symmetrical boudinage of a competent marble, illustrating a component of vertical stretch of the rock	36
4.5a: Re-orientation of breccia fragments into parallelism with L_2 stretch and F_2 fold axes	37
4.5b: Fold-hinge normal tensile fractures that record the subhorizontal stretch during D_2	37
4.6: Cross-sections across the Navachab synform	41
4.7: Formline map of the Navachab synform with stereoplots for S_0 , S_2 and L_2	42
4.8a: Small-scale example of detachment folding	44
4.8b: Re-folded boudin capped with quartz-tremolite	44
5.1: Lithological subdivision of unit 5 at Gecko prospect	46
5.2: Outcrop appearance of the subdivision of unit 5 at Gecko prospect	48

5.3: Geological map for the Gecko prospect	49
5.4: Stereoplots for S_0 and L_2 at Gecko prospect	50
5.5: Formline map for Gecko prospect	50
5.6a: Cross-sectional view to the SW of the subdivision of unit 5 and location of zones of mineralisation at Gecko prospect	51
5.6b: Cross-section through the Gecko prospect	51
5.7: Stereoplots for S_0 , S_2 and L_2 at Grid A prospect	52
5.8a: Photo of the NE wall of Grid A pit showing the location of figure 5.9	54
5.8b: Cross-section of the Grid A prospect	54
5.9: 90 m photo panel and accompanying cross-section across the central parts of the Grid A prospect	55
5.10: Geological map of the Klipspringer prospect	56
5.11: Stereoplots for S_0 , S_2 and L_2 for Klipspringer prospect	57
5.12: Formline map of the Klipspringer prospect	57
5.13: Cross-section across the Klipspringer prospect	58
5.14: Geological map of the Steenbok prospect	60
5.15: Stereoplots for S_0 and L_2 at Steenbok prospect	60
5.16: Formline map of the Steenbok prospect	61
5.17: Cross-section across the Steenbok prospect	61
6.1: Stereoplot for S_2P veins at (a) Gecko, (b) Grid A, (c) Klipspringer and (d) Steenbok	63
6.2: Deformation characteristics of S_2P veins	64
6.3: Stereoplots for ac veins at (a) Gecko, (b) Grid A, (c) Klipspringer and (d) Steenbok	65
6.4a: Photo showing the growth of tremolite needles normal to the vein wall	67
6.4b: Photo showing the gentle folding of ac veins	67
6.5a: Stereoplot for shallow, sheeted quartz veins at Gecko	68
6.5b: Outcrop appearance of shallow, sheeted quartz veins	68

6.6a: Stereoplot for shear veins at Klipspringer	69
6.6b: Photo showing sigmoidal shear veins	69
6.7: Simplified diagram illustrating the formation of shear veins	69
6.8a: Photo showing the orientation of the conjugate set with regards to S_2P and ac veins	70
6.8b: Stereoplot for the conjugate set at Gecko	70
6.8c: Photo illustrating the cross-cutting relationship between conjugate set and S_2P veins	70
6.9a: Line diagram of Klipspringer-type mineralisation	72
6.9b: Photo of stockwork veining in the neck of a boudin	72
6.10: Simplified diagram of anastomosing shear zones illustrating the formation of dilational sites	74
6.11: Photo showing the formation of dilational jobs as a result of shearing and folding	74
6.12: Photo of dilational sites that have undergone brecciation of dolomitic marble	74
6.13a: Cross-sectional photo to the NE of Trial Pit 2 at Gecko	75
6.13b: Photo showing mosaic breccia of angular dolomitic marble fragments	75
6.14: Geological map of Gecko showing the location of boreholes and panels mapped	78
6.15a: Simplified stratigraphic column of borehole AWD-3	81
6.15b: Typical wall-rock alteration of dolomitic marble shown in core	81
6.15c: Photo of core showing wall-rock alteration containing sulphides, oxides and visible Au	81
6.15d: Photo showing the appearance of dolomitic marble surrounding the zones of minerlisation	84
6.15e: Photo showing the appearance of dolomitic breccia in borehole	84
6.16a: Photo showing alteration halo around a quartz vein	82
6.16b: Photo showing alteration halo around a boudinaged quartz vein	82
6.17: Photo of the NE wall of Grid A showing the location of panels mapped on the pit wall	84
6.18: Geological map of Klipspringer showing the location of the road cut analysed	86
6.19: Geological map of the road cut analysed at Steenbok	87

7.1: Schematic diagram showing the development of a stepover at the Navachab main pit	95
7.2: Photo showing intense alteration at the intersection of ac and S ₂ P veins	98
7.3: Stage 1 of mineralisation	100
7.4: Stage 2 of mineralisation	101

List of Tables

2.1: Correlation of structural elements between previous workers for the Central Zone of the Damara Belt	9
2.2: Lithostratigraphic subdivision of rocks in the Karibib district	12
4.1: Summary of the structural elements observed in the Karibib district	30
6.1: Summary of the raw data for veins of panels mapped at the prospects and boreholes logged from Gecko and Grid A	77

Chapter 1 Introduction

1.1. Background and Rationale of Project

Lode-gold deposits are epigenetic, hydrothermal in origin and commonly associated with auriferous quartz veins. Quartz veining is structurally controlled and testifies to the mainly fracture-controlled fluid-flow in the commonly greenschist-facies, but also higher-grade metamorphic wall-rocks (e.g. Sibson et al., 1988; Groves, 1993; Ridley, 1993; McCuaig and Kerrich, 1998; Phillips and Powell, 2009). The vein systems show a close spatial and temporal association with shear- and fault zones or folds (e.g. Hodgson, 1989; Vearncombe, 1998; Goldfarb et al., 1998, 2001; Groves et al., 2003). This also highlights the role of deformation for fluid-flow. Veining is commonly concentrated in second- or third-order structures related to larger first-order structures and may be concentrated in zones of strain incompatibility, such as jog geometries, or along lithological contacts (e.g. Groves et al., 1998; Robert and Poulsen, 2001).

The analysis of auriferous vein systems is one key aspect for our understanding of the formation of gold deposits. In particular, constraining the structural controls of vein formation and mineralisation aids the delineation and improves the predictability of ore-body geometries (Robert and Poulsen, 2001). Fluid-flow follows hydraulic gradients from areas of high- to low mean rock stress. Any fracture (vein) formation indicates localized dilatancy, which, in turn, represents zones of relatively low mean stress (e.g. Ridley, 1993; Ferry, 1994; Oliver, 1996). Zones of extensive veining have, thus, represented fluid sinks during regional deformation and associated fluid-flow. An identification of regional-scale fluid-flow patterns and variations in mean rock stress is, thus, of paramount importance for the exploration of vein-hosted gold deposits.

The Navachab Gold Mine is situated some 10 km to the SW of the town of Karibib (Fig. 1.1), located in the southern Central Zone of the Damara Belt in Namibia. It is currently the only operating gold mine in Namibia (as of August 2011). The gold mine is hosted in high-grade metamorphic, Neoproterozoic rocks of the Damara Supergroup, a heterogeneous

metasedimentary sequence made up of alternating siliciclastic schists and metapsammities and calcitic and dolomitic marbles (Badenhorst, 1992). Mineralisation in the main pit of the Navachab Gold Mine is hosted by a swarm of shallowly-dipping, sheeted quartz veins and bedding-subparallel, massive quartz-sulphide bodies along a prominent lithological contact, locally referred to as the MC-type mineralisation (MC: interlayered marble calc-silicate felses) (Moore et al., 1998, 1999). The mineralisation occurs on the steep, SE limb of the regional-scale, NE-trending, doubly-plunging antiform of the Karibib dome. The geometry, orientation and progressive deformation of the quartz-vein sets suggests quartz veining and fluid-flow during regional-scale folding and fold amplification (e.g. Kisters, 2005; Kitt, 2008). Alternate models involve sinistral wrench tectonics at the time of mineralisation accommodating the anticlockwise rotation of dome structures (e.g. Steven et al., 2008).

In recent years, exploration has identified several prospects with auriferous quartz veins scattered over an area of some 30 km² to the NW of the main open pit (Fig. 1.1). These prospects are collectively referred to as the “zoo prospects” in the mine terminology. The four most important prospects are the Gecko, Grid A, Klipspringer and Steenbok prospects and are shown on Figure 1.1.

The zoo prospects are hosted by stratigraphically higher units compared to the main open pit and are developed in the heterogeneous, marble-dominated sequence of the Karibib Formation. The several hundred metre thick marble succession is preserved in the core of the first-order Navachab synform to the immediate NW of the Karibib dome where the main open pit is situated. Quartz veining and associated gold mineralisation in each of these prospects testify to the fact that these sites represented zones of increased fluid-flow and permeability through which regional-scale fluid-flow was channelled outside the main open pit.

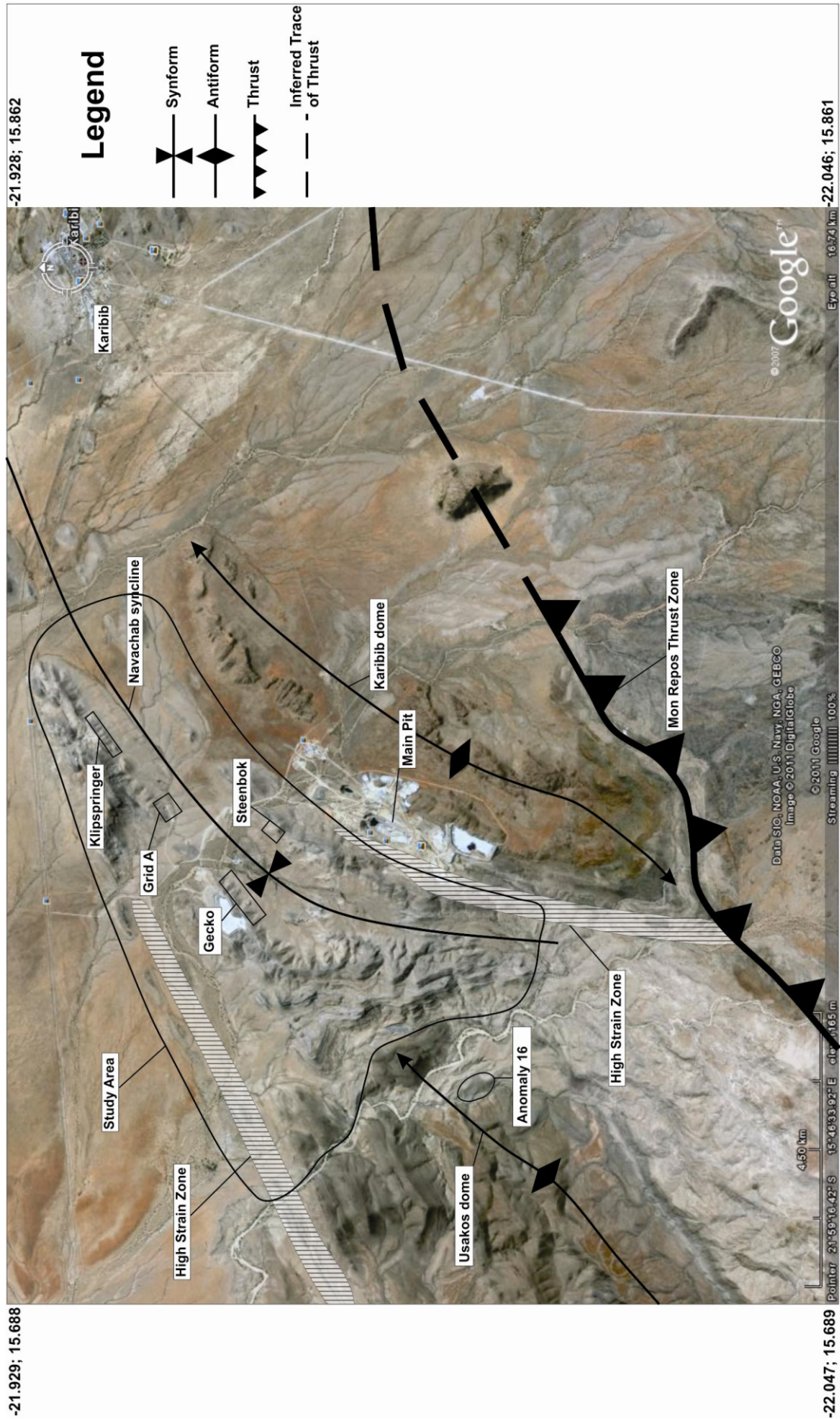


Figure 1.1: Locality map of the study area SW of Karibib. The location of the study area in Namibia is shown on Figure 2.1. The figure includes the locations of four prospects investigated in this study, as well as the axial traces of the first-order Karibib and Usakos domes and the intervening Navachab synform. The figure also shows the location of high-strain zones (shaded) mentioned in the text (chapter 4) and the regional-scale Mon Repos Thrust Zone (Kisters et al., 2004) that places Palaeoproterozoic basement gneisses (in the SE) onto the rocks of the Damara Supergroup (in the NW); Google Earth image.

1.2. Aims of the Study

The study area covers some 56 km², bounded by the lines of longitude (15.748° and 15.757°), and the lines of latitude (-21.941° and -22.003°), located NW of the main pit of the Navachab Gold Mine (Fig. 1.1). The main aim of the study is to determine the structural and lithological controls of quartz veining in the four main zoo prospects, also with respect to their location in the Karibib Formation and in relation to the main open pit.

In detail, the aims of the study are as follows:

1. to document the wall rocks and wall-rock structures in the zoo prospects and the geometry, distribution, orientation, and deformation of quartz veins with respect to wall-rock structures and lithologies in order to constrain the structural and/or lithological controls on quartz veining;
2. to establish the broader structural controls and position of the prospects within the Navachab synform. While the first-order synform (>20 km strike length, 6 km half-wavelength) has been delineated on regional maps, this study aims to provide a detailed lithological and structural map through which e.g. marker horizons within the thick marble succession can be correlated. This would allow to position each prospect structurally and stratigraphically within the Karibib Formation and the Navachab synform. At this stage, prospects are only linked in plan view, but the potential 3D connectivity of the prospects can only be delineated once the structural and stratigraphic framework of the host structure has been established. This requires the detailed lithological and structural mapping of units in the Karibib Formation and correlation across the synform;
3. to combine the local and district-wide controls of quartz veining and prospects. The aim is to delineate regional-scale fluid-flow patterns through which individual prospects and the main mineralisation were possibly linked. Were fluid-flow patterns influenced by adjacent fluid sinks, i.e. mineralized areas and prospects? Do these sinks show a systematic distribution and consistent spacing? Do fluid channels follow certain lithological packages or do they follow certain structures or structural levels?

The overall rationale and idea behind this project is to establish the geometry and architecture of a paleoplumbing system for the hydrothermal mineralizing fluids around the Navachab Gold Mine.

1.3. Methodology

Mapping of the study area was done in three field seasons over altogether 12 weeks in April and June/July 2010 and concluded by a final, two-week field season in March 2011. A Clar-type structural compass was used in the field. Planar elements are given as dip and dip direction, whereas linear structural elements are given as plunge direction and plunge. Satellite images obtained from Google Earth were used as base maps. An acid bottle containing HCl acid was used in the field to distinguish dolomitic marble from calcareous marble. A 1:21 000 regional map was produced to identify the lithological and structural elements of the Navachab synform. The lithology, stratigraphy and structure of the four zoo prospects were mapped at 1:2000 scale. In addition, the characteristics of the quartz veins were recorded including the orientation, thickness and spacing of veins. Mining and initial prospecting at the Grid A and Gecko prospects had already exposed detailed and clean benches, which were mapped on a 1:20 scale to document the quartz-vein inventory in relation to wall-rock structures and lithologies. In addition, several diamond drill boreholes were logged in order to gain subsurface information about the distribution and density of quartz veins in the prospects. The maps were produced using ArcGIS 9.3.1 and all diagrams were produced using Corel Draw X5. All stereoplots were produced using Stereo32 and data are plotted as equal area projections into the lower hemisphere.

Chapter 2 Regional Geology and Background

2.1. Regional Geological Setting

The system of Pan-African orogenic belts formed during the collision of cratonic blocks and the amalgamation of the Gondwana supercontinent in the outgoing Proterozoic (e.g. Miller, 1983; 2008; Porada, 1989; Frimmel, 2009). The Damara Orogen, comprising the coastal Kaoko and Gariiep Belts and the intracontinental Damara Belt, formed at the triple junction of the Kalahari, Congo and Rio-de-la-Plata Cratons (Fig. 2.1) (Prave et al., 1996; Poli and Oliver, 2001).

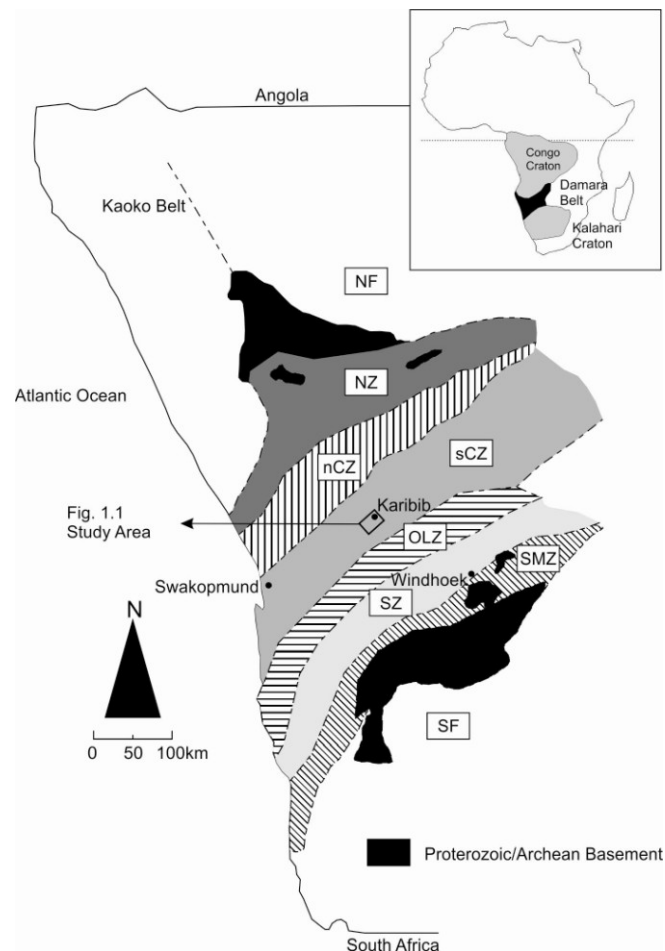


Figure 2.1: Simplified tectonic map of the Damara Belt in central Namibia (after Miller, 1983). The figure shows the distribution of tectonostratigraphic zones and the location of the study area and the insert shows the location of the Damara Belt in Africa and the bounding Congo and Kalahari Cratons. NF: Northern Foreland; NZ: Northern Zone; nCZ: northern Central Zone; sCZ: southern Central Zone; OLZ: Okahandja Lineament Zone; SZ: Southern Zone; SMZ: Southern Marginal Zone; SF: Southern Foreland.

The belts evolved through successive stages of intracontinental rifting, continental break-up, spreading, reversal of plate motion, subduction and continental collision (Miller et al., 2009). In the Damara Belt, this sequence of events is chronicled by the deposition of the Damara Supergroup (Miller, 2008). Intracontinental rifting commenced at ca. 750 Ma, evidenced by the emplacement of rift-related syenites (e.g. Jung et al., 2007) and the deposition of the thick succession of the coarse-clastic, rift-type Nosib Group and the accompanying felsic volcanism preserved in the Naauwpoort Formation (Porada, 1989; Hoffman et al., 1996; Miller et al., 2009). Progressive rifting led to the formation of two oceanic basins, namely the N-S trending Adamastor Ocean and so-called inland sea of the Khomas Ocean, the latter marking the future trace of the Damara Belt. The Adamastor Ocean produced a break-up unconformity and eastward transgression over the Kalahari and Congo Cratons, and the Khomas Ocean developed between the two cratons, associated with break-up unconformities and ultimately the development of mature, mixed siliciclastic-carbonate shelves (e.g. Stanistreet et al., 1991). This sedimentation was punctuated by two glacial events, evidenced by the deposition of diamictites of the Chuos Formation at ca. 740 Ma (Hoffman et al., 1996; Miller et al., 2009) and the Ghaub Formation at ca. 635 Ma (Hoffmann et al., 2004).

Subduction in the northern Adamastor Ocean was initiated at ca. 655 Ma with passive-margin sedimentation occurring elsewhere (Goscombe et al., 2005; Gray et al., 2006). Development of the southern Adamastor Ocean and the Khomas Ocean most likely continued through 600 Ma (Gray et al., 2006). Carbonate and turbidite sedimentation along the southern margin of the Congo Craton led to the deposition of the Swakop Group (Stanistreet et al., 1991; Gray et al., 2006). Closure of the Khomas Ocean was initiated at 580-570 Ma with the northward subduction of the Kalahari Craton under the Congo Craton. The subduction polarity is evidenced by the presence of the accretionary prism of the Southern Zone above the downgoing plate of the Kalahari Craton and the occurrence of the main magmatic axis of the Damara Belt on the leading edge of the overriding Congo Craton (Fig. 2.1) (Miller, 1983, Kukla and Stanistreet, 1991; Goscombe et al., 2005; Gray et al., 2006). Closure of the Khomas Ocean occurred at ca. 550-540 Ma with continent-continent collision in the Damara Belt, followed by the late- to post-tectonic intrusion of granitoids

between ca. 535 and 470 Ma. The post-tectonic magmatism was succeeded by final cooling and uplift of the Damara Belt at ca. 470 Ma (Gray et al., 2006).

2.1.1. Structural Geology

Miller (1983, 2008) subdivided the Damara Belt into several tectonic zones: the Northern Platform, Northern Margin, Northern, Central, and Southern Zones, Southern Margin Zones, and the Southern Foreland (Fig. 2.1). The Central Zone is further divided into the northern Central Zone and the southern Central Zone (Fig. 2.1), the latter of which hosts the mineralisation of the Navachab Gold Mine. The southern Central Zone forms the leading edge of the Congo Craton, separated from the accretionary wedge of the Southern Zone by the Okahandja Lineament Zone (Miller, 1983; Kasch, 1983a). In the southern Central Zone, up to three main phases of deformation have affected the rocks of the Damara Supergroup. However, an exact correlation and also the relative and absolute timing of these deformation phases is a matter of conjecture (Table 2.1) (Jacob, 1974; Coward, 1983; Kasch, 1983a; Miller, 1983; Oliver, 1994; Poli and Oliver, 2001; Kisters et al., 2004).

The first deformation phase, D_1 , is thought to be the result of the early convergence stage and subduction of the Kalahari Plate below the Congo Craton at ca. 580 Ma. D_1 is associated with the development of open- to isoclinal, recumbent folds and nappes (F_1), low-angle thrusting and the development of a bedding-parallel penetrative foliation, designated S_1 by Kasch (1983a). The vergence of the thrusts and folds is variably given as to the east by Blaine (1977) and Sawyer (1981) and to the NW by Downing (1982). Good evidence of the early D_1 deformation is only locally preserved.

Table 2.1: Correlation of structural elements between previous workers for the Central Zone of the Damara Belt. Many of the studies are based on structural interpretations of specific locations and probably does not refer to structural features across the entire Central Zone.

Deformational Phase	Jacob (1974)	Coward (1983)	Kasch (1983a)	Poli and Oliver (2001)	Kisters et al. (2004)	Miller (1983; 2008)
D₁	S ₁ is axial planar to mesoscopic isoclinals F ₁ folds	Large, SE verging recumbent folds	Isoclinal, SE verging folds, numerous low-angle thrusts and development of bedding-parallel S ₁	Strong S ₁ fabric defined by biotite and quartz alignment parallel to S ₀ . L ₁ fabrics are formed by sillimanite, cordierite and feldspar	Bedding sub-parallel foliation and associated intrafolial folds, low angle thrusting and truncation faults	Local D ₁ thrusts and large scale F ₁ recumbent folds
D₂	Large scale folding with F ₂ defining the NE structural trend of many areas in the Central Zone	Large recumbent, SW-closing sheath folds with associated NE-plunging L ₂ stretching lineation	Tight- to isoclinal, non-cylindrical and recumbent folds (F ₂), low-angle thrusting and development of axial planar S ₂	Axial planar S ₂ sporadically developed with no preferred orientation. SW verging sheath folds	Refolding of S ₀ /S ₁ around domes (F ₂) and a N-NE trending axial planar S ₂ foliation. Local development of sheath folds	Tight- to isoclinal, non-cylindrical and recumbent folds, low angle thrusting, and development of axial planar S ₂ foliation to F ₂
D₃	Minor F ₃ open folds on steep F ₂ . S ₃ fanning cleavage is occasionally developed	Refolding of recumbent F ₂ into more upright, SE verging F ₃ folds	Large, upright, SE-verging folds and steep thrusts and reverse faults			Large, upright, NE-trending, SW-verging domes and the development of the main structural grain of the south Central Zone

Progressive convergence between the Kalahari and Congo Cratons between ca. 550-540 Ma (D_2 deformational phase) resulted in tight- to isoclinal, non-cylindrical and recumbent folds (F_2), low-angle thrusting, and the development of an S_2 foliation axial planar to F_2 folds (Kasch, 1983b; Miller, 2008). Miller (2008), after Coward (1983), describes the F_2 folds as large recumbent, SW-closing sheath folds associated with a NE-plunging L_2 stretching lineation. The D_2 deformation defined by Miller (1983, 2008) corresponds to the D_1 deformation defined by Jacob (1974) and Kisters et al. (2004). Jacob (1974) did not find F_1 folds, but describes a bedding-parallel foliation (S_1). Kisters et al. (2004) notes a bedding-parallel S_1 foliation that becomes weaker towards the top of the Damara Supergroup, associated isoclinal, intrafolial folds and low-angle, bedding-subparallel shear zones that truncate lithological packages.

Miller (1983, 2008) associates the third deformational phase (D_3) at ca. 540 Ma with large, upright, NE-trending, SE-verging domes that resulted in the development of the main NE-trending structural grain of the south Central Zone (Miller, 1983, 2008). This deformation is thought to mark the final collisional stage between the Congo and Kalahari Cratons (Miller, op cit.). The D_3 deformation corresponds to the D_2 deformation defined by Jacob (1974) and Kisters et al. (2004). Kisters et al. (op cit.) describe F_{2a} folds, Miller's (1983) F_3 folds, as the regional-scale, NE-trending, NW-verging dome structures and intervening synforms that refolded bedding (S_0), and the bedding-parallel S_1 foliation in the Karibib and Usakos districts. The F_{2a} folds (of Kisters et al., op cit) are associated with a regionally developed, NE- to NNE-trending, moderate- to steep SE-dipping axial-planar foliation (S_2). In addition, the S_2 foliation is associated with a regionally developed L_2 lineation, corresponding to Miller's (1983) L_3 . A later refolding (F_{2b}) of F_{2a} folds about NW-trending axes is attributed by Kisters et al. (2004) and Johnson (2005) to the lateral, orogen-parallel extrusion of rocks in areas of granite intrusion and, in particular, partial melting of the Damara Supergroup and basement. This refolding results in the sheath-fold like geometries of regional-scale folds (F_2 folds after Coward, 1983; Miller, 1983, 2008) that seem restricted to the higher-grade SW parts of the southern Central Zone, but are not recorded in the Karibib district (Kisters et al., 2004). The folding and refolding of the high-grade rocks also forms the basis for the tectonic models by e.g. Oliver (1994) and Poli and Oliver (2001), who regard fold development as part of one progressive event, recording the lateral, SW-directed extrusion of rocks. This

highlights the differences in interpretation and also timing of fold development in the high-grade rocks of the southern Central Zone.

2.1.2. Metamorphic Evolution

The Central Zone experienced high-T and low-P peak-metamorphic conditions that reached lower granulite facies in the west, along the Atlantic seaboard (Kasch, 1983a; de Kock, 1992; Miller, 2008). Masberg (2000), Jung and Mezger (2003) and Ward et al. (2008) suggest peak-metamorphic conditions of T ca. 750-800°C at P ca. 5-6 kbar. Steven (1993) and, more recently, Wulff et al. (2010) suggest peak-metamorphic conditions of T ca. 550-600°C and P ca. 2-3 kbar for the area around Karibib. Jung and Mezger (2003) also highlight the evidently polyphase metamorphic evolution, with peak temperatures reached at ca. 535, 505-515 and 490 Ma. Miller (2008) suggests a post-D₃ age of ca. 535 Ma for the main Damaran metamorphism, M₂, as is indicated by the supposedly post-tectonic, peak-metamorphic mineral assemblages and by the numerous anatexitic leucosomes, which lack a tectonic fabric.

2.2. Lithostratigraphy of the Karibib District

The rocks in the Karibib district and around the Navachab Gold Mine include a Paleoproterozoic granite-gneiss basement in the SW and the overlying supracrustal succession of the Damara Supergroup. Table 2.1 is a simplified stratigraphic column for the rocks found in the Karibib district. Since most of these units are developed outside the study area, only a brief lithological characterization is presented in the following.

Table 2.2: Lithostratigraphic subdivision of rocks in the Karibib district (after Miller, 2008)

Group	Subgroup	Formation	Member	Description	
Damara Supergroup	Swakop Group	Navachab	Kuiseb	Biotite and quartzo-feldspathic schists with cordierite porphyroblasts, calc-silicate felses	
			Karibib	Grey- to white calcitic and dolomitic marble with calc-silicate felses and intraformational breccia horizons	
			Ghaub	Similar to the Chuos Formation, but with rather local distribution, may contain iron formations	
		Usakos	Arandis	Oberwasser	Well-bedded dark-grey biotite-cordierite schist, calc-silicate felses, quartzites; includes interbedded amphibolites of the Daheim basalts in the upper parts of the member
				Okawayo	Calcitic and dolomitic marbles with calc-silicate felses, locally intruded by mafic sills and dykes
				Spes Bona	Well-bedded, dark-grey biotite-cordierite schist, calc-silicate felses, quartzites and metagraywacke
			Chuos	Glaciomarine diamictite; highly variable lithology; matrix is commonly schistose and dark-grey greenish	
		Nosib		Etusis	Well-bedded, pinkish-red feldspathic quartzites, arkoses, conglomerates and minor pyroclastics
		Abbabis Metamorphic Complex			

Abbabis Metamorphic Complex

The Abbabis Metamorphic Complex contains the oldest rocks found in the Karibib district, exposed in an erosional window in the core of the Karibib dome and 3-5 km south of the Usakos dome along the up-thrown block of the Mon Repos Thrust Zone (Steven, 1993; Kisters et al., 2004). The quartzo-feldspathic, pink- to grey gneisses, schists, amphibolites and pegmatites mainly represent Palaeoproterozoic basement, forming the leading edge of the Congo Craton (Jacob, 1974; Miller, 1983). U-Pb zircon ages for the Abbabis Metamorphic

Complex in the Ida dome area are interpreted as the time of igneous crystallization and constrain a minimum age for the supracrustal rocks in the complex to 2038 ± 5 Ma (Tack and Bowden, 1999). U-Pb ages for a migmatitic orthogneiss in the Khan dome yielded a ca. 1.1 Ga age and records a second granite-forming and possibly tectonometamorphic event in Kibaran (*sensu lato*) times (Tack and Bowden, op cit.).

Etusis Formation

The Etusis Formation unconformably overlies the Abbabis Metamorphic Complex and forms the lowermost unit of the Damara Supergroup (Miller, 1983; 2008). In the Karibib dome, the continental rift-type sequence comprises well-bedded, pink- to red feldspathic quartzites and arkosic metasediments and minor metavolcanic rocks with locally well-developed cross-beds and channel-fill conglomerates (Badenhorst, 1992; Kisters et al., 2004; Kitt, 2008; Miller, 2008). The Etusis Formation attains its maximum thickness of 1500 m along the NW side of the Karibib dome, but is not exposed in the Usakos dome (Kisters et al., 2004; Kitt, 2008).

Chuos Formation

The Etusis Formation is overlain by diamictites of the Chuos Formation. The Chuos Formation is a dark-grey to greenish, typically schistose rock made up of calc-silicate assemblages (Miller, 2008). The Chuos Formation reaches a maximum thickness of 180 m in the Karibib dome (Kisters et al., 2004; Kitt, 2008). Locally, the Etusis Formation may not be developed and rocks of the Chuos Formation are in direct contact with the basement gneisses (Kisters et al., 2004). Hoffman et al. (1996) give a maximum age constraint for the Chuos Formation of 746 ± 2 Ma, based on U-Pb zircon ages from underlying metavolcanics of the Etusis Formation.

Spes Bona Member

The mainly metapelitic Spes Bona Member overlies the Chuos Formation. The Spes Bona Member comprises banded biotite and biotite-cordierite schists and calc-silicate felses with minor amphibolites, metapsammities and marbles (Badenhorst, 1992; Kisters et al., 2004; Kitt, 2008). The thickness of the Spes Bona Member varies from <20 m on the SE flank of the Karibib dome to ca. 150 m in the hinge zone and ca. 80 m on the NW limb of the dome. In contrast, a minimum thickness of ca. 600 m is assumed for the Spes Bona Member in the hinge of the Usakos dome (Kisters et al., 2004).

Okawayo Member

The Spes Bona Member is overlain by the Okawayo Member which consists of dark grey- to off-white massive and finely banded marbles, sedimentary marble breccias and intercalated calc-silicate felses (Badenhorst, 1992; Kisters et al., 2004). The thickness of the Okawayo Member ranges from ca. 50 m on the Karibib dome to 150 m on the NW flank of the Usakos dome (Kisters et al., 2004; Kitt, 2008).

Oberwasser Member

The Oberwasser Member overlies the Okawayo Member. It is lithologically similar to the Spes Bona Member in that it consists of biotite schists, calc-silicate rocks, minor quartzites, marble horizons and amphibolites (Kisters et al., 2004). It forms the hangingwall sequence to the main ore body in the main pit of the Navachab Gold Mine (Kitt, 2008). The Oberwasser Member has an average thickness of 60-80 m in the Karibib dome and is up to 240 m thick in the Usakos dome (Kisters et al., 2004). The uppermost part of the Oberwasser Member contains interbedded amphibolites of the Daheim Member that represent mafic volcanic rocks (Badenhorst, 1992). In the study area, the Daheim Member directly underlies the Karibib Formation.

Ghaub Formation

The Ghaub Formation is the second diamictite that occurs in the Karibib district and overlies the Oberwasser Member. The depositional environment was an elevated rift shoulder and, as such, the clast suites of both the Chuos and Ghaub diamictites are dominated by quartzites, gneiss and granite, therefore making it difficult to distinguish the two diamictites in the field unless stratigraphic relations are known (Miller, 2008). The age of the Ghaub Formation is given as 635 ± 1.2 Ma (Hoffmann et al., 1996).

Karibib Formation

A detailed description of the Karibib Formation is given in Chapter 3, since the marble-dominated succession underlies large parts of the study area.

Kuiseb Formation

The topmost unit of the Damara Supergroup is made up of the turbiditic Kuiseb Formation, comprising mainly biotite-cordierite schists and metapsammities (Badenhorst, 1992). The Kuiseb Formation is only exposed in a small outlier in the core of the Navachab synform, here only preserved as a < 15 m thick erosional remnant, but reaching a thickness of > 800 m in the southern Central Zone (Owen, 2010).

Intrusive Rocks

In the Karibib district, the rocks of the Damara Supergroup have been intruded by various syn- to post-tectonic granitoids, mafic sills/dykes, pegmatites and aplites.

To the east of the Karibib dome the Damara Supergroup has been intruded by diorites of the Goas Suite, which includes the Mon Repos granodiorite and diorite (Jacob et al., 2000). The SE limb of the Usakos dome has been intruded by smaller dioritic plugs (Kisters et al., 2004). Ameglio et al. (2000) describe the Mon Repos diorite as a zoned, sheet-like body of 1-2 km thickness with one or two deeper root zones. U-Pb single zircon ages indicate an

emplacement of the Mon Repos diorite at 546 ± 6 Ma (Jacob et al., 2000). The Rote Kuppe granite cross-cuts the Mon Repos diorite and U-Pb SHRIMP dating puts the emplacement age at 543 ± 5 and 539 ± 6 Ma (Jacob et al., op cit.).

Numerous generations of syn- to post-tectonic pegmatite and aplite dykes have intruded the Abbabis Metamorphic Complex and the Damara Supergroup (Brandt, 1985; Steven, 1993; Kisters et al., 2004; Kitt, 2008). Kitt (2008) found that the NW-trending pegmatite dykes in the Navachab main pit are commonly restricted to the siliciclastic units of the Spes Bona Member and almost absent in the marble units of the Okawayo Member. This suggests the control of rheological contrasts between more competent siliciclastics and less competent marble units on dyke propagation and emplacement. The Karibib Formation in the study area is almost devoid of pegmatites and aplite dykes.

Lamprophyre sills and dykes intrude into the Damara Supergroup. In the main pit, the Okawayo Member is intruded by a prominent metalamprophyric sill, which locally has dyke-like offshoots into the overlying Oberwasser Member (Moore et al., 1998, 1999; Kitt, 2008).

2.3. Previous Work

Previous works at the Navachab Gold Mine have mainly focused on the origin and controls of the gold mineralisation in the main pit. Moore et al. (1998, 1999) were the first to provide a more detailed account of the structural controls and ore- and alteration mineral parageneses of the mineralisation. They concluded that the gold-quartz veins formed as conjugate anti- and synthetic Riedel shears in a non-coaxial shear zone represented by the steep NW limb of the Karibib dome, centred around the highly strained marbles of the Okawayo Member. In addition they explained the formation of large replacement skarn lenses in the MC unit (MC: interlayered marble calc-silicate felses) as the intersection between the vein system and the host rocks and that the intersection between shallowly-dipping sheeted quartz veins and bedding would explain the shallow NNE plunge of the ore body.

Nörtemann et al. (2000) referred to the gold mineralisation as a reduced gold skarn, envisaging skarn development in three stages:

- A first stage involves isochemical metamorphism with an exchange of volatiles associated with the intrusion of the central, synmetamorphic lamprophyre sill, which caused dehydration of the banded marble and, thus, an increase in fluid pressure;
- the second stage is characterized by further dehydration and decarbonization of the marbles with initial metasomatic transport and exchange of elements, mainly Fe and Mn, to form a garnet- and pyroxene skarn;
- the third stage includes retrograde alteration, hydrothermal fracturing and precipitation of the ore. Mineralisation is a function of decreasing temperatures and increasing sulphur fugacities.

Nörtemann et al. (2000) indicate pressures of 2-2.5 kbar and temperatures of 590°C and 575±15°C for the mineralisation, based on sphalerite and arsenopyrite geobarometry and thermometry.

Kisters (2005) refers to the origin of different vein sets as being closely related to the different stages of fold development of the regional-scale Karibib dome during D₂ fold and thrust tectonics. The first set (MC unit) formed as a result of localized flexural-slip during the initiation and amplification of the Karibib dome along the contact between the Spes Bona Member and the rheologically much weaker marbles of the Okawayo Member. The second set of subhorizontal quartz veins formed during the later lock-up stages, when flexural-slip was no longer possible on the steepened NW limb of the Karibib dome, resulting in extensional fractures.

Kitt (2008) proposes a similar structural model to that of Kisters (2005), but takes into account the formation of sheeted quartz veins in the hinge of the Usakos dome. Kitt (2008) states that the regional-scale dome formation represents a first-order control on quartz-vein formation, and that local lithological and/or structural controls exert a more localized control on quartz-vein formation. Furthermore, Kitt (2008) suggests that the actual location of economic-grade vein clusters seems to be controlled by dilational stepovers between overlapping D₂-related thrusts.

Steven et al. (2008) suggest a model that postulates the anticlockwise rotation of F_2 dome structures during a D_4 event as described by Steven (1993), with D_3 as the dome forming event. They suggest that the veins formed during a late stage and in NNE-trending corridors that record sinistral strike-slip movement. This would explain the localization of the mineralisation of the main pit on the NW limb of the Karibib dome and slightly oblique to the overall NE-trending $D_{2/3}$ structural grain of the Damara Belt. For the Grid A prospect, Steven et al. (2008) propose a model involving WNW-ESE shortening during early D_4 , which caused vertical extension and necking of competent dolomite units. Further WNW-ESE compression caused tight folding, thrust faults and sheeted quartz-vein development.

Wulff et al. (2010) develop a genetic model for the fluid-flow during the mineralisation, in which fluids generated at deeper crustal levels are derived from metamorphic dehydration reactions of the biotite schists at subsolidus conditions, rather than a magmatic source of fluids. Wulff et al. (op cit.) suggest that at deeper crustal levels, the initial fluid release from the rocks was likely controlled by gradients in fluid pressure created in dilational fractures during ongoing deformation and that the far-field transport of the fluid occurred along high-permeability structures such as fractures and shear zones on regional-scale lithologic contacts within the Damara Supergroup.

For a description of the geology of the main pit, the reader is referred to Kisters (2005) or Kitt (2008). Two main sets of quartz veins are developed in the main pit and include (1) bedding-parallel, shallowly-dipping ore lenses and shoots situated at the base of the Okawayo Member and overlying schists and calc-silicate felses of the Spes Bona Member (the MC-type mineralisation, Moore et al., 1998, 1999), and (2) a laterally extensive swarm of shallowly-dipping quartz veins that truncate the host rock at high angles (the sheeted quartz veins, after Moore et al., 1998, 1999).

Chapter 3 Lithostratigraphy of the Navachab Synform

The Karibib Formation forms the core of the Navachab synform and underlies much of the study area. For the Karibib district, Badenhorst (1992) describes the Karibib Formation as consisting of a basal section comprising interbedded, dark- and light-grey marble, white dolomitic marble, ribbon marble and intraformational marble breccias, and an upper section comprising interbedded banded, dark- and light-grey marble, fine-grained, dark-grey laminated marble, carbonate conglomerate lenses and silicified pisolith and fenestrated structures.

In this study, a new detailed lithostratigraphy of the Karibib Formation was established through mapping and stratigraphic profiling along sections through the several hundred metre thick, marble-dominated unit. Based on correlations between the different sections and lithological characteristics, the Karibib Formation in the Navachab synform has been subdivided into six main units. The subdivision allowed for easier structural analysis and stratigraphic correlation within the Navachab synform.

3.1. Unit 1

The lowermost unit 1 consists of alternating horizons of calcareous marbles and calc-silicate felses that are interlayered with marble breccia horizons (Fig. 3.1a) The laminations observed in the calcareous marble are typically on the scale of <1cm – 10 cm, but may be up to 20 cm thick and are interlayered with calc-silicate felses that may be up to 10 cm thick. The calc-silicate felses are rusty brown in colour and weather positively. The calcareous marble is light- to medium- grey in outcrop and weathers negatively.

Intraformational breccia horizons contain two types of fragments, namely white calcitic and dark dolomitic marble set in a medium-grey calcareous matrix. The fragments are typically angular to subrounded and have long axes of <1 – 10 cm, but locally may be up to 100 cm. The breccias commonly fine upwards from clast- to matrix-supported breccias. In most

cases, the top quarter of the breccias is matrix supported. In places, there are erosive contacts, where the breccias cut into the underlying banded marbles (Fig. 3.1b). The intraformational breccias show large thickness variations and undergo a thinning and thickening along strike. This is considered to be a primary feature and there are cases where breccia horizons pinch out altogether only to re-appear further along strike.

Near the hinge of the Usakos dome, the fragments have a random orientation. In high-strain zones, however, the long axis of fragments is typically rotated into parallelism with the regional L_2 lineation and fold axis of F_2 folds and flattened fragments are parallel to the regional NE-trending S_2 foliation (chapter 4.2). Along the highly-strained NW limb of the Karibib dome, breccia fragments are flattened in the S_2 foliation plane to such an extent that they resemble bedding and banded marbles.

The intraformational breccia horizons weather positively and form good marker horizons, despite the thickness variations that can be used for a correlation between different sections. The breccia horizons in this unit have a true thickness of <1 and up to 20 m, but due to the shallow dips in the southern parts of the Navachab synform, the apparent thickness can be up to 50 m. The packages of banded marble horizons show a large range in true thickness, varying from merely several metres to up to 150 m.

3.2. Unit 2

Unit 2 consists of alternating horizons of calcareous marble, with only few or no calc-silicate felses. The unit includes intraformational marble breccia horizons. The calcareous marble typically contains fine, millimetre-scale black laminations (Fig. 3.1c). The black laminations give the marble a streaky appearance. The start of the unit is taken at the first marked appearance of the black laminations. The calcareous marble weathers negatively and is often covered by alluvium in lower-lying areas, providing few outcrops. The breccia horizons are as in unit 1. The true thickness of the breccia horizons are <1 to 10 m. As with unit 1, the laminated marble horizons have a variable thickness ranging from several metres to up to 50 m.

3.3. Unit 3

Unit 3 is lithologically similar to unit 1. However, towards the top of unit 3, the number of calc-silicate felses found in the calcareous marble decreases in abundance. The start of the unit is taken as the first re-appearance of thick calcareous marble horizons containing calc-silicate felses. However, in some sections, the contact of unit 2 and unit 3 is gradational in that several horizons of calcareous marble with fine, black laminations occur after the first re-appearance of thick calcareous marble horizons containing calc-silicate felses. The true thickness of the breccia horizons is <1 to 10 m. The vertical thickness of the banded marble horizons is highly variable and ranges from several metres up to 100 m.

3.4. Unit 4

Unit 4 consists of alternating horizons of calcareous marble, with dolomitic marble bands and intraformational breccias (Fig. 3.1d). The start of the unit is taken as the first appearance of thick calcareous marble horizons containing dolomitic marble bands. The unit contains fewer intraformational breccias horizons than the lower units. The calcareous marble is typically darker in colour than the calcareous marble found in units 1-3, but white beds of calcareous marble do occur within the unit. There are few calc-silicate felses within this unit and when they do occur, they are seldom thicker than 0.5 cm. The dolomitic bands are typically on the scale of <1 – 10 cm, but may be up to 50 cm thick. The thicker dolomitic bands are susceptible to rectangular boudinage and boudin necks are commonly filled with carbonate (Fig. 3.1d). The calcareous marble weathers negatively while the dolomitic marble weathers positively. The breccia horizons are as in unit 1, although dolomitic fragments have locally been observed in some breccias horizons. The breccia horizons have a true thickness of <1 to 25 m. The banded marble horizons have a variable vertical thickness ranging from several metres up to 100 m.

3.5. Unit 5

Unit 5 is an up to 100 m thick dolomitic unit that weathers negatively. The dolomitic marble has an overall massive appearance that, in places, appears to be bedded. The bedding is defined by thin, millimetre- (up to 1 cm) scale calcareous marble bands. The dolomitic marble is light-grey in outcrop and has a typical elephant-skin weathering (Fig. 3.1e). The start of the unit is taken as the first appearance of a thick massive dolomitic horizon. Unit 5 hosts the mineralisation at the zoo prospects. More detailed mapping in these areas found that the dolomitic marble in the Karibib Formation in the Navachab synform can be further subdivided into several subunits. Details of this are presented later in chapter 5.

3.6. Unit 6

The topmost unit of the Karibib Formation in the Navachab synform is a calcareous banded marble. The start of the unit is taken as the first appearance of calcareous marble overlying a thick, massive dolomitic marble and the upper boundary as the first appearance of the Kuiseb Formation. The marble is dark-grey in colour (Fig. 3.1f). The laminations are typically <1 – 20 cm wide, but up to 50 cm thick layers also occur. In places, the unit shows a strong magnetic response. The dark-grey, banded marble is mostly covered by alluvium, forming the core of the Navachab synform, so that the true thickness of the unit is unknown. The minimum thickness is 40 m as measured in the vicinity of the Klipspringer prospect.

Figure 3.2 is a geological map of the Navachab synform produced during this study and shows the distribution of units 1-6 of the Karibib Formation. In addition the figure also shows the location of the zoo prospects and the sections (1-6) traversed. Note that faults are observed in the Navachab synform, but are too small to be included on the geological map.

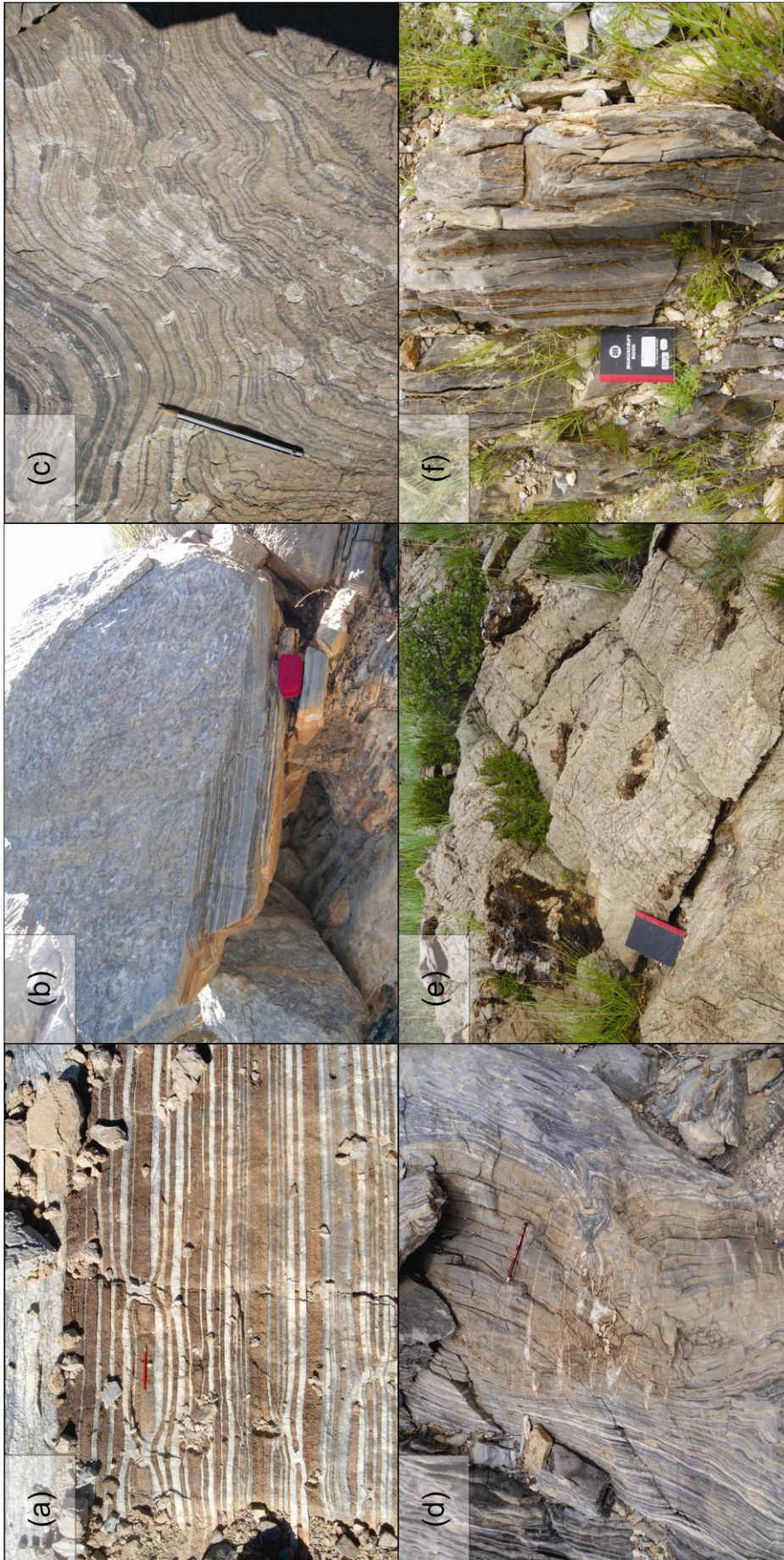
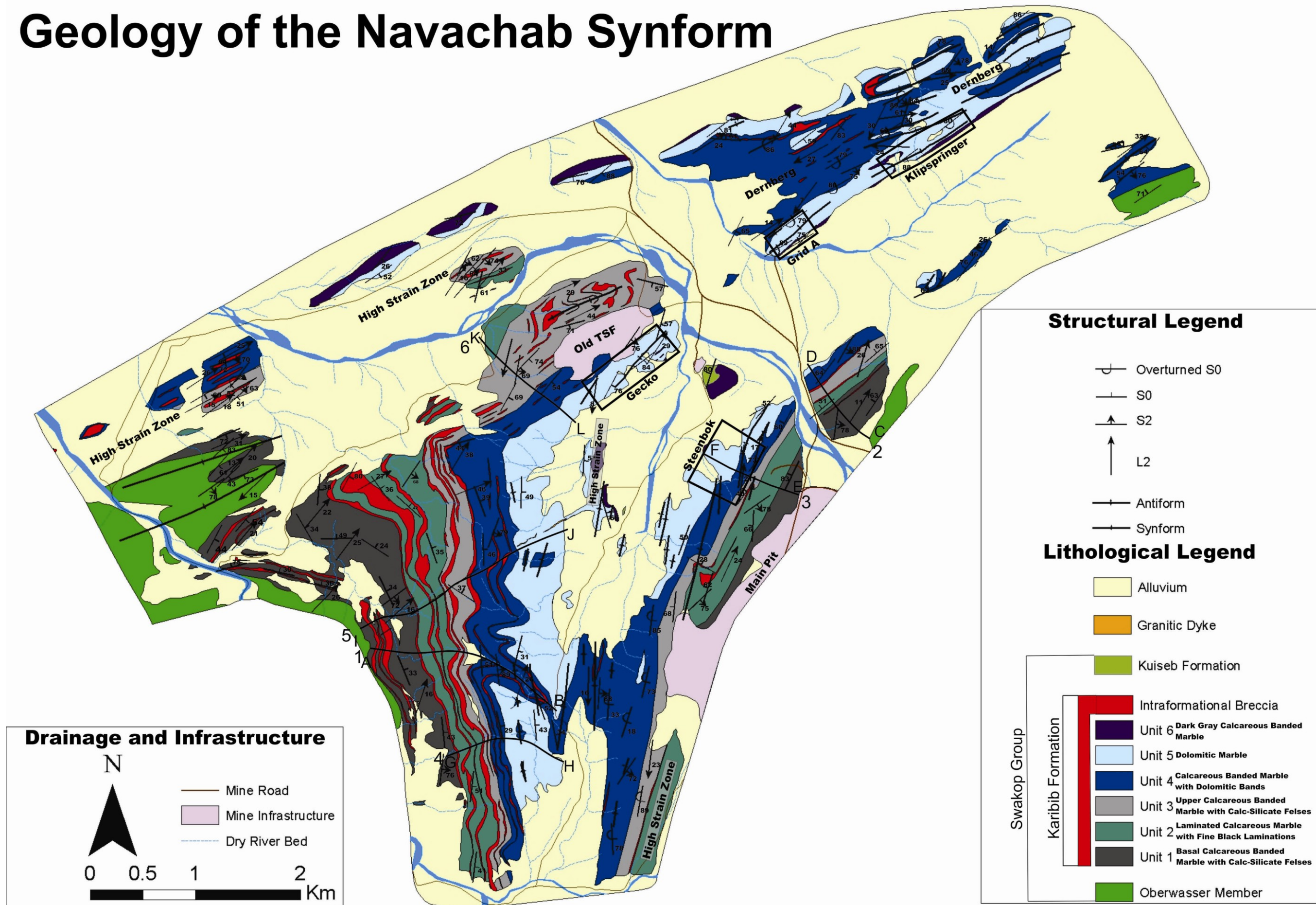


Figure 3.1: Outcrop appearance of the main units in the Karibib Formation. (a) Calcareous banded marble with calc-silicate felses (unit 1 and 3). The calc-silicate beds are more competent than the calcareous beds and are prone to rectangular boudinage. View to the NE. (b) Disconformity formed by an erosional surface caused by intraformational mass-flow breccia eroding into layered marbles of unit 1. View to the north. (c) Calcareous marble with fine black laminations (unit 2) that give the marble a streaky appearance. The black laminations are prone to internal disharmonic folding. View to the SW. (d) Calcareous banded marble with dolomitic bands (unit 4). Left of photo is the typical outcrop appearance of the unit. The thick and competent beds of dolomitic marble commonly show boudinage. Boudin necks are filled by carbonate veins. View to the north. (e) Typical outcrop appearance of unit 5. Massive light-beige, elephant-skin weathering. View to the NW. (f) Outcrop appearance of a banded grey marble of unit 6. View to the SW.

Geology of the Navachab Synform



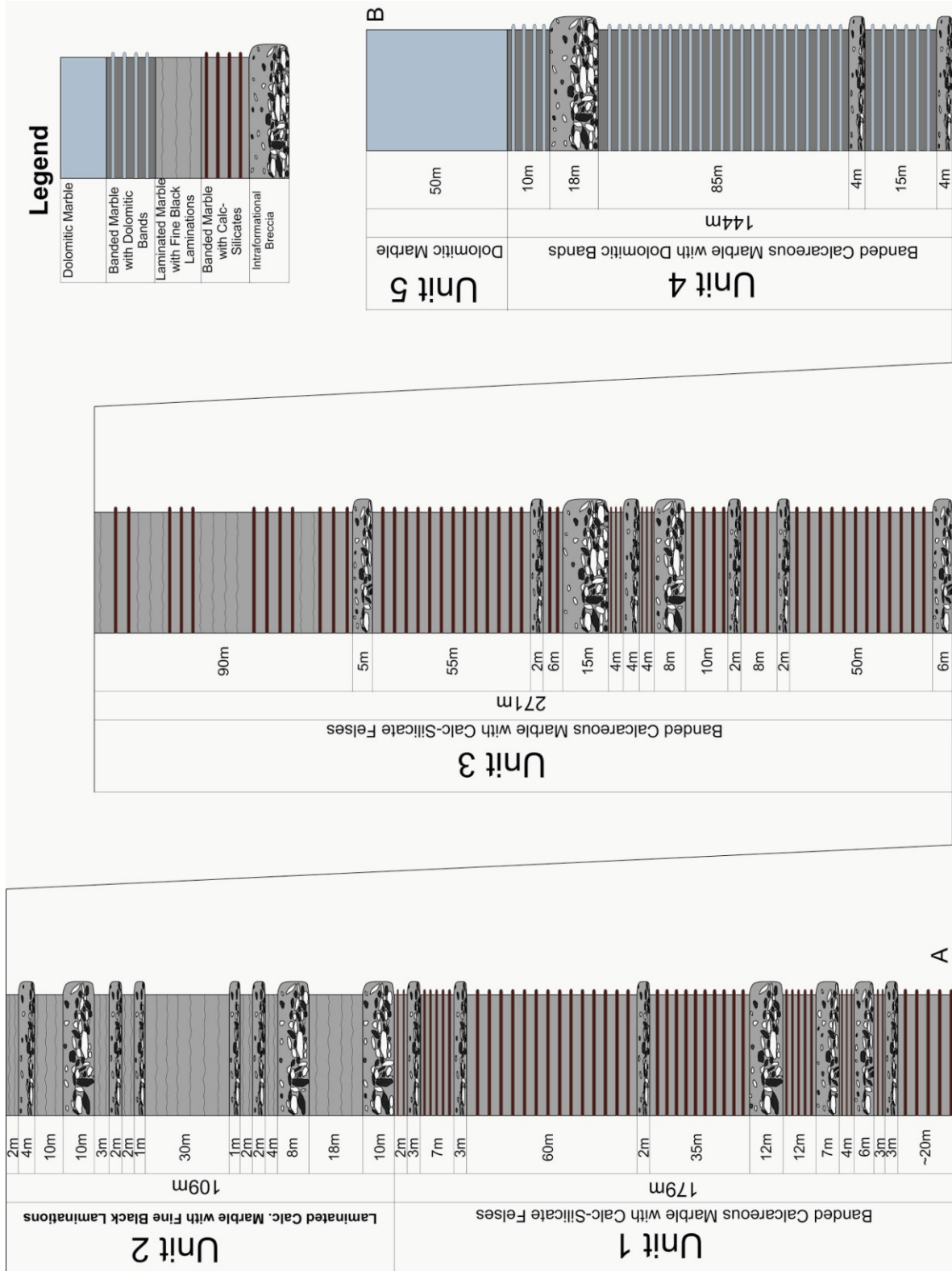
3.7. Stratigraphic profiles

In total six sections were traversed which allowed for the subdivision of the Karibib Formation in the Navachab synform (Fig. 3.2). Up to now, on a regional scale, the Karibib Formation in the Navachab synform has only been subdivided into calcareous or dolomitic marble. The six sections showed that there are distinct lithological characteristics in the Karibib Formation that allow for the subdivision of the Karibib Formation. Details of the six section traversed are shown below.

Figure 3.3 illustrates the stratigraphy of the most complete and best preserved section (Section 1) through the Karibib Formation located in the hinge of the Usakos dome where the rocks have undergone little internal deformation and only gentle folding. Correlation of the other sections is made against this section. The correlation of breccia horizons is not made because of the thinning and eventual termination of breccia horizons that make a regional correlation almost impossible. Intense folding and transposition in other areas of the map has resulted in the structural attenuation and 'loss' of individual horizons and/or units (Fig. 3.2). The NW and SE boundaries of the map show the development of distinct high-strain zones, corresponding to the NW limbs of the Usakos and Karibib domes, respectively. In these areas, the carbonates are highly attenuated and transposed into a NE-trending, steeply-dipping tectonic fabric (S_2 , chapter 4.2) resulting in structurally condensed and thinner columns through the Karibib Formation.

Sections 2 and 5 (Fig. 3.2 and 3.4) represent complete sections, i.e. sections comprising the entire Karibib Formation. Section 2 occurs in an area that has undergone bedding transposition and a pervasive fabric development (S_2 and L_2 , chapter 4), especially well displayed in the breccia horizons. Overall, the thickness of the section 2 (ca. 555 m) is less than section 1. The upper units (2-4) in section 2 are thinner than those in section 1, resulting from the structural attenuation of the marble units. Correlation of the lower units (1-2) of section 5 with section 1 is difficult due to the poor outcrop conditions in the lower parts of section 5. The exact contact of unit 2 and unit 3 is unknown in section 5 due to the poor outcrop and the often gradational contact observed between the two units. The thickness of unit 2 and unit 3 is estimated on Figure 3.4.

Figure 3.3: Section 1, stratigraphic column through the Karibib Formation in the hinge of the Usakos dome taken from the Kachab River (See Fig. 3.2 for location). Thickness of the column is ca. 750 m and excludes unit 6 which does not crop out on surface.



Sections 3, 4, 6 (Fig. 3.2 and 3.4) show most of the units, but lack most of unit 1 (sections 3 and 4), and unit 1 and parts of unit 2 (section 6). This is a result of alluvial cover. Section 3 occurs ca. 1 km SW of section 2. The thickness of the units is similar to that of section 2. Section 4 occurs to the SW of section 1. Unit 2 of section 4 is thicker than that of section 1 and unit 3 is thinner than that of section 1. Unit 4 is of similar thickness to that of section 1. Section 6 shows similar thicknesses for the complete units 3 and 4 of section 1. To the immediate NE of section 2, units 1 to 3 seem to have been excised from the Karibib Formation, juxtaposing marbles of unit 4 against the schist-dominated Oberwasser Formation. This suggests the presence of a hitherto unidentified structure along which at least 250 m of stratigraphy has been omitted. The nature of this structure is unclear, although metre-wide mylonites are developed in the basal sections of the Karibib Formation in section 2.

This compilation of litho-units within the Karibib Formation illustrates that although units can be correlated throughout the Navachab synform, they show a rather lensoid geometry, which underlines their origin as turbiditic mass-flow deposits (e.g. Badenhorst, 1992; Miller, 2008). Moreover, the subdivision and correlation of marble units enable the identification of structures with significant displacement to have affected the seemingly monotonous sequence (see chapter 4).

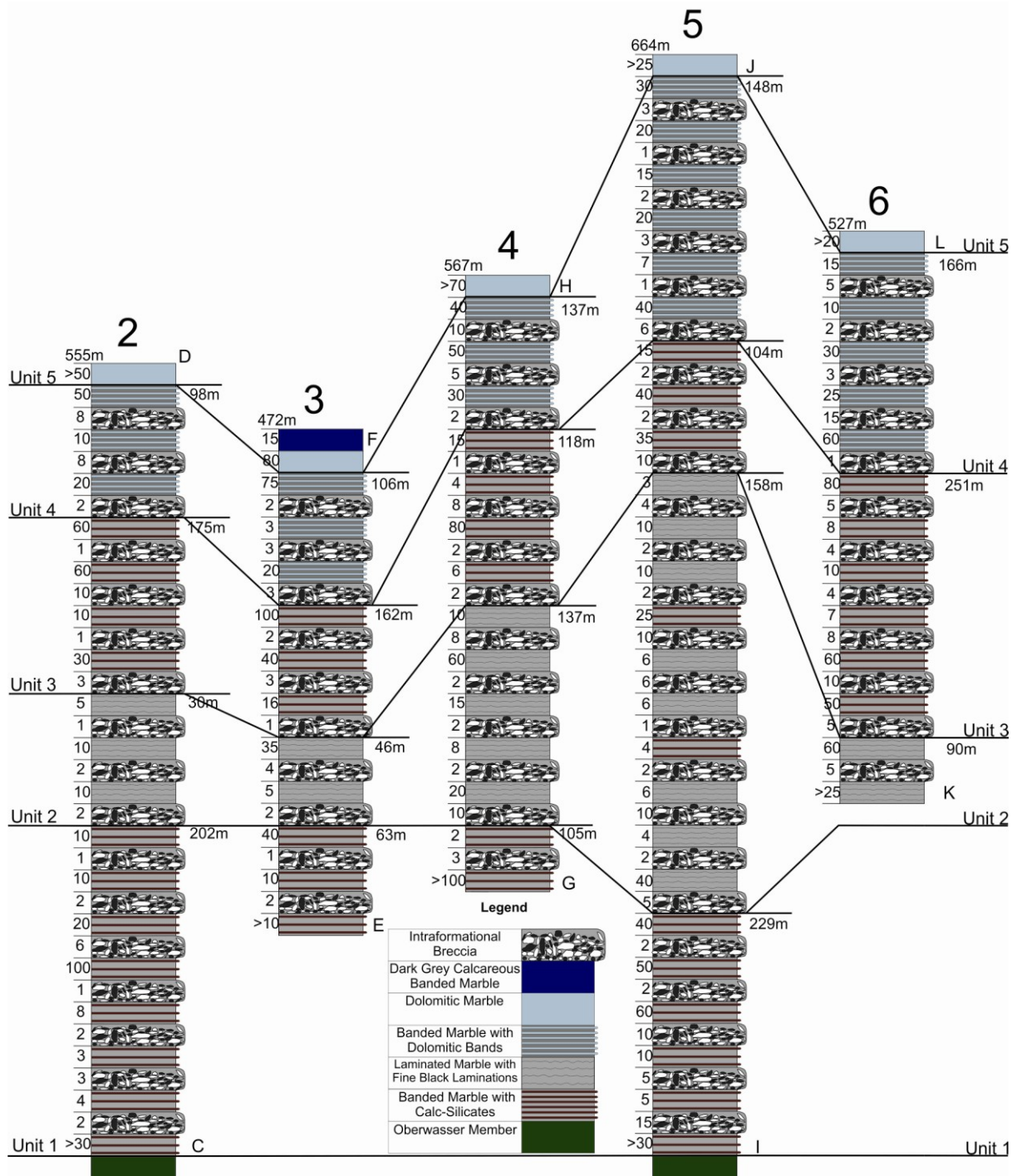


Figure 3.4: Sections traversed across the southern part of the Navachab synform, not to scale. The locations of the sections are shown on the geological map (Fig. 3.2). Thicknesses of individual horizons are shown on the left of each respective column, and the thickness of each unit within each section is shown on the right of each column. The total thickness of each section is shown above each respective column.

Chapter 4 Structural Geology of the Karibib District

The most prominent, regional-scale structures in the Karibib district are the Karibib and Usakos domes, which are separated by the Navachab synform (Fig. 1.1). These kilometre-scale, NE-trending folds define the regional grain of the southern Central Zone and are referred to as F_3 (Miller, 1983; 2008) or F_2 folds (Jacob, 1974; Kisters et al., 2004). The following terminology is used in the text to denote different fabric elements:

- D deformational phase
- S planar penetrative fabric
- L linear penetrative fabric
- F fold phase

Suffixes 1, 2, 3 etc. denote the structural order resulting from the respective deformational phase, e.g. S_1 refers to foliation developed during the D_1 deformational phase.

Kisters et al. (2004) identified two main phases of deformation, D_1 and D_2 , in a study of dome structures in the Karibib district. The D_1 deformation of Kisters et al. (2004) corresponds with that of e.g. Miller (1983) and resulted in the formation of a variably developed S_1 foliation. The truncation of marker horizons along the contacts between the lower formations of the Damara Supergroup suggests the presence of low-angle shear zones which may also account for the dramatic thickness variations of the units (Kisters, 2005). The D_2 deformation (after Kisters et al., 2004) represents the periclinal folding and dome formation and correlates with the D_3 event of other regional studies (e.g. Miller, 1983, 2008). SW-verging sheath-fold structures (F_2) are only developed to the SW of the Karibib dome in the SW hinge of the Usakos dome (Johnson, 2005) and in adjoining domes further to the SW (Poli and Oliver, 2001; Kisters et al., 2004; Johnson, 2005). The F_2 dome structures are doubly-plunging, asymmetric, NW-verging antiforms that refold bedding (S_0) and the

bedding-subparallel S_1 and/or S_0/S_1 transposition fabric. The regionally developed, SE-dipping to vertical S_2 foliation is axial planar to the F_2 folds with a NE- to NNE trend and would indicate a coeval relationship with the dome structures. Steven (1993) describes a fourth deformation phase, D_4 , which involves sinistral wrenching and an anticlockwise rotation of domes. The anticlockwise rotation of F_2 fold structures resulted in NNE-trending bedding- and foliation domains between e.g. the adjacent Karibib and Usakos domes that are parallel to lineament structures geophysically identified by Corner (1983).

Table 4.1: Summary of the structural elements observed in the Karibib district (after Kisters et al., 2004; Johnson, 2005; Kitt, 2008; Owen, 2010)

Deformational Phase	Fabric element	Field expression, orientation and occurrence
Primary	S_0	Primary compositional layering
D_1 Early low-angle shearing	S_1 and S_0/S_1	Bedding-subparallel foliation parallel to low-angle shear zones; locally developed as a transposition fabric; not observed in the study area
	F_1	Isoclinal, intrafolial folds; not observed in study area
D_2 Top to the NW thrusting and periclinal NW-vergent folding	S_2	Steep NE-trending axial planar foliation to F_2 ; developed as pressure-solution seams and flattening of breccias clasts parallel to S_2
	F_2	Large-scale NE-trending, NW-verging, NE-SW doubly-plunging dome and basin structures (Karibib and Usakos domes and Navachab synform); includes parasitic folds observed in the Navachab synform
	L_2	Includes intersection lineation (L_{2i}) between S_2 and S_0 or S_0/S_1 , and variably developed mineral stretching lineation (L_{2m}); shallow NE-SW plunge parallel to first-order F_2 ; stretched fragments observed in marble breccias

4.1. Bedding (S_0)

Bedding in rocks of the Karibib Formation is well preserved on all scales. Bedding is represented by alternating grey- and dark-grey banding in schists and alternating bands of grey marble and calc-silicate felses in marble horizons (Kitt, 2008). In the Navachab synform, bedding is well developed in the lower parts of the Karibib Formation indicated by alternating units of calcareous marble, calc-silicate felses and sedimentary marble breccias.

In addition, layering of dolomitic and calcareous marble towards the top of the formation also reflects original compositional layering. Individual beds range in thickness from fine laminations (mm-scale) to several 10's of metres wide, massive horizons such as the intraformational breccias. Graded bedding is common in the breccias horizons, where the basal part of the breccias is coarse-grained and clast supported, fining upwards into matrix-supported tops.

4.2. Planar Tectonic Fabrics (S_1 and S_2)

4.2.1. Bedding-Parallel Foliation (S_1)

Kitt (2008) describes the S_1 foliation as the result of the preferential alignment of biotite, forming a penetrative bedding-subparallel foliation in the metapelitic units and suggests that the lack of S_1 in the marble units to possibly be the result of the obliteration of the fabric by pervasive recrystallisation. Kisters et al. (2004) recorded isoclinal, intrafolial folds, which refolded the compositional banding (S_0), in the banded marbles of the Okawayo Member and shows that the S_1 foliation is, at least locally, a transposition fabric (S_0/S_1). Furthermore they recorded low-angle truncation of marker units in the lower parts of the Damara Supergroup, which they related to the presence of D_1 low-angle shear zones. Kisters et al. (op cit.) also noted the heterogeneous development of S_1 and the, in general, decrease in fabric intensity from the lower formations, close to the basement-cover interface, to the upper formations, including the Karibib Formation. In agreement with this, S_1 is not observed in the Navachab synform.

4.2.2. Steep, axial planar foliation (S_2)

S_2 is a regionally-developed, NE- to NNE-trending, steeply-dipping foliation and is axial planar to F_2 folds. In the Karibib Formation, the S_2 foliation is expressed as dark-grey, spaced (1 mm-1 cm) pressure-solution seams (Fig. 4.1a) or defined by the preferred orientation of flattened carbonate breccia clasts in the intraformational marble breccias (Fig. 4.1b). The pressure-solution seams are best developed in unit 4, where the dark bands contrast prominently against the white calcareous marble horizons. The breccia clasts are typically angular, but take on a more elongate shape when flattened in the S_2 plane. S_2 is difficult to distinguish from S_0 on the limbs of folds where S_0 is steeply-dipping. The dark-grey pressure-solution seams and flattened clasts are developed throughout the study area, although fabric intensities vary considerably.

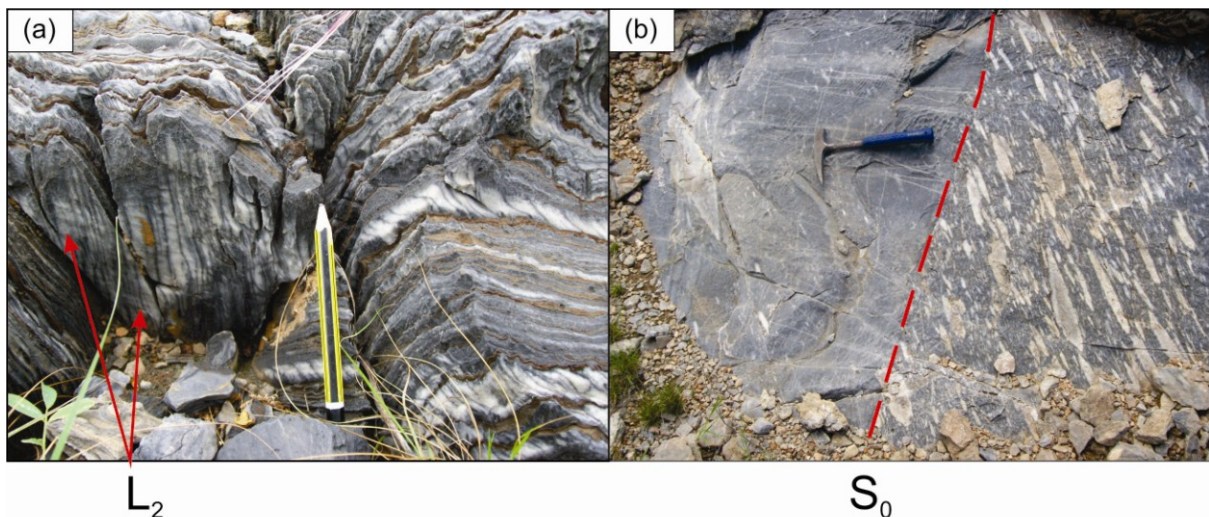


Figure 4.1: (a) Closely- (1 mm to 1 cm) spaced, dark-grey pressure-solution seams in white calcareous marble bands in unit 4. Note that on the bedding surface, an intersection lineation is developed (See below). View to the SW, oblique cross-sectional view. (b) Flattened and re-orientated breccia fragments define the S_2 foliation in this outcrop. The red dashed line annotates S_0 ; note the angular relationship between the long axis of fragments (S_2) and bedding (S_0). Oblique plan view, view is to the NE.

In the prospects, transposition of bedding into the S_2 fabric delineates high-strain zones. Bedding transposition originates either along steep S_2 foliation domains developed on fold limbs, which then are further attenuated to yield shear zones, or as high-strain zones where incompetent calcareous marbles wrap around competent rocks such as quartz pods or dolomitic marble to form highly-attenuated S_2 foliation domains. Figure 4.2a is a

diagrammatic illustration of the development of S_2 along the limbs of tight folds gradually developing into anastomosing shear zones that envelop F_2 folds. Figure 4.2b shows the development of high-strain fabrics when, in particular, bedding of calcareous marble wraps around pods of more competent rocks to develop an S_2 fabric.

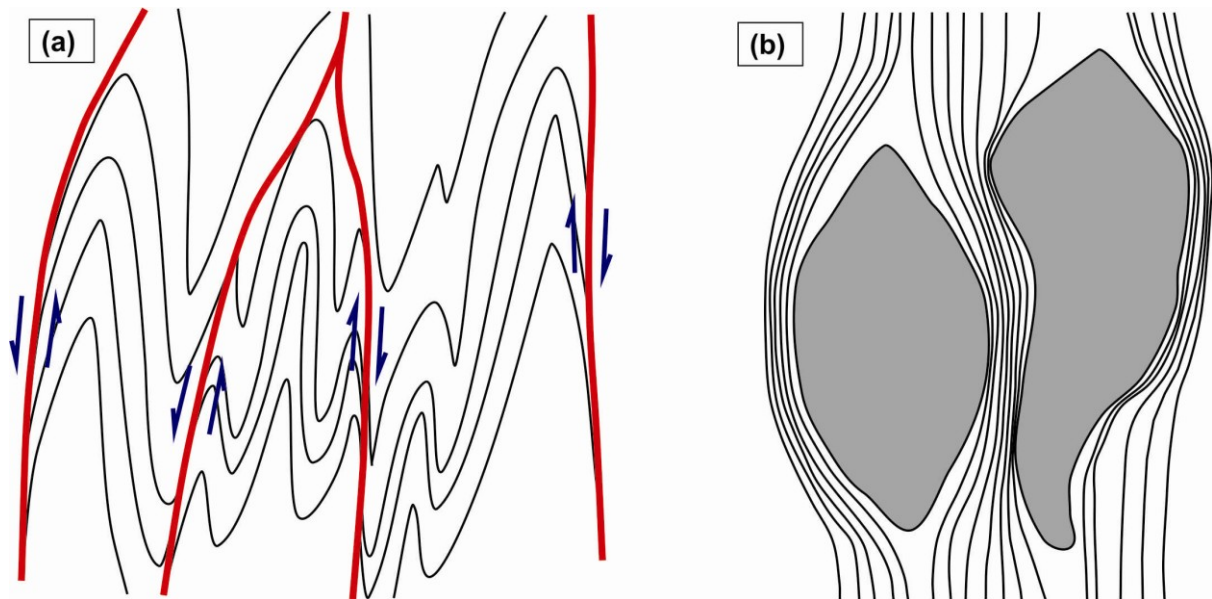


Figure 4.2: Field sketches illustrating (a) the development and attenuation of the S_2 foliation on fold limbs. During progressive deformation, the bedding-parallel S_2 on fold limbs develops into anastomosing, low-displacement shear zones (red) enveloping folded domains and F_2 fold hinges. Note the inconsistent sense of displacement along the shear zones that suggests that deformation occurred during largely coaxial shortening; and (b) a similar accentuation of S_2 fabric domains when the foliation wraps around more competent rocks (e.g. calcareous marbles enveloping fragments, boudins or relict hinges of more competent dolomitic marble), resulting in strain caps and strain shadows around the competent blocks (here: dark grey). These features are recorded on a scale of centimetres to tens of metres.

4.3. High Strain Zones

Three high-strain zones occur in the Karibib district. Kitt (2008) identified NE-trending and up to 100 m wide high-strain zones in marbles of the Karibib Formation preferentially developed on the steep- to overturned NW limbs of the Usakos (1) and Karibib (2) domes. The third high-strain zone occurs in the hinge of the Navachab synform.

In this study, the first high-strain zone which occurs along the NW limb of the Usakos dome can be shown to be continuous through the NW part of the study area and up to the

Dernberg locality (Fig. 3.2). The SW strike extent of the high-strain zone can be traced for some 30 km along the entire extent along the NW limb of the Usakos dome, described by Johnson (2005) and Owen (2010) in their respective studies of the Usakos dome and the adjacent Kranzberg synform. This underlines the regional significance of the high-strain zone in the Karibib marbles and far beyond the boundaries of the study area. The NW high-strain zone in the study area is, for the most part covered by alluvium and calcrete, but its width must be assumed to be at least 300 m, while the strike extent can be followed for at least 5 km. The NW zone occurs between the coordinates (-21.957; 15.723) and (-21.949; 15.742). The high-strain zone appears to terminate at the Dernberg locality.

The second high-strain zone occurs along the NW limb of the Karibib dome and extends from the south to the NE for ca. 2 km in the study area (Fig. 3.2). The high-strain zone occurs between coordinates (-21.998; 15.753) and (-21.978; 15.761). This zone corresponds to the steep- to overturned NW limb of the Karibib dome, also hosting the main pit of the Navachab Gold Mine.

In the NW high-strain zone, parts of the Karibib Formation have been transposed. Transposition has particularly affected unit 2 in the west and unit 4 towards the NE of the zone. Breccia clasts provide good strain markers and are flattened and orientated parallel to S_2 . In places, the breccia clasts are attenuated to such a degree that the breccia horizons resemble banded marbles. Figure 4.3 shows the transposition of bedding in the southern zone where individual folds have been attenuated between two subparallel, slightly anastomosing high-strain zones, parallel to S_2 . The attenuation and rupture of fold limbs ultimately leads to the separation of fold hinges and the formation of rootless, intrafolial (F_2) folds. Fold hinges dismembered in such a way can be found on a centimetre-scale, but also in a metre- to tens-of-metre scale (see also Johnson, 2005). Figure 4.2a shows the initial stages of transposition. With further tightening of folds, accompanied by progressive slip and pressure-solution, individual fold limbs are attenuated and eventually separated from their hinge zones (Fig. 4.3). This may eventually form a pseudostratigraphy and the banding in the marbles is the result of multiply folded bedding transposed into S_2 . The transposition folds in these high-strain zones show similar shallow plunges to the F_2 folds and the largely symmetrical folding. The chocolate-tablet boudinage of the competent horizons contained within the transposed fabric indicate that the high-strain zones record a largely coaxial

flattening strain normal to the transposition fabric, i.e. the S_2 foliation, and a near-equal component of vertical and horizontal stretch (Fig. 4.4). This indicates that the high-strain zones are related to D_2 fabrics and folds.

A third high-strain zone has been identified in the hinge of the Navachab syncline near the Gecko prospect (Fig. 3.2). The outcrop of the high-strain zone is small, ca. 540 m along strike and ca. 110 m wide, and contains mylonites.

4.4. Linear Fabrics (L_2)

In the Navachab synform, two types of lineations are regionally developed, including (a) a prominent intersection lineation between S_0 and S_2 (L_{2i} ; Fig. 4.1a), and (b) a pervasively developed stretching lineation (L_{2m}). The two lineation types are parallel to each other and plunge shallowly to the NE and SW. The intersection lineation is most pronounced where the S_2 foliation is defined by dark-grey, closely-spaced pressure-solution seams (Fig. 4.1a). Given that S_2 is an axial-planar foliation to F_2 folds (see below), it is considered as a δ -lineation that can be used to ascertain the plunge of F_2 folds. The stretching lineation is most pronounced in intraformational breccias, expressed by the preferred orientation of breccia fragments, resulting from the flattening and stretching of breccia fragments in the S_2 foliation plane. The shape-preferred orientation of breccia fragments (Figs. 4.1b and 4.5a), thus, delineates the XY-plane of the finite strain ellipsoid ($X \geq Y \gg Z$, with $X \geq Y \geq Z$). Notably, the stretching lineation is also parallel to F_2 fold hinge lines (Fig. 4.5a). F_2 hinge-parallel stretch is also recorded by the separation of small-scale crenulations hinges in calc-silicate felses (Fig. 4.5b).

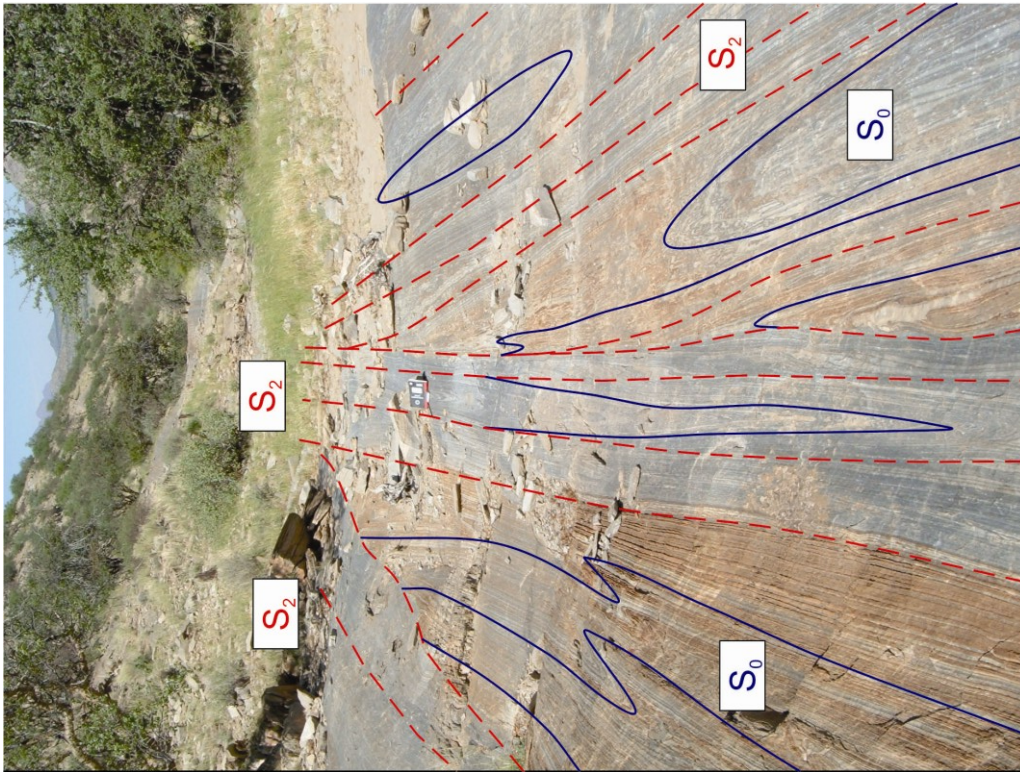


Figure 4.3: Transposition of bedding (solid purple lines) where individual folds have been attenuated by progressive slip (S_2 foliation, dashed red lines) and have ultimately been separated from their hinge zones. View to the south.



Figure 4.4: Cross-sectional view of the symmetrical boudinage of a competent marble (centre of photo, to the right-hand side of the notebook), illustrating a component of vertical stretch of the rocks. The boudinage of competent layers is equally recorded in plan view (see below), and is indicative of chocolate-tablet boudinage and a principal stretch in the horizontal and vertical. View to the NE, the open cut of Grid A in the background.

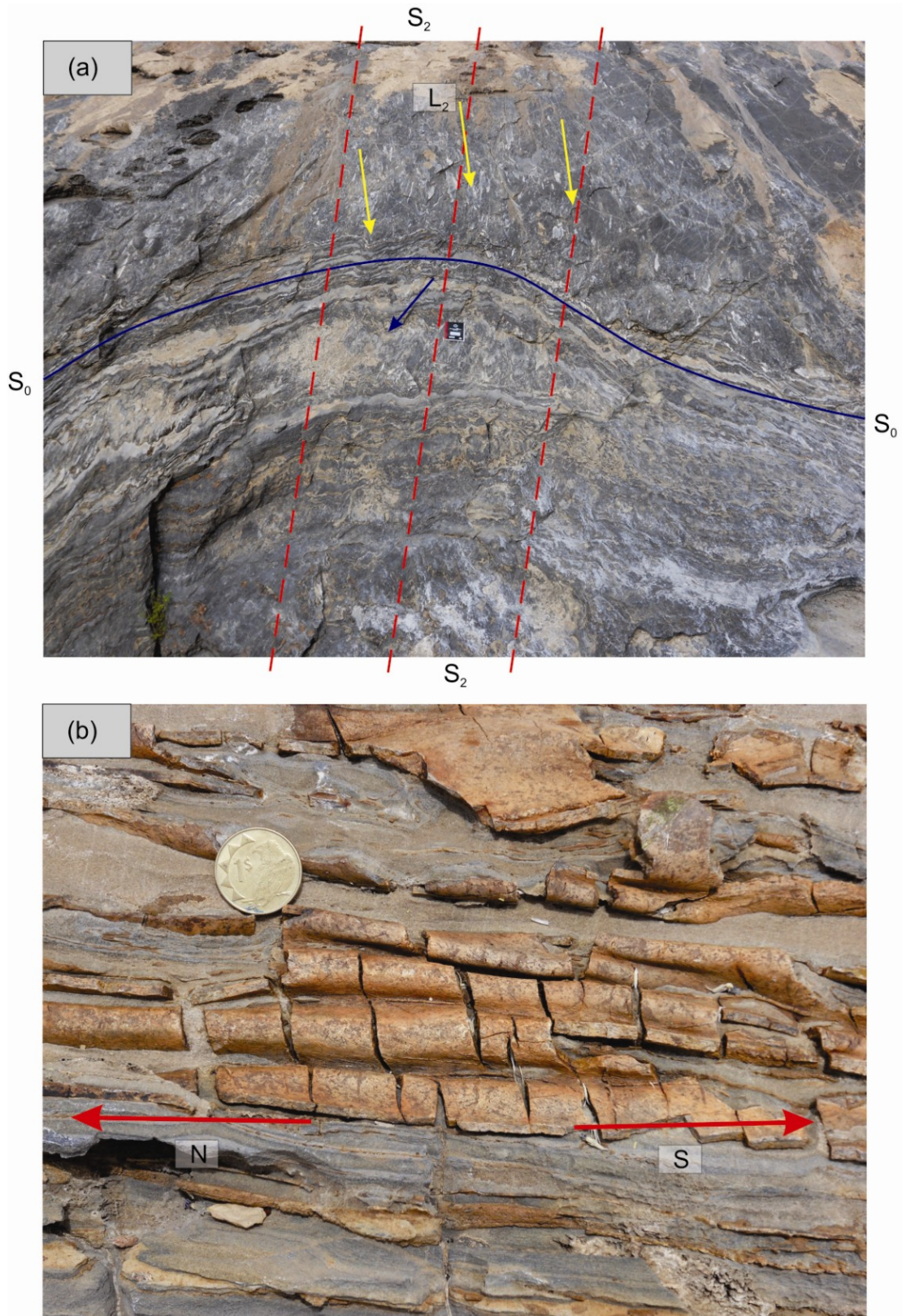


Figure 4.5: (a) Breccia fragments re-orientated into parallelism with L_2 stretch and F_2 fold axes. Purple line shows openly folded S_0 . Breccia fragments (above the purple line) are elongated in the bedding plane and define a L_2 m. Yellow arrows show the plunge direction of the fragments. The long axis of flattened clasts in the plane of bedding defines S_2 (red dashed lines), corresponding to the XY-plane of the finite strain ellipsoid. View is to the SW. (b) Fold-hinge normal tensile fractures separating the F_2 hinges in calc-silicate felses in the south of the study area. The tensile fractures record the subhorizontal stretch during D_2 .

4.5. Folds

4.5.1. F₁ Folds

F₁ folds were not observed in the Karibib Formation in the Navachab synform. The F₁ folds are commonly small-scale (cm- to m-scale) isoclinal, intrafolial folds that refold S₀ and were observed by other studies in the Karibib district (e.g. Kisters et al., 2004; Kitt, 2008), but they are mainly confined to the lower formations (see chapter 2.1.1).

4.5.2. F₂ Folds

The dominant structures in the Karibib district are F₂ folds represented by the Karibib and Usakos domes and the intervening Navachab synform. The folds trend NE to NNE and are doubly plunging at shallow angles to the SW and NE. The first-order domes and intervening synform show half-wavelengths of 3-5 km, with smaller-scale parasitic F₂ folds recorded down to the centimetre scale. The L_{2m} and L_{2i} lineations are parallel to F₂ folds showing shallow plunges to the NE and SW. On a regional-scale, F₂ folds are associated with a major thrust zones exposed to the SE of the Navachab synform, the Mon Repos Thrust Zone (Kisters et al., 2004). This thrust zone can be traced for > 70 km along its NE, slightly-undulating strike, showing moderate- to steep SE dips. The thrust is situated on the shallowly-dipping SE limbs of the Karibib and Usakos domes (Fig. 1.1), recording a top-to-the-NW thrust sense of movement in which basement gneisses of the Abbabis Metamorphic Complex and the Etusis Formation are thrust on top of rocks of the Karibib Formation. The NE trend and top-to-the-NW kinematics along the Mon Repos Thrust Zone are related to the overall NW vergence of the F₂ folds in the Karibib district and Kisters et al. (2004) suggested a D₂ timing for thrusting. The Navachab synform and study area is located in the footwall of the thrust zone and while the NW vergence of F₂ folds is related to the overall D₂ fold-and-thrust tectonics, direct evidence of the thrust in form of e.g. splays is not recorded in the study area.

Figure 4.6 shows a series of cross-sections drawn across the Navachab synform and illustrates the complex nature of the folds observed in the Navachab synform. Figure 4.7 is a formline map of the study area and shows the axial trace of the Navachab synform as well as the orientation of structural elements (Fig. 4.7a-h for bedding (S_0), S_2 and L_2). Five main fold orders identified in the field are shown on the formline map:

- The first fold order has a half-wavelength of ca. 2 km. First-order folds are represented by the Karibib and Usakos domes and the Navachab synform.
- The second fold order with a half-wavelength of up to 1 km is represented by an anticline that extends from the SW of the map through to the NE and the Dernberg locality. This antiform is henceforth referred to as the Dernberg anticlinorium.
- Third-order folds show half-wavelengths of 300-400 m.
- The fourth fold order is of particular interest, since the zoo prospects mostly occur on the limbs of these folds. These folds have a half-wavelength of 175-300 m.
- Fifth-order folds half-wavelengths of 50-150 m.

The Navachab synform has a NE trend in the NE part of the study area. Towards the SW, the axial trace of the synform shows a bifurcation and two smaller synclinal structures are developed, northern and southern synforms, separated by the hinge of the Usakos dome. This bifurcation occurs between the Gecko and Steenbok prospects (Fig. 4.7).

The northern synform is bordered by a second-order antiformal structure in the NW and the first-order hinge of the Usakos dome in the SE. Along its SW strike continuation, the NW antiform forms part of the NW limb of the first-order Usakos dome. Further to the NW, the antiform is bordered by the NW high-strain zone that forms the NW limb of the antiform. Figure 4.7a shows S_0 , S_2 and L_2 for the NW high-strain zone. S_0 and S_2 are subparallel to each other with steep dips and L_2 has a moderate NE-SW plunge and all have similar NE trends. Along strike and towards the NE, the closely folded antiform and related third-order folds grade into the tight- to isoclinal Dernberg anticlinorium (Fig. 4.7).

The SE branch of the Navachab synform is deflected to NNE trends around the broad hinge of the Usakos dome and is, further to the south, truncated by the Mon Repos Thrust Zone (Kisters et al., 2004). This also illustrates the en-echelon nature of regional-scale F_2 folds.

In the south, the average bedding for the Navachab synform generally dips at moderate angles to the east on the western limb of the synform (Fig. 4.7h), but dips are steep- to overturned on the eastern limb (Fig. 4.7f). S_2 is steep and dips ESE to SE. L_{2m} and L_{2i} in the south are doubly plunging to the N- to NNE and south with shallow- to moderate plunges (Fig. 4.7g).

In the NE of the map, bedding on the eastern limb of the Navachab synform shows steep NW dips (Fig. 4.7e). At the Gecko prospect, bedding is steep to the SE as is S_2 (Fig. 4.7b). In the Dernberg anticlinorium, F_2 folds verge to the SE on the eastern limb and to the NW on the western limb of the second-order fold (Fig. 4.7c). S_2 in the NE of the map has a steep, SE dip (Fig. 4.7c,e) and L_2 is moderately doubly plunging to the NE and SW (Fig. 4.7d).

The fold symmetry and interlimb angles change systematically along the axial trace of the Navachab synform. The first- and lower-order folds are commonly asymmetric and NW-verging in the SW of the synform, becoming symmetrical and near-upright towards the NE.

The change in vergence direction is associated with a systematic change in the interlimb angles of F_2 folds from the SW to the NE of the study area. In the SW, corresponding to the hinge of the Usakos dome, the interlimb angles of F_2 folds are open- to close. The only exceptions are tight- to isoclinal folds along the NW D_2 high-strain belt. F_2 folds become progressively tighter towards the NE where fold shapes are commonly tight- to isoclinal. In the area around Dernberg, in the NE of the study area (Fig. 4.6), tightening of the Dernberg anticlinorium and associated lower-order folds has resulted in the doubly-verging nature (NW and SE) of the anticlinorium, resulting in a positive flower-type geometry (Fig. 4.6). This tightening of folds has also resulted in highly-irregular and disharmonic fold shapes. The disharmonic folding arises from the detachment of layers in fold profiles, which is particularly pronounced where dolomitic and calcareous marble are in close proximity.

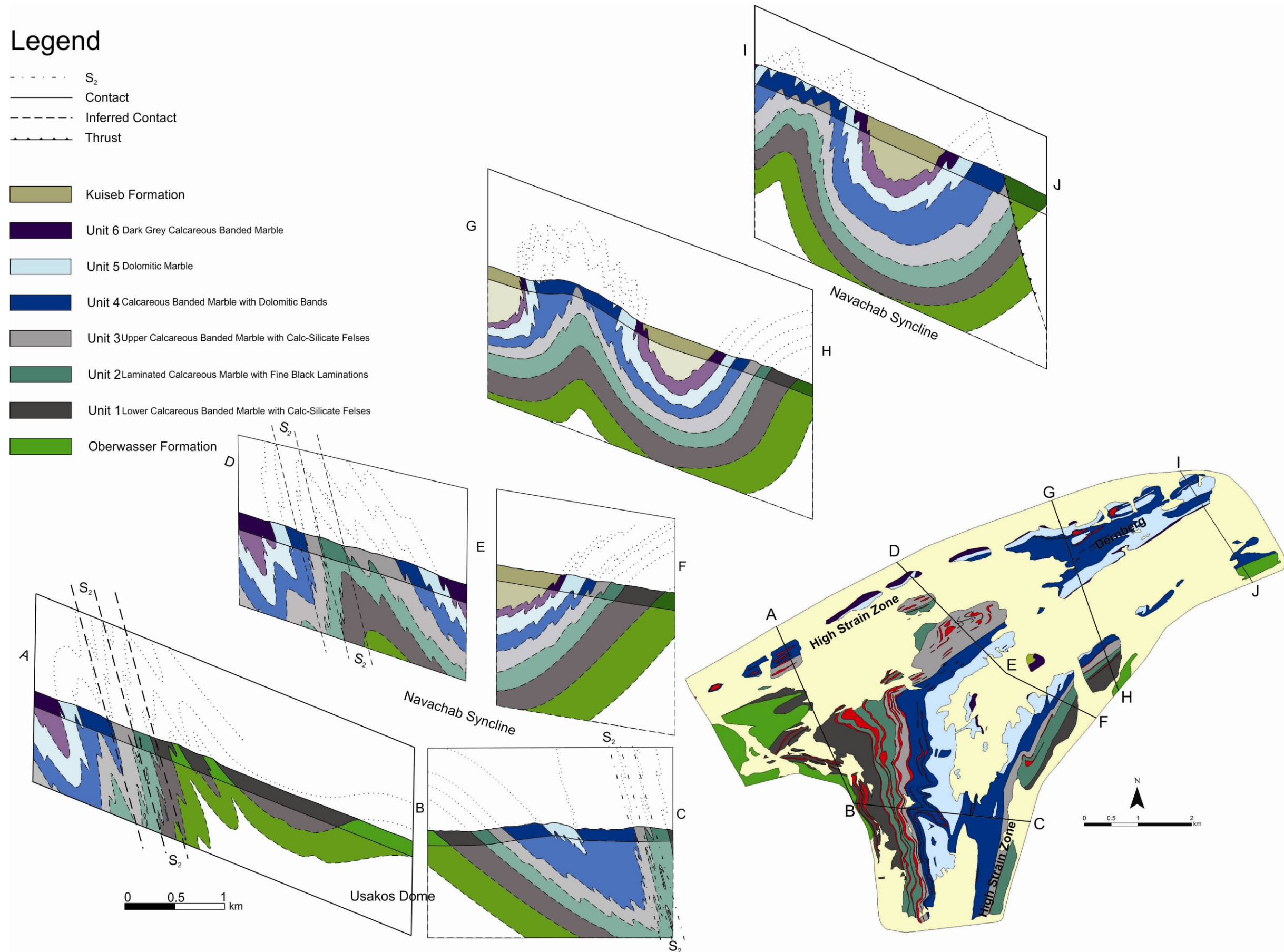


Figure 4.6: Cross-sections across the Navachab synform. Insert shows the locations of cross-sections. F_2 fold symmetry in the Navachab synform changes from asymmetric in the south to symmetrical and near-upright in the NE. The folds have a moderate NW vergence in the south and have a slight SE vergence in the NW. The folds of Dernberg near Grid A (G-H) have a doubly-verging nature, both to the NW and the SE, and give Dernberg positive flower-type geometry. In addition detachment of folds has occurred at Dernberg resulting from the tightening of the Navachab synform. Cross-section B-C shows transposition folds as well as the steep axial planar S_2 foliation.

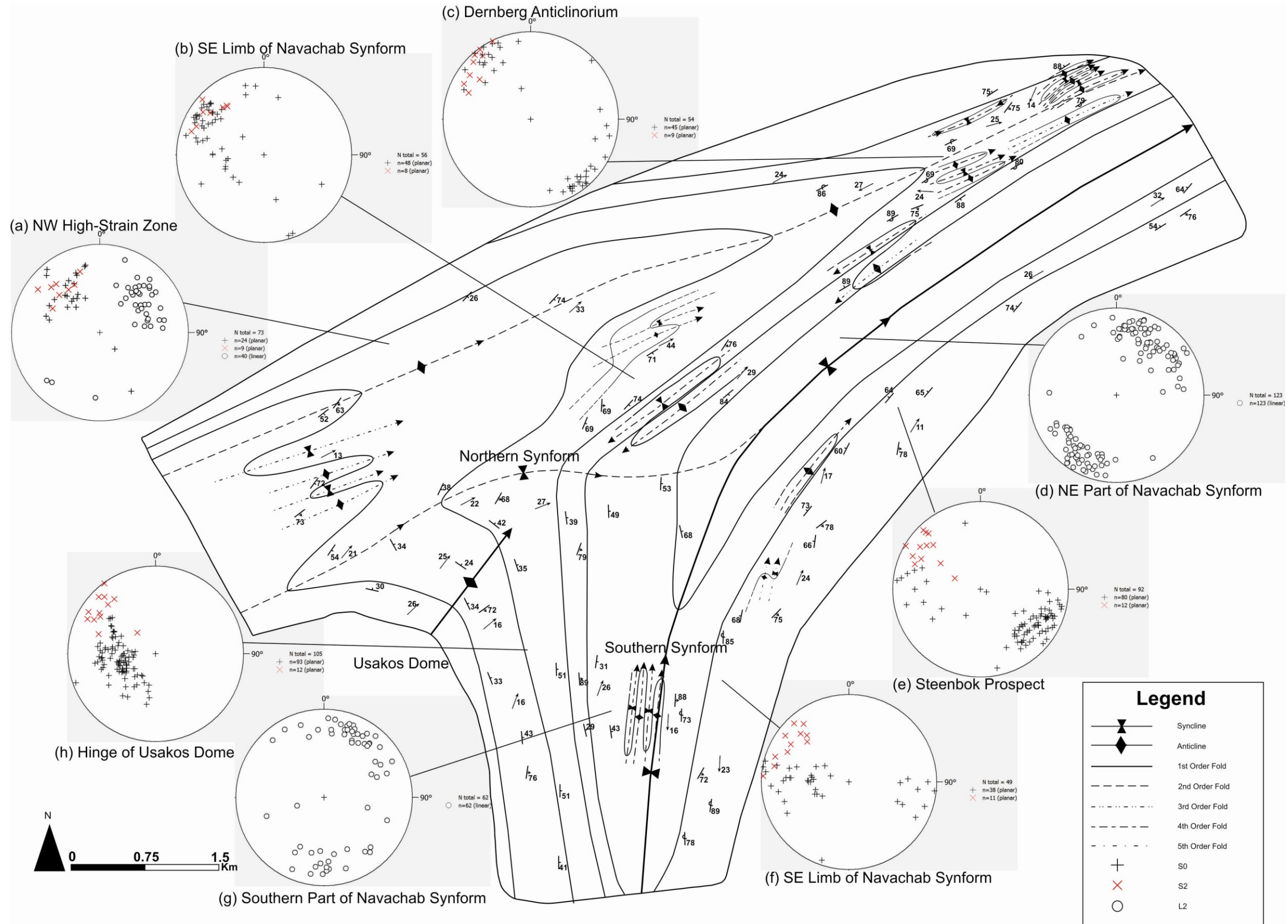


Figure 4.7: Formline map of the Navachab synform showing fold orders and stereoplots for bedding (S_0), axial planar foliation (S_2) and lineation (L_2). All stereoplots are equal area, lower hemisphere projections. (a) Poles to S_0 , S_2 , and L_2 plots for the NW high-strain zone. (b) Poles to S_0 and S_2 for Gecko. (c) Poles to S_0 and S_2 for Dernberg. (d) L_2 for the NE part of the Navachab synform. (e) Poles to S_0 and S_2 for the area from Steenbok Prospect to NE part of study area. (f) Poles to S_0 and S_2 for the SE limb of the Navachab synform. (g) L_2 plots for the southern part of the Navachab synform. (h) Poles to S_0 and S_2 for the area near the hinge of the Usakos dome. S_0 near the Usakos dome (h) has a moderate east dip and steepens and rotates to SE dips in the area around Gecko (b) eventually reaching subvertical dips at Dernberg with a NE strike (c). S_0 along the NW limb of the Karibib dome (f) is steep- to overturned with a NNE to NE strike. S_0 from Steenbok to the NE part of the study area (e) is moderate- to steep and NW dipping. The stereoplots (a,b,c,,e,f,h) show that S_2 is axial planar to the first-order F_2 folds and has an overall NE strike with moderate- to steep dips. L_2 lineations (d,g) are doubly plunging in both the NE and the south and plunge at shallow to moderate to the NNE to NE and to the SSW to SW.

Figure 4.8a illustrates a small-scale example of a detachment fold exposed on the NE wall of the Grid A prospect. The competent dolomitic marble shows rounded F_2 hinges. The concentric- and parallel-type folding is not able to accommodate further tightening of the fold, and less-competent calcareous marble layers display tight cusp- or flame-like shapes that accommodate the strain incompatibilities arising during folding.

This type of detachment folding is also most likely the case on a larger scale, affecting the entire sequence of heterogeneous marbles of the Karibib Formation. However, the actual location of e.g. regional detachment surfaces and resulting fold geometries must remain speculative. Hence, a conservative approach was taken during the construction of the regional cross-sections (Fig. 4.6), assuming rather parallel or only slightly similar fold geometries that are, in fact, unlikely to be realized in the area.

In outcrop and for fourth- and fifth-order folds, fold shapes throughout the Navachab synform are similar, showing thickened hinges and thinned limbs as is to be expected during folding of the marble sequence at or close-to peak amphibolite-facies conditions. Locally, and especially in the area of the Dernberg anticlinorium, fold shapes assume a chevron-type geometry, with sharp hinges and straight limbs. Refolded boudins are common in the area of the Dernberg anticlinorium where calcareous marble is in contact with dolomitic marble with the mechanically softer calcareous marble forming neck folds against the stiffer dolomitic marble. The refolded boudins are typically capped by calcite or quartz-tremolite and, thus, represented originally dilational sites (Fig. 4.8b).

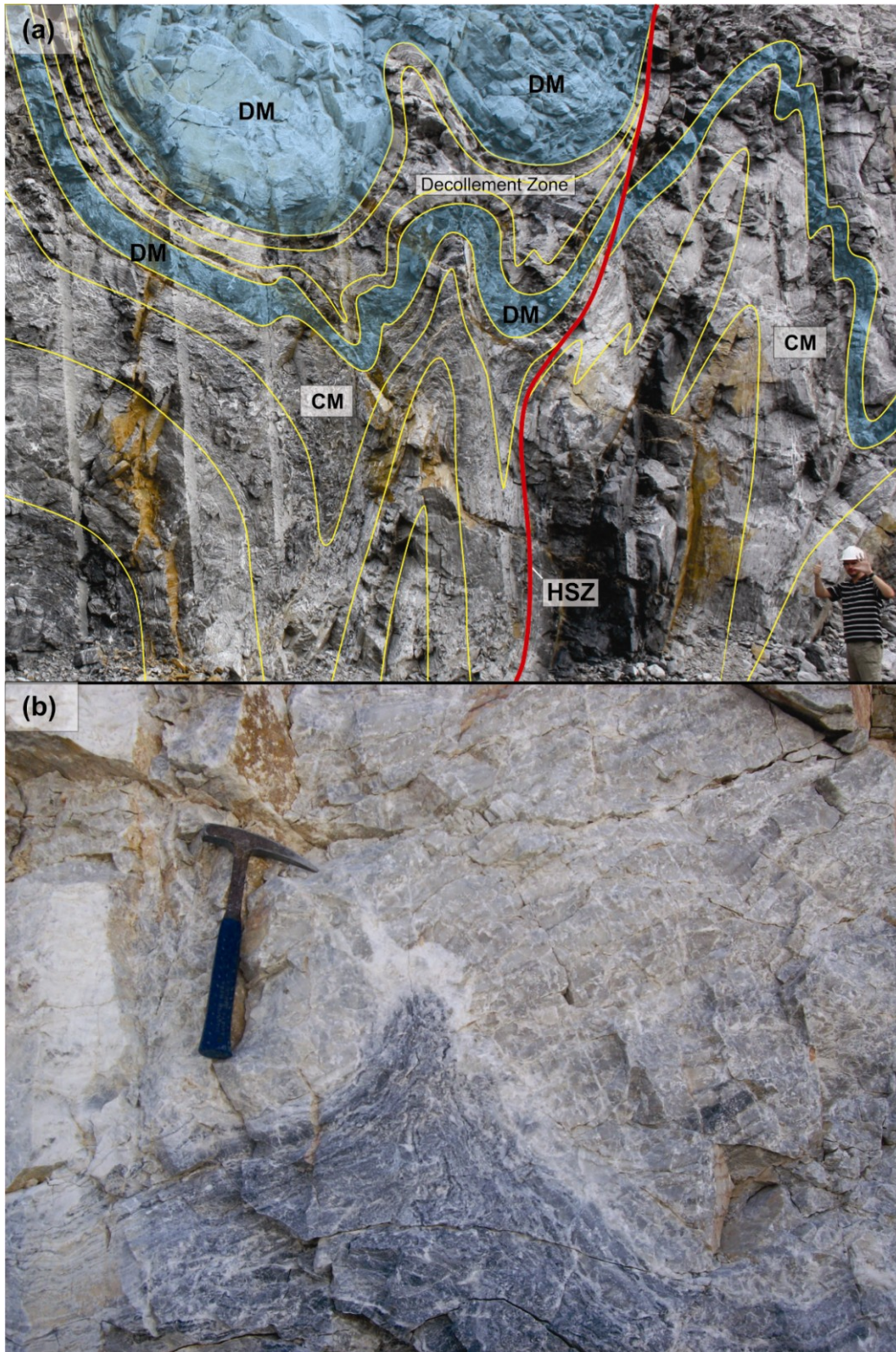


Figure 4.8: (a) Small-scale example of detachment folding; note the author in the lower right hand corner for scale. Detachment of folded layers is the result of different fold shapes in fold profile caused by the marked competence contrasts between dolomitic marble (DM) and calcareous marble (CM). The detachment is achieved by layer-parallel slippage and differential ductile flow of different rocks. View to the NE, NE wall of Grid A. Zoomed in photo of Domain A, Figure 5.9. Bedding annotated by yellow lines. (b) Example of a refolded boudin. The original necking is indicated by the neck fold of calcareous marble (dark) against dolomitic marble (lighter) and the localization of quartz-carbonate veining in the neck. View to the NE, Grid A.

Chapter 5 Geology of the Zoo Prospects

The locations of the four zoo prospects is shown in Figures 1.1 and 3.3. Three of the prospects (Gecko, Grid A, Klipspringer) occur on the NW limb of the Navachab synform (Fig. 3.3), whereas Steenbok occurs on the SE limb that the synform shares with the adjacent Karibib dome. Active mining at Grid A was in effect at the time that the study was undertaken. Surface outcrop at the prospects is good and road cuts for drilling access provide fresh outcrop at all the prospects.

5.1. Lithological Subdivision of Unit 5

All of the zoo prospects are hosted in the dolomitic unit 5 of the Karibib Formation. The detailed mapping of the Gecko prospect allowed for a further subdivision of the dolomitic unit 5 into five subunits. This further lithological subdivision was deemed necessary, since the abundance of quartz veins appears to be controlled by distinct lithologies and lithological packages within unit 5 (Chapter 6). The lithological subdivision is best observed at Gecko, where a complete section through unit 5 is exposed at the SW end of the prospect (Fig. 5.1). This lithological subdivision is also encountered at the other zoo prospects and is therefore of regional extent and significance, although exposure in the other prospects is not be as good as at Gecko.

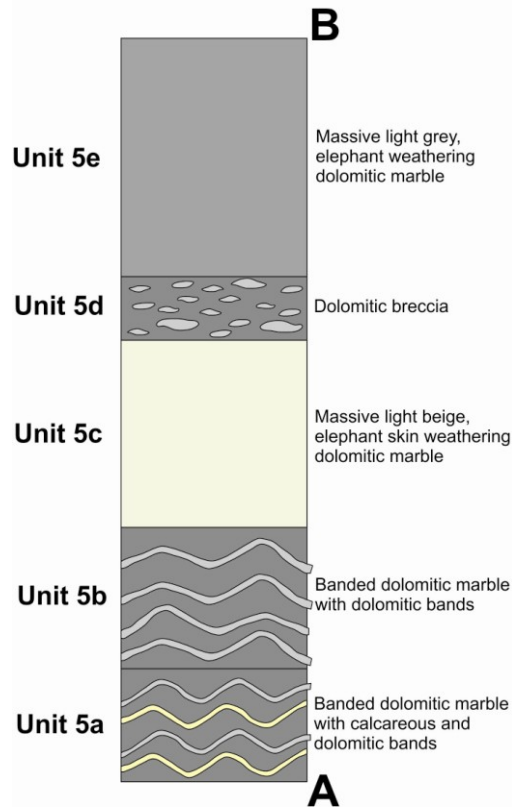


Figure 5.1: Lithological column, from old (bottom) to young (top), showing the subdivision of unit 5 into 5 subunits. Note that unit 5a is not always present. The column is based on a section traversed at the SW end of the Gecko prospect, the location of which is shown as line A-B on Figure 5.3. A and B refer to the location of the section traversed on Figure 5.3. The thickness of the measured section is ca. 260 m.

Unit 5a and 5b are banded dolomitic marbles in the lower parts of unit 5 (Fig. 5.2a). Unit 5a is located at the contact with the upper calcareous marble of unit 4, although it is not always present. The unit consists of interlayered calcareous and dolomitic marble in approximately equal amounts, whereas unit 5b is mostly dolomitic, with only minor calcareous intercalations. The contact between unit 5a and the overlying unit 5b is gradational. Individual bands of dolomitic and calcareous marble are commonly less than 5 cm thick. The dolomitic bands are positively weathering, light-grey to beige and the calcareous bands are white- to cream in colour. The banded dolomitic marble of unit 5a and unit 5b shows intense internal folding. Competence contrasts between adjacent calcareous and dolomitic bands are clearly indicated by different fold styles and geometries. The calcareous marble is tightly folded showing similar-type folds with thickened hinges and thinned fold limbs. The dolomitic marble, in contrast, shows constant thicknesses, parallel fold shapes and tends to form rectangular boudins and carbonate-filled extensional fractures.

Unit 5c is a positively weathering, massive dolomitic marble. On surface, it shows a light-beige elephant-skin weathering (Fig. 5.2b). Internal strain is difficult to record in this unit due to the homogeneous nature of the dolomitic marble and internal folding is difficult to identify.

Unit 5d is a positively-weathering dolomitic sedimentary breccia (Fig. 5.2c). The breccia is matrix supported and the majority of the fragments are dolomitic in composition, similar to the matrix of the breccias, so that clasts are, on weathered surfaces, difficult to identify. As a result, this unit appears similar in outcrop to the underlying dolomitic unit 5c. Fragments are commonly angular, ranging in size from merely a few centimetres up to 50 cm. The long axis of fragments is orientated parallel to L_2 and F_2 fold axes. Light- and dark-grey calcareous clasts also occur, but are subordinate. Where exposed, contacts between Unit 5c and unit 5d are sharp.

Unit 5e forms the upper contact with calcareous marbles of the overlying unit 6 (chapter 4). The unit is similar to unit 5c in that it is massive with an elephant-skin weathering (Fig. 5.2d). It has a light-grey to steel-grey colour. As with unit 5c, the homogenous nature of the dolomitic marble makes it hard to identify internal strain. The unit has a sharp contact with unit 5d and the overlying calcareous marble of unit 6.

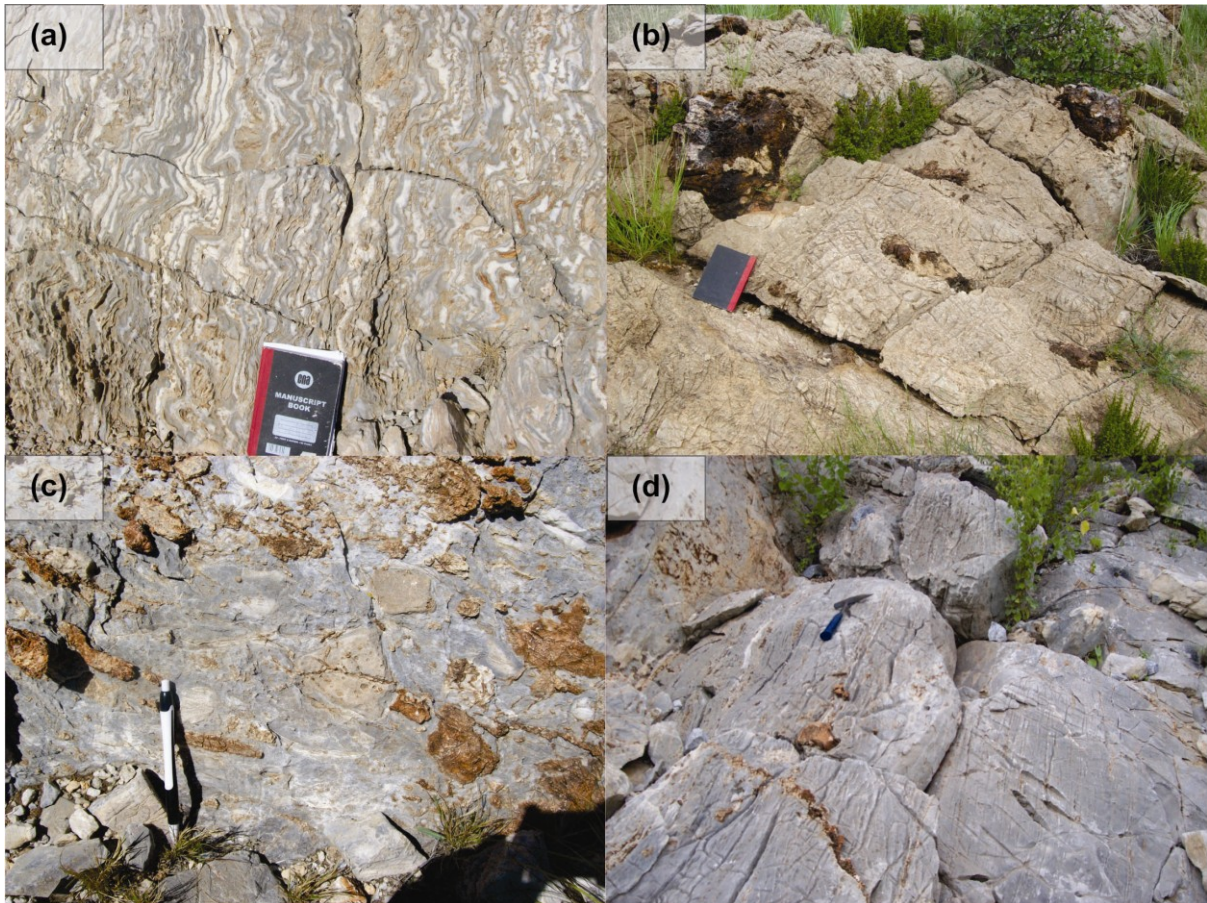


Figure 5.2: Outcrop appearance of the subdivision of unit 5. (a) View to the SW of banded dolomitic marble (units 5a and 5b) showing small-scale internal folding. Calcareous marble bands are light-cream to white in colour and the dolomitic bands are grey to beige. (b) View to the NW of a massive, beige dolomitic marble of unit 5c. The homogeneous nature of the massive dolomitic marble makes it difficult to record strain. (c) View to the SW of dolomitic breccias of unit 5d. The fragments in the breccia are slightly lighter grey than the matrix. Note the preferred orientation of the fragments defining L_{2m} . (d) View to the SW of light-grey weathering, massive dolomitic marble of unit 5e.

5.2. Gecko Prospect

The Gecko prospect is located on the NW limb of the Navachab synform (Fig. 3.2). Figure 5.3 is a geological map of the Gecko prospect and shows the location of the lithostratigraphic column that forms the basis of the subdivision of unit 5 (Fig. 5.1). Bedding at Gecko is steep to the SE with a NE strike (Fig. 5.4a). The two main fold structures underlying the prospect form a fifth-order antiform-synform pair. Parasitic sixth- and seventh- order folds are particularly well developed along the contact between units 5 and unit 6 (Fig. 5.3 and 5.5), whereas the central and lower parts of unit 5 remain largely unaffected by the sixth-order

folding. This highlights the role of rheological contrasts for the formation of parasitic F_2 folds in the Navachab synform. The thickness of the dolomitic marble at Gecko thins from the SW towards the NE. This is as a result of the fold closure of a fourth-order antiform. The thickness of unit 5a decreases from ca. 30 m in the SW to ca. 15 m in the NE, and unit 5b is ca. 40 m thick. Unit 5c thins from ca. 70 m in the SW to ca. 30 m in the NE (Fig. 5.3). The thickness of unit 5d is ca. 15 m. The true thickness of unit 5e is unknown due to the presence of numerous lower-order parasitic folds (sixth- and seventh- order), but the apparent thickness is 180 m. S_2 is not observed in the dolomitic marble. In general, folds show shallow- to moderate SW plunges. L_2 lineations and fold axes measured at Gecko are shown on Figure 5.4b, illustrating the parallelism of the two elements. Figure 5.5 is a S_0 formline map of Gecko.

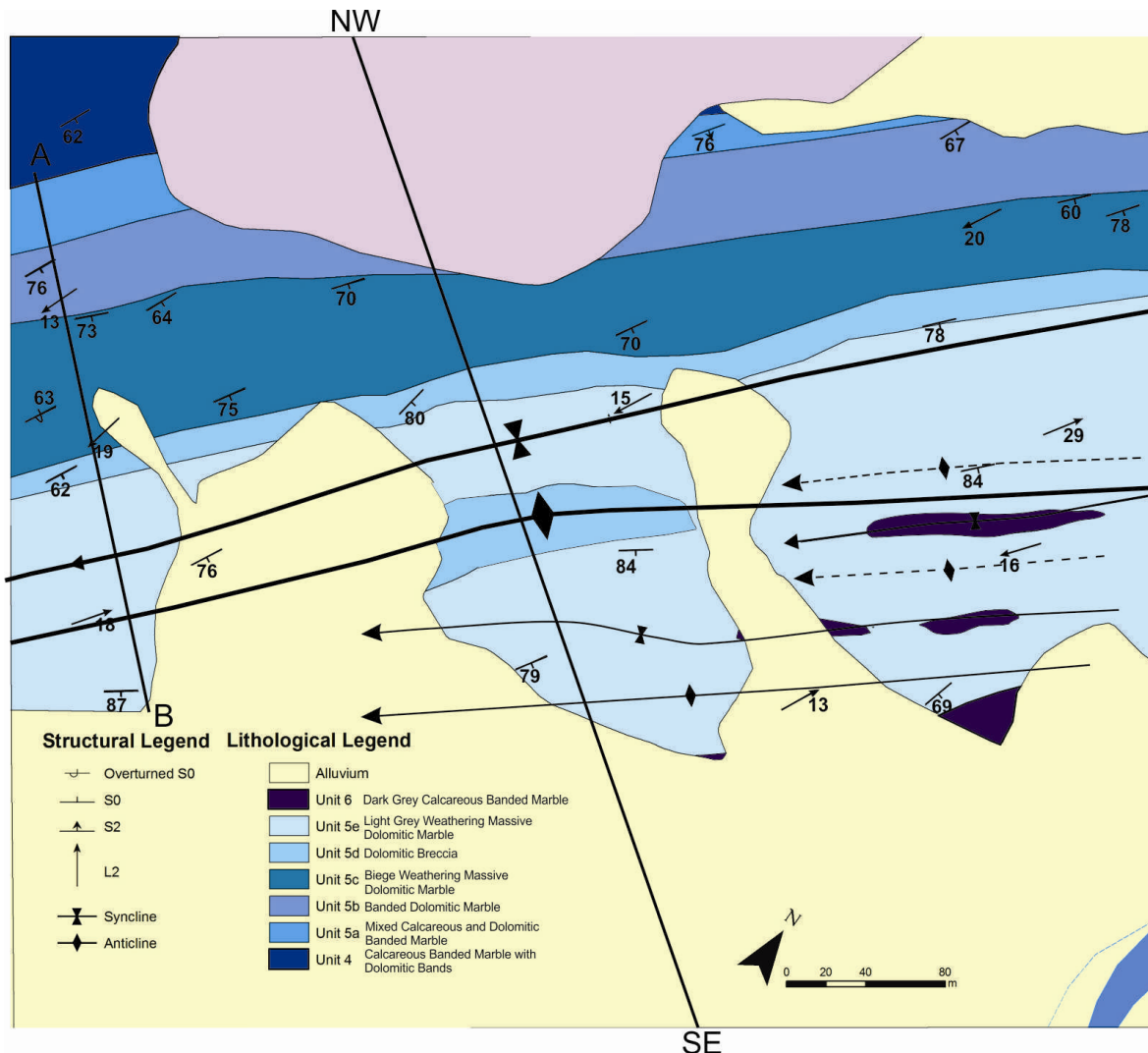


Figure 5.3: Geological map for the Gecko prospect. Dips for S_0 and S_2 are steep, both with a NE strike (Fig. 5.4a). Plunges of folds are shallow to the SW (Fig. 5.4b) and are shown as arrow heads of fold axial traces. The NW-SE line indicates the location of the cross-section drawn across the Gecko prospect (Fig. 5.8b) and the line A-B is the location of figure 5.1.

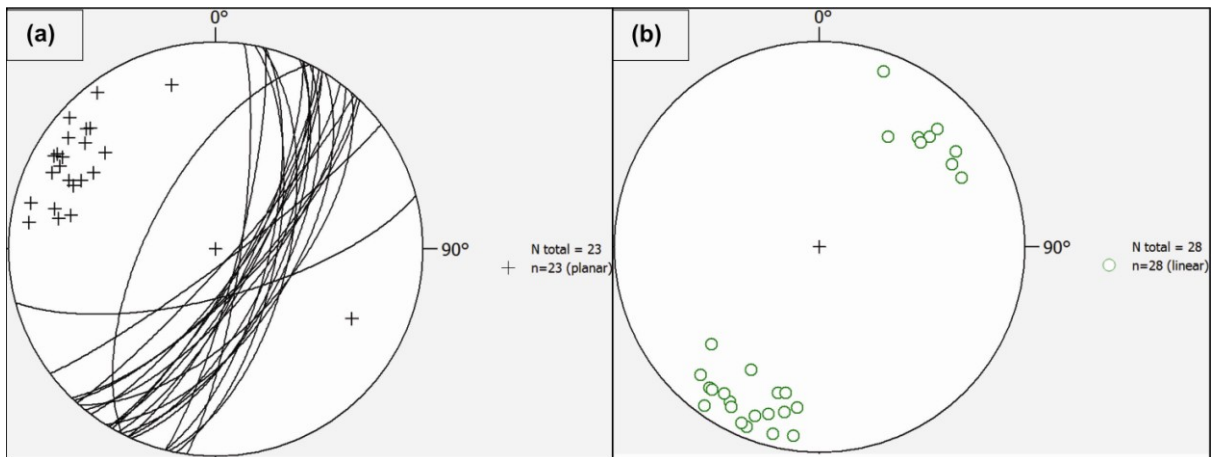


Figure 5.4: (a) Stereoplot for S_0 at Gecko. Dips are steep- to overturned with a NE strike (poles (+) and great circles to S_0). (b) Stereoplot for L_2 and fold axes at Gecko. Plunges are moderate- to shallow and doubly plunging to the NE and SW.

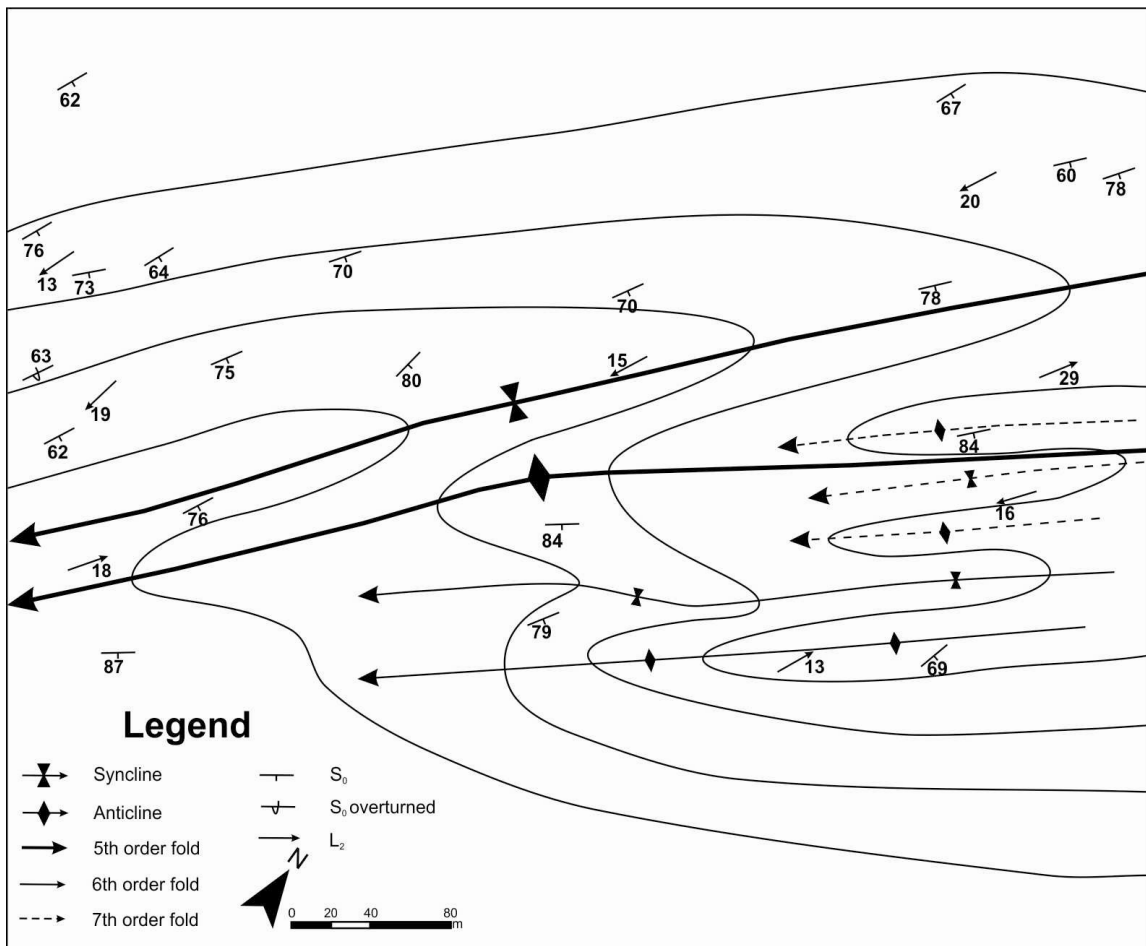


Figure 5.5: Formline map of Gecko, showing the presence of a fifth-order antiform-synform pair and sixth- and seventh-order parasitic folds. Note that folding mainly affects the contact zone between unit 5 and unit 6 (compare Fig. 5.3). Legend for fold orders is shown on Figure 5.5.

Figure 5.6a is a view to the SW taken at the Gecko prospect showing the subdivision of the dolomitic marble (Unit 5) into 5 subunits and also the location of the two zones of main quartz veining and mineralisation. The two zones of main quartz veining and mineralisation

occur at the contact between unit 5e and unit 6, and at the contact of unit 5c and unit 5d. Figure 5.6b is a cross-section drawn across Gecko (indicated on Fig. 5.3), also illustrating the asymmetry of the folds. The folds are NW vergent and have thickened hinges, i.e. a similar fold shape. The main mineralisation and prospect occurs on the SE limb of a fourth-order antiform, but the individual zones of mineralisation are inferred to be localized on the limbs of a sixth-order antiform and fifth order-synform for Zone 1 and Zone 2 respectively.

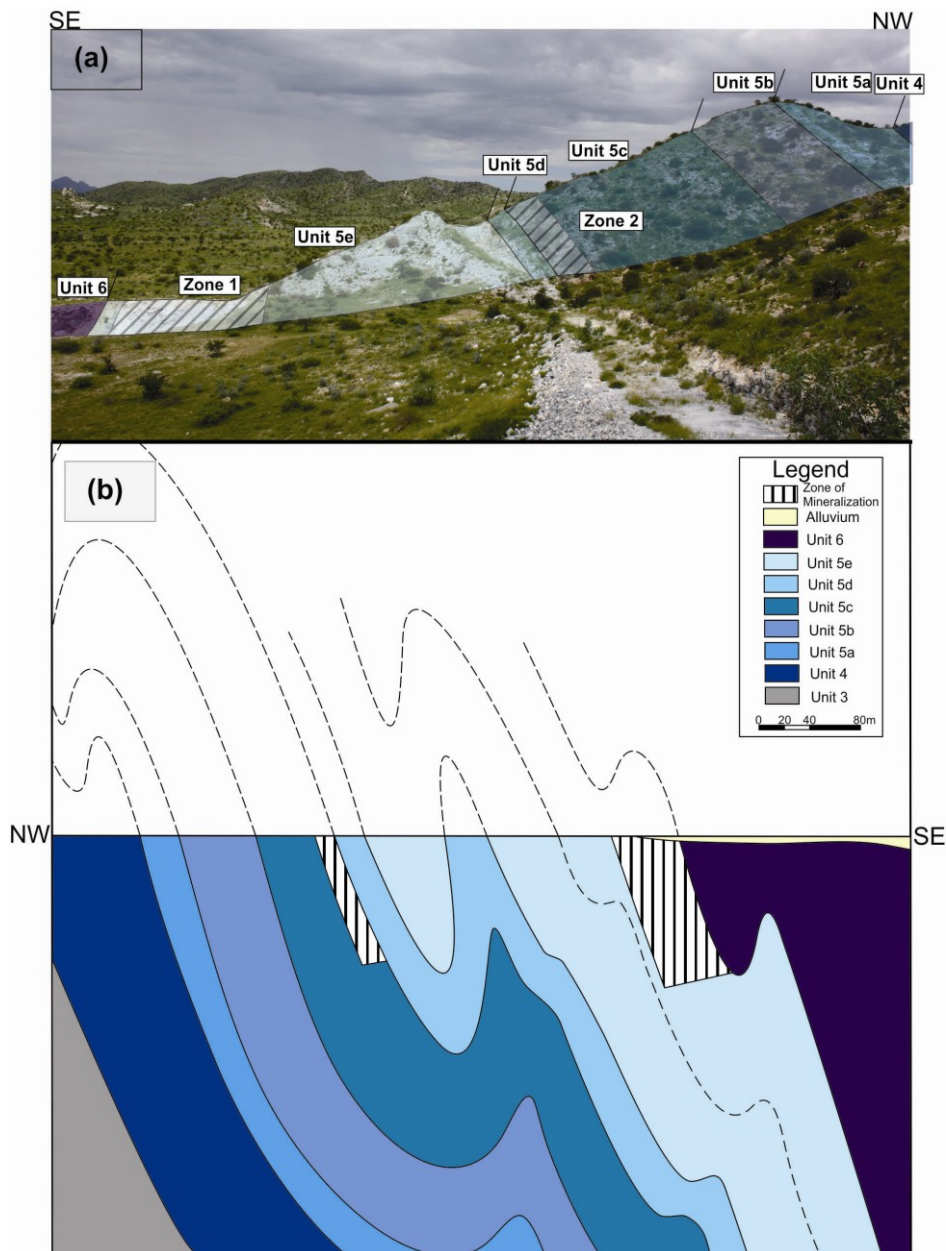


Figure 5.6: (a) Cross-sectional view (to the SW) of the Gecko prospect showing the subdivision of unit 5 and the location of the two zones of mineralisation at the contact of unit 5c/5d and unit 5e/6. Note that the width of the photo is 200m and the dip of strata is, on average, 134/73°. (b) Cross-section through the Gecko prospect, looking NE. Location of cross-section is shown on Figure 5.3. The prospect occurs on the SE limb of a fourth-order antiform and the individual zones of mineralisation are inferred to occur on the NW limb of a sixth-order synform.

5.3. Grid A Open-Pit

The Grid A open-pit is located along the NW limb of the Navachab synform (Fig. 3.2). At the time this study was undertaken, mining at Grid A was already in progress. As such, a geological map for the prospect could not be completed, but the pit walls provided excellent 3D exposure and detailed cross-sections and longitudinal-sections through the mineralized zone and wall rocks that led to a better understanding of the controls of the mineralisation. Figure 5.7a shows the orientation of S_0 and S_2 and Figure 5.7b is a stereoplot for L_2 . S_0 at Grid A is steep- to overturned and S_2 is steep, both having a NE strike. The dolomitic marble at Grid A is that of unit 5b. The other sub-units are not observed at Grid A so that unit 5b is in direct contact with the calcareous marbles of the underlying unit 4 and overlying unit 6. In places, thin (<1 m thick) layers of massive dolomitic marble are observed. F_2 fold axes and L_2 mainly plunge shallowly to the SW, although L_2 plunges are locally highly variable (see below). F_2 folds at Grid A verge to the NW and SE, with the majority of the folds verging to the SE. Fold geometries are highly variable. Fold shapes are mainly similar, with thickened, rounded hinges, but chevron folds with angular hinges are also common. Detachment folds and highly irregular fold profiles are observed particularly near the contact of dolomitic marble and calcareous marble (Fig. 4.8a and Fig. 5.9).

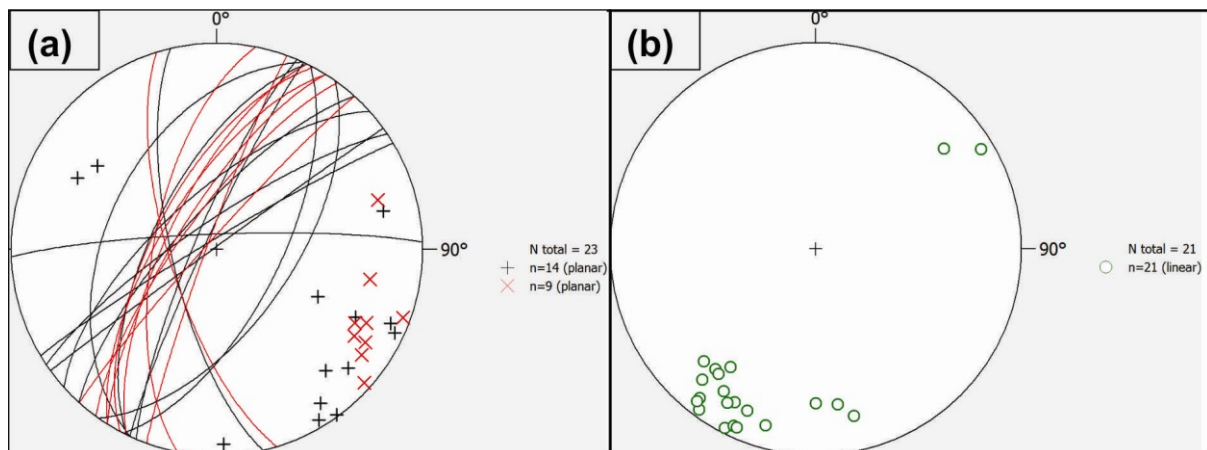


Figure 5.7: (a) Stereoplot for S_0 and S_2 at Grid A. S_0 (black +) is steep- to overturned and S_2 (red X) is steep, both have a NE strike. (b) Stereoplot for L_2 . Lineations at Grid A show moderate plunges to the SW and NE.

Figure 5.8a represents a view of the NE wall of the Grid A pit and the accompanying Figure 5.8b is a geological cross-section of this field of view, including bedding formlines. The section illustrates the presence of a tight, piercement-type fold of the stratigraphically overlying calcareous marble unit 6 into dolomitic marbles of unit 5. Figure 5.9 also shows the location of a 90 m cross-sectional panel mapped across the NE wall of Grid A. The mapping of this panel documents the disharmonic F_2 folding at the contact between unit 5 and unit 6. The overall SE vergence of folds is explained by the location of Grid A on the overturned, NW-dipping limb of the Dernberg anticlinorium. The disharmonic folding originates particularly at the interface between calcareous and dolomitic marbles and the formation of detachments is the result from the highly different fold shapes and fold amplitudes and wavelengths (parallel, close- to tight in dolomitic marble with amplitudes and half-wavelengths > 5 m; similar and tight-to isoclinal in calcareous marble, with amplitudes > 10 m, but wavelengths down to 50 cm). The tight and similar fold geometries in calcareous marble may eventually take on a chevron-like fold shape. Anastomosing S_2 -parallel high-strain zones separate folded domains. The high-strain zones have been observed on and develop from the highly attenuated, commonly overturned limbs of folds. Individual shear zones are only 5-15 cm wide and are characterized by highly-foliated marbles, the attenuation of bedding and a drag of bedding into the shear zones. Where exposed, the planes of the shear zones contain a prominent stretching lineation with highly variable plunges, ranging in orientation from subhorizontal to down-dip. Displacement on the shear zones does not exceed a few metres at most. The shear zones show mostly a top-to-the-SE sense of movement. Closer towards the contact of dolomitic marble with unit 6 in the east, top-to-the-NW kinematics are more pronounced.

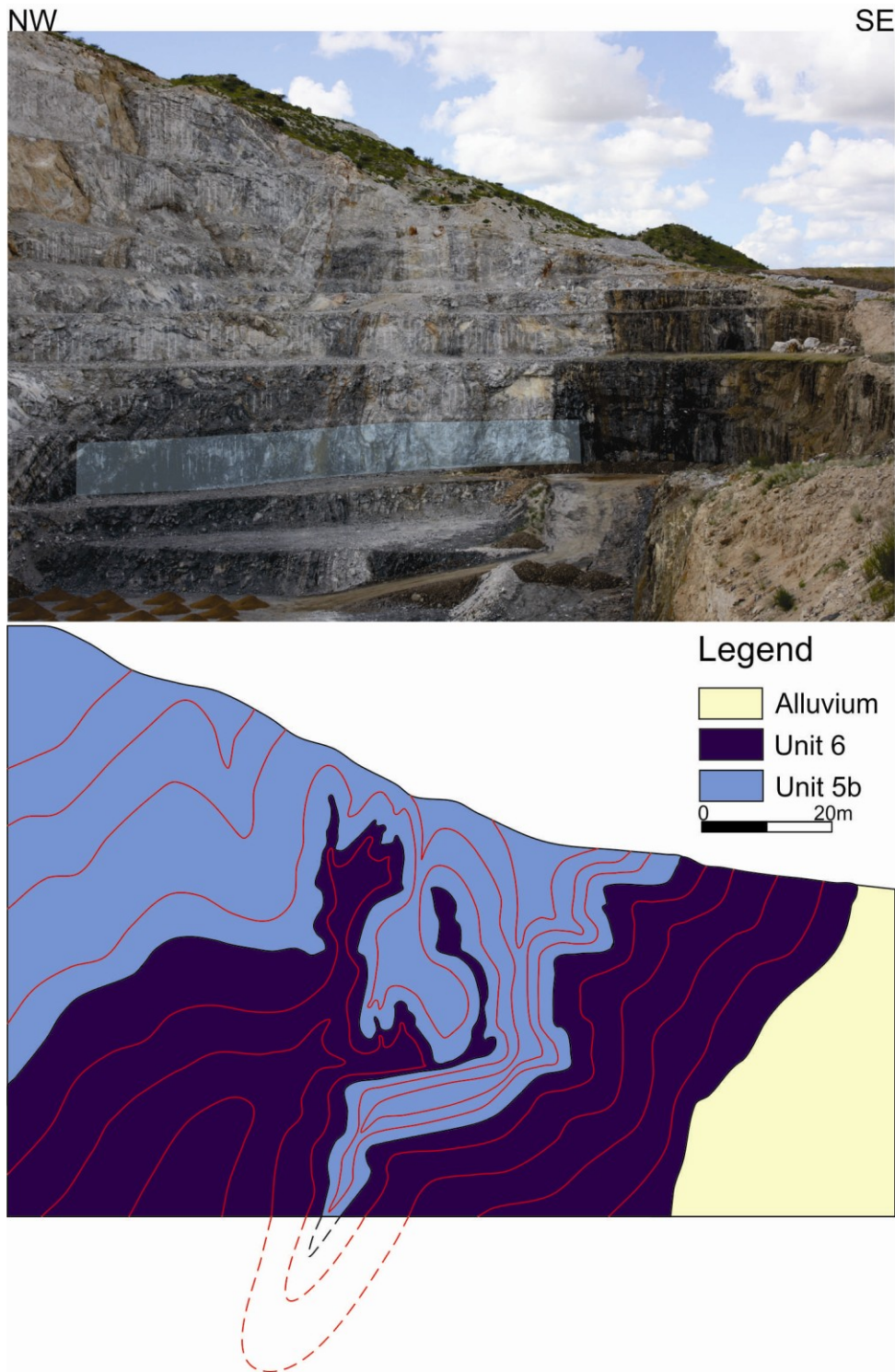


Figure 5.8: (a) Photo of Grid A, looking NE. Light blue shaded area is the location of Figure 5.9. (b) Cross-section of the NE pit wall of Grid A based on the detailed mapping of panels shown in (a). Red lines indicate formlines of S_0 . This cross-section illustrates that the wall-rock geology of Grid A is made up of an antiform-synform pair in structurally overturned strata. Folding occurs along the contact between the stratigraphically underlying, but structurally overlying dolomitic marble of unit 5 (light blue) against the stratigraphically higher calcareous marbles of unit 6. The central antiform represents an antiformal syncline of calcareous marble (unit 6) that is infolded with the unit 5 dolomitic marble. Note the flame- or piercement-like geometry of folds as a result of the competence contrast between the marble units.

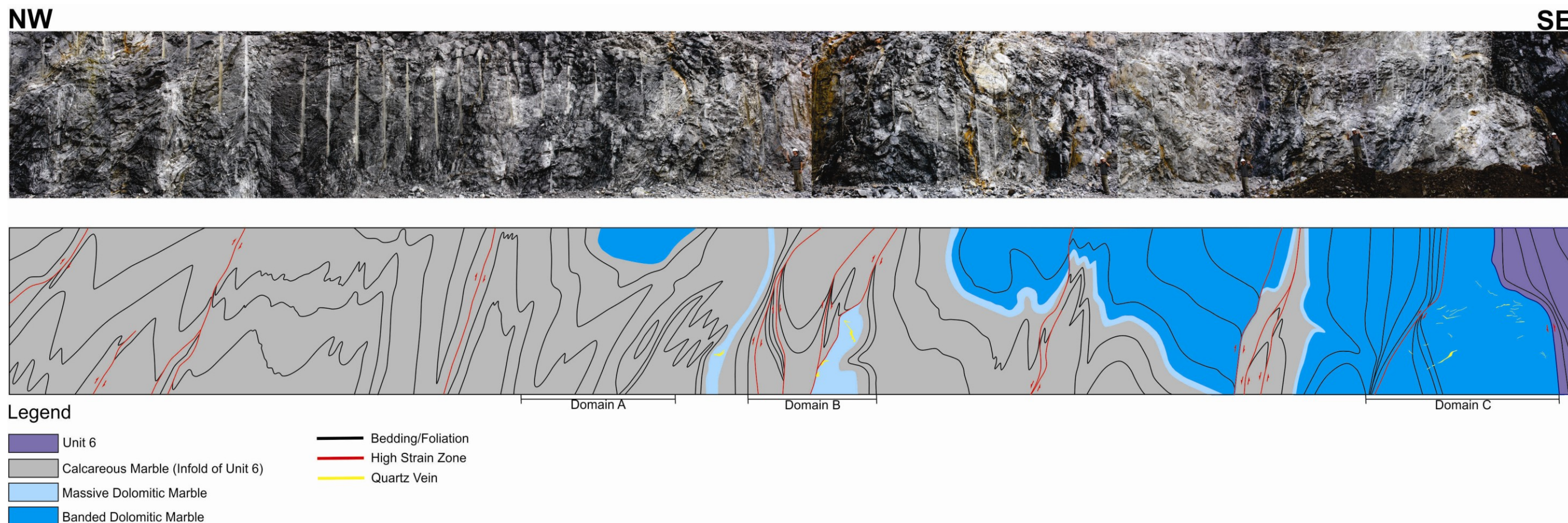


Figure 5.9: 90 m photo panel (above) and cross-section (below) across the central parts of the Grid A Prospect, NE wall (see Fig. 5.8 for location). The panel illustrates (1) the strongly disharmonic folding in the Karibib Formation that arises from competence contrasts between different marble units (black lines are S_0 formlines); (2) the mullion- or piercement-type folding of the incompetent calcareous marbles against dolomitic marbles; (3) the nucleation of small-scale, anastomosing, S_2 -parallel shear zones (red lines) particularly along the overturned limbs of F_2 folds. The high-strain zones show both a top-to- the SE and NW sense of displacement together with an oblique component, indicated by highly variable lineation patterns on foliation planes; and (4) the presence of seemingly allochthonous blocks and slivers of dolomitic marble (light blue) intercalated with the calcareous marble of unit 6. F_2 folds show an overall SE vergence and form part of the eastern limb of the doubly-verging Dernberg anticlinorium (Refer to Figure 4.6). Domain A is a good example of detachment folding with the dolomitic marble having a rounded fold shape and the calcareous marble having a chevron shape (Fig. 4.8a). Note that the folds in domain A are NE-verging. Domain B illustrates the enveloping nature of the shear zones (chapter 6.6). The shear zones mostly have top-to-the-east movement, but top-to-the-west do occur. Domain C is a dilational jog that occurs at the contact of the dolomitic marble and unit 6 resulting from shearing and folding and is explained in chapter 6.6.

5.4. Klipspringer Prospect

Figure 5.10 is a geological map of the Klipspringer prospect. The subdivision of unit 5 is similar to that of Gecko with the exception that unit 5a is not present at Klipspringer and unit 5b is in direct contact with unit 4. S₀ is steep- to overturned and S₂ is steep, and both have a NE strike (Fig. 5.11a). L₂ and F₂ fold axes at Klipspringer are shallow and doubly plunging to the ENE and WSW (Fig 5.11b). The doubly-plunging nature of the folds is not only indicated by variations in the plunge of lineations, but also by the closure pattern of marble units around fold hinges in map view (Fig. 5.10). F₂ folds verge to the NW and have similar fold shapes. As with Gecko, the fragments in the dolomitic breccia at Klipspringer have a preferred orientation parallel to L₂ and in the S₂ foliation. Figure 5.12 is a formline map of Klipspringer. Unlike Gecko, the folds at Klipspringer occur in all subunits of unit 5 and are not confined to the upper subunits. The prospect occurs along the SE limb of a fourth-order antiform and the zones of increased quartz veining and associated mineralisation occur on the NW limbs of fifth- and sixth- order folds (Fig. 5.13). Near the contact of unit 5e and unit 6, there is a doubly-plunging fifth- order synform-antiform pair. The intense folding observed at Klipspringer makes it difficult to determine the true thickness of the subunits. At its thinnest, unit 5b is 18 m, unit 5c is 20 m, unit 5d is 6 m, and unit 5e is 24 m.

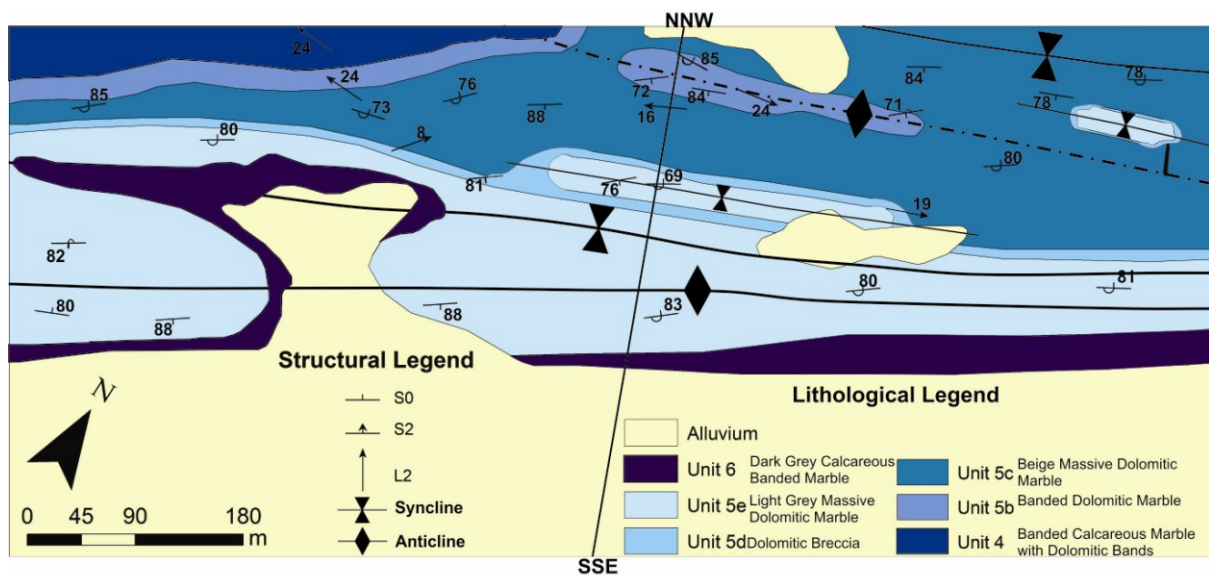


Figure 5.10: Geological map of Klipspringer. Dip of S₀ at Klipspringer is steep- to overturned with a NE strike. The folds at Klipspringer are doubly plunging and shallow to the NE and/or SW. Note the closure patterns of marble units around fold hinges. Location of the cross-section drawn across Klipspringer (Fig. 5.13) is shown on the map. Refer to Figure 5.12 for legend to fold orders.

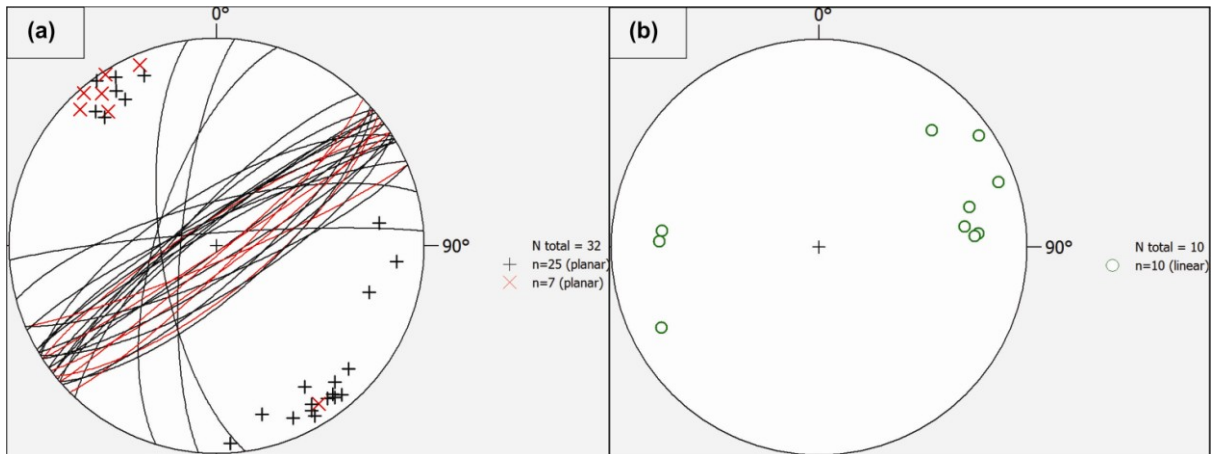


Figure 5.11: (a) Stereoplot for S_0 and S_2 at Klipspringer. S_0 (black +) at Klipspringer is steep- to overturned and S_2 (red X) is subvertical, both have a NE strike. (b) Stereoplot for L_2 at Klipspringer, illustrating the moderate doubly-plunging orientation of the lineation to the ENE and WSW.

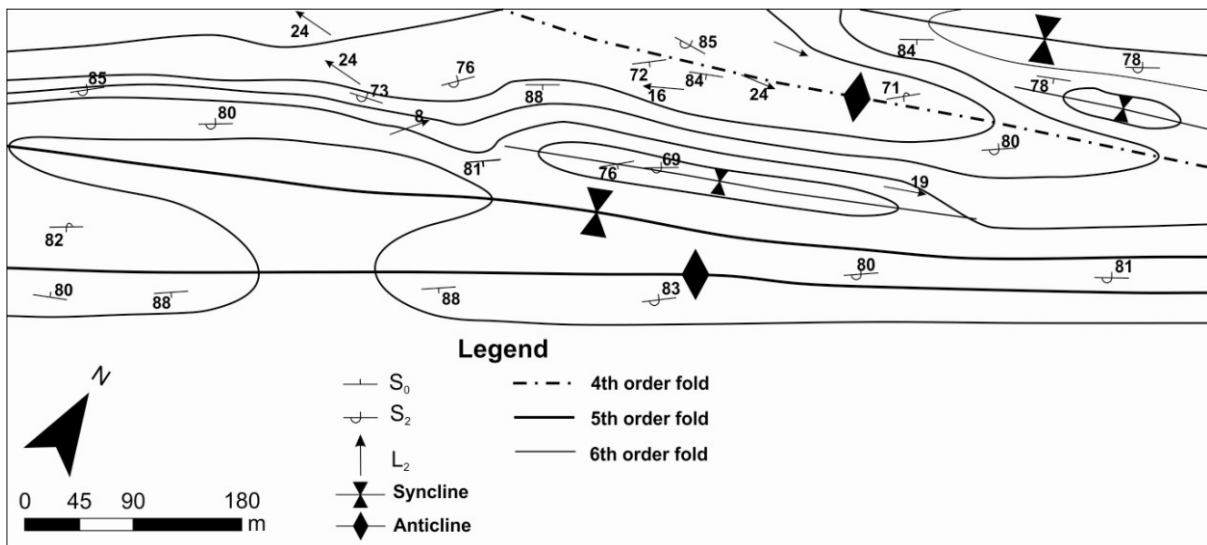


Figure 5.12: Formline map of the Klipspringer prospect. The formline map shows that the F_2 folds at Klipspringer occur in all subunits of unit 5, which is in contrast to Gecko. The main fold at Klipspringer is a fourth-order antiform. Near the contact of unit 5e and unit 6 is a fifth-order synform-antiform pair (refer to Figure 5.10).

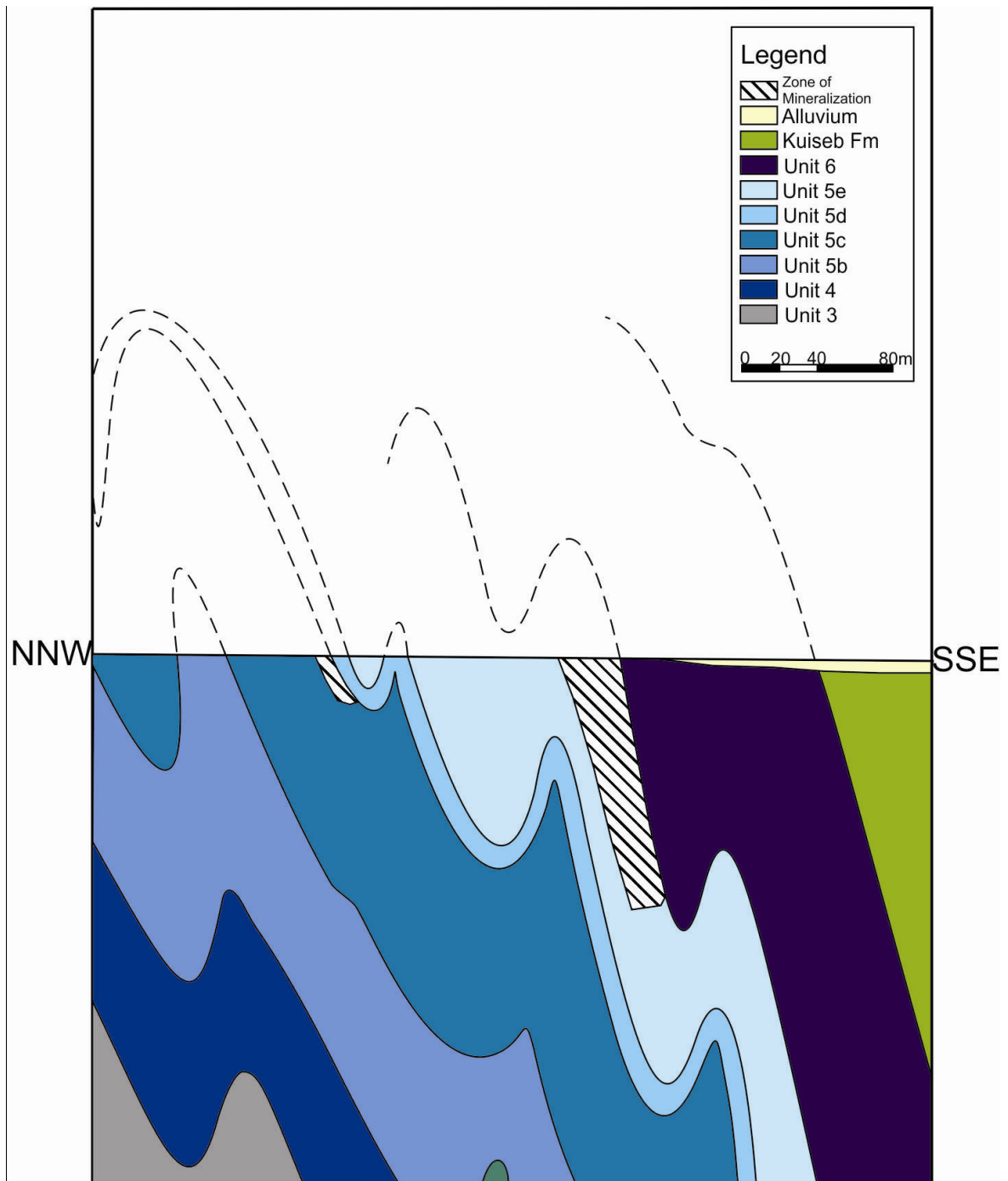


Figure 5.13: Cross-section across the Klipspringer prospect. The zones of increased quartz veining and mineralisation occur on the SE limb of a fourth-order antiform of the NW limb of the Navachab synform. On a more local scale, quartz veining seems to be controlled by the NW limbs of sixth-order folds.

5.5. Steenbok

The Steenbok prospect is smaller than the other three prospects and it occurs on the SE limb of the Navachab synform to the immediate north of the main open pit (Fig. 3.2). S_0 at Steenbok is steep- to overturned with a NNE strike (Figs. 5.14 and 5.15a). L_2 and F_2 fold axes at Steenbok are shallow and doubly plunging to the NNE and SSW (Fig. 5.15b). Steenbok lacks the well-developed subdivision of unit 5 that is observed at e.g. Gecko and Klipspringer. Instead, the dolomitic marble at Steenbok appears massive and is inferred to be unit 5e. However, along the contact between the dolomitic marbles of unit 5 and underlying calcareous marbles of unit 4, a thin, only up to 1 m wide horizon of banded dolomitic marble occurs, which may correlate with units 5a or unit 5b developed on the NW limb of the Navachab synform. The true thickness of unit 5e is not possible to determine at Steenbok due to the presence of sixth- and seven-order F_2 folds in which the marbles are duplicated. The massive nature of the dolomitic marble does not record strain and as such folding within the dolomitic marble is difficult to observe, however, the close proximity of the dolomitic marble to the calcareous marble (unit 4) allowed for the identification of the folds at the prospect. A granitic dyke occurs in the vicinity of the prospect and is shown on the geological map.

Quartz veining is centred around a fifth-order synform-antiform pair with lower order (sixth- and seventh- order) parasitic folds on the limbs (Fig. 5.16). There is only one zone of increased quartz veining and associated mineralisation confined to the folded contact between the dolomitic unit 5 and calcareous marbles of unit 6. This probably reflects the homogeneity of unit 5 and the lack of the lithological contrasts within the unit. The folds at Steenbok verge to the NW, show similar fold shapes and mostly plunge shallowly to the NNE. Figure 5.17 is a cross-section across Steenbok and shows that the zone of mineralisation occurs on the SE limb of the Navachab synform and locally occurs on the NE limb of a fifth-order antiform.

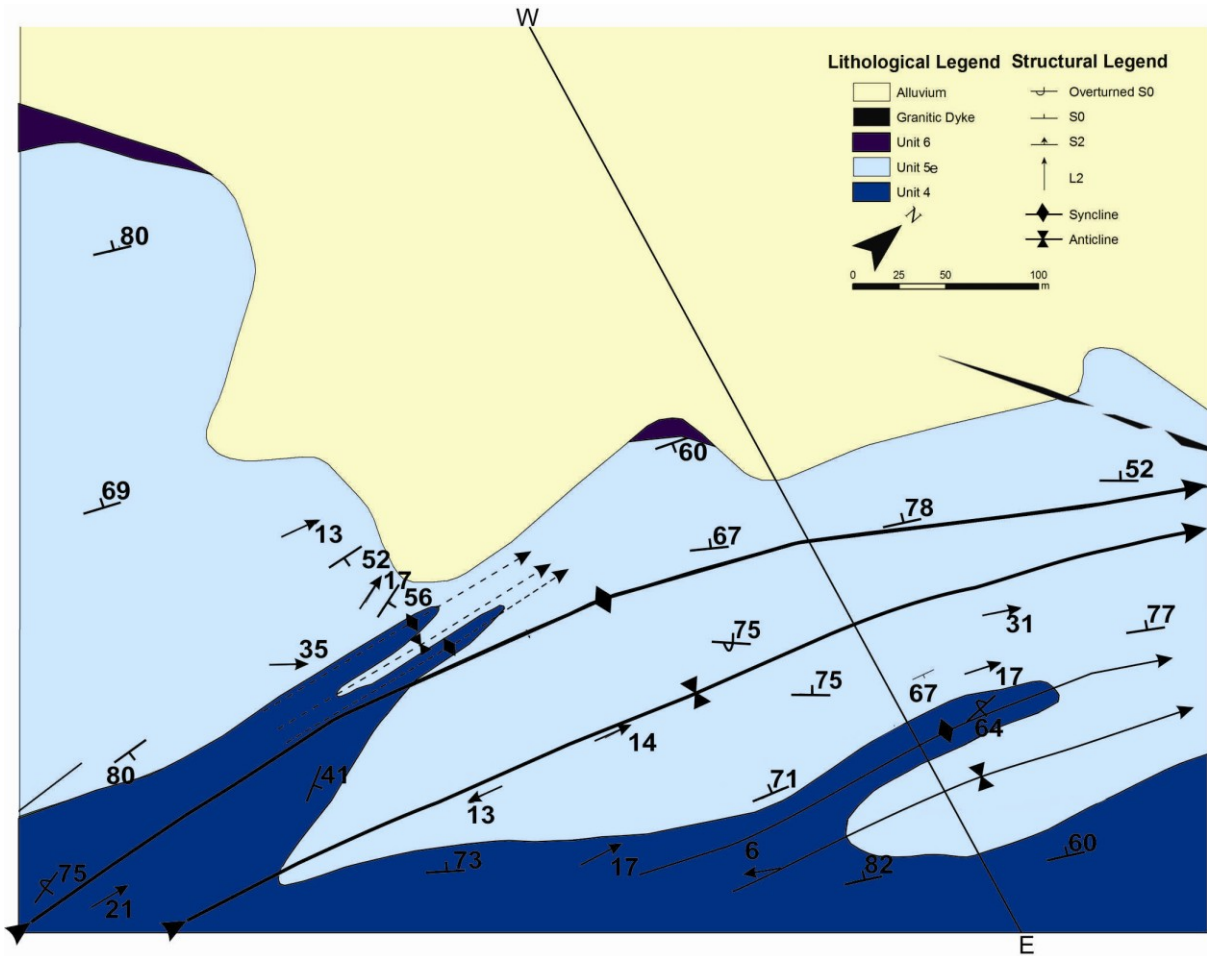


Figure 5.14: Geological map of the Steenbok prospect. The dolomitic marble at Steenbok lacks the compositional variations as observed at Gecko and is dominated by the thick, massive dolomitic unit 5e. The dips are steep- to overturned with a NNE strike. Fold plunges and L_2 is shallow doubly plunging to the NNE and SSW. Location of the cross-section drawn across Steenbok (Fig. 5.17) is shown on the map. Note the granitic dyke. Refer to Figure 5.16 for legend to fold orders.

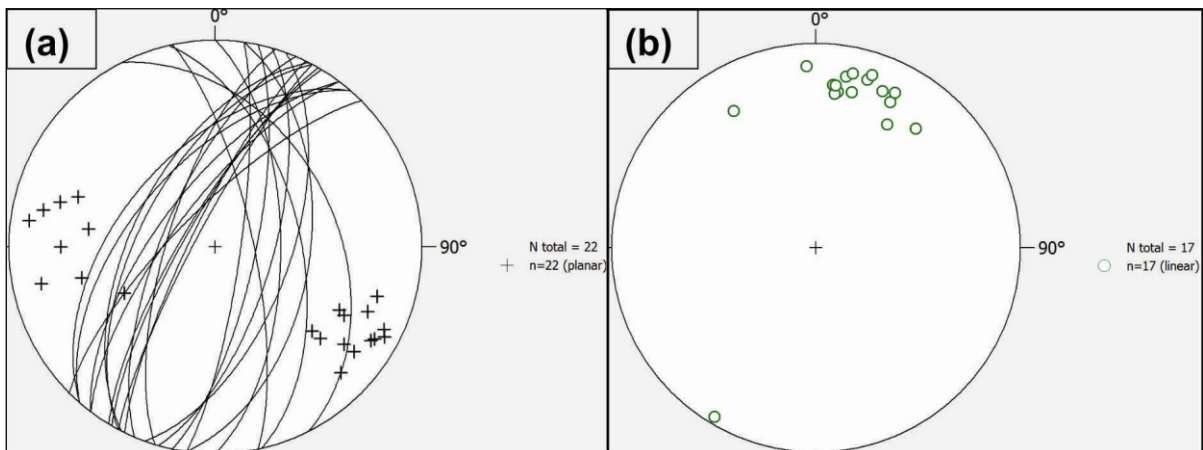


Figure 5.15: (a) Stereoplot for S_0 at Steenbok prospect. S_0 at Steenbok is steep- to overturned with a NNE strike. (b) Stereoplot for L_2 at Steenbok prospect. L_2 at Steenbok prospect is shallow and doubly plunging mostly to the NNE but also to the SSW.

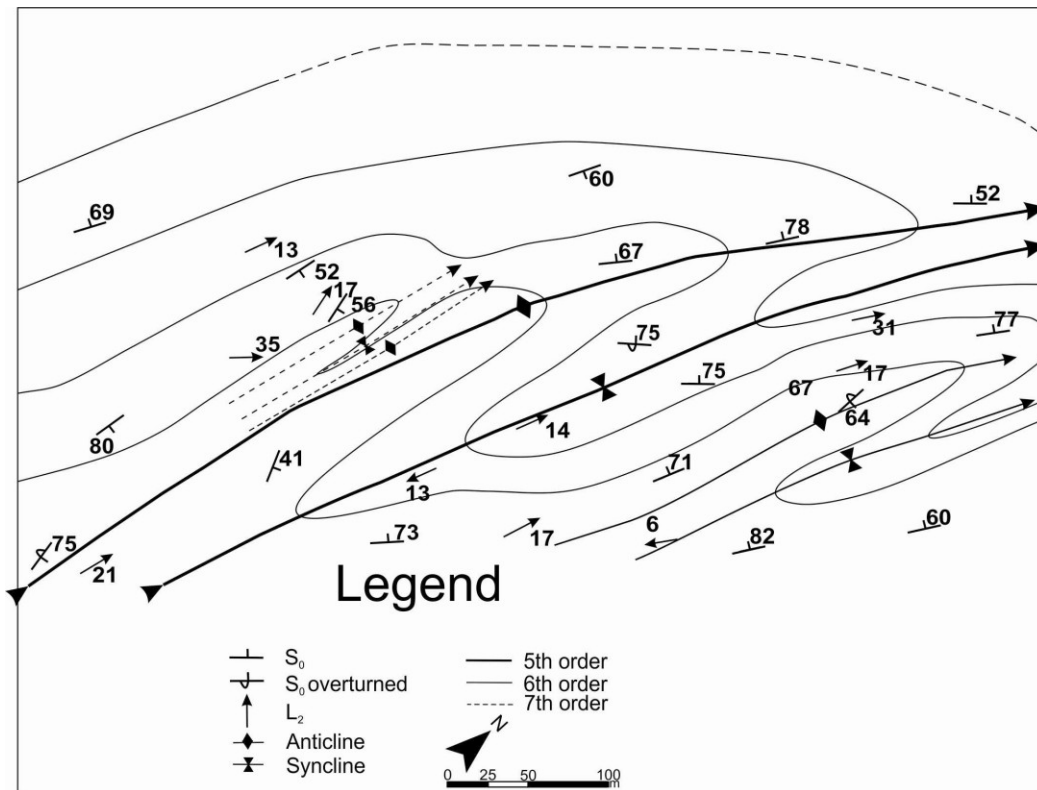


Figure 5.16: Formline map of Steenbok. The prospect is centred around a fifth-order synform-antiform pair. Lower order parasitic folds occur on the limbs of the pair.

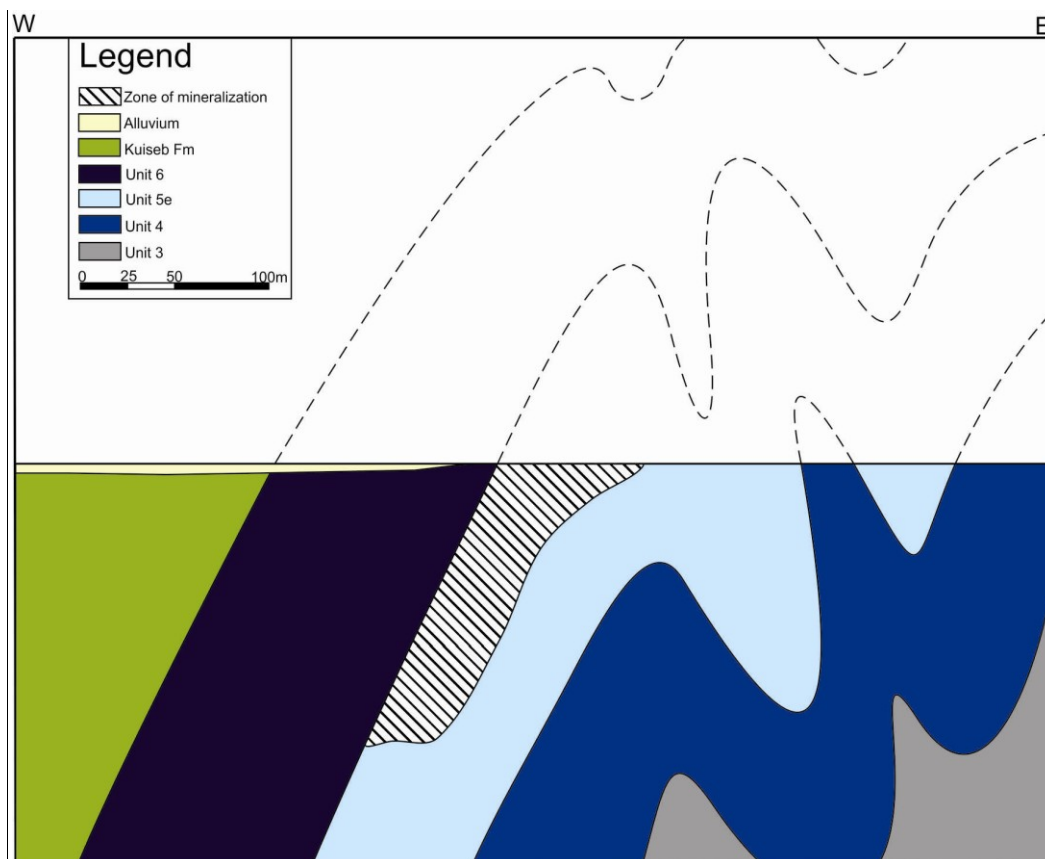


Figure 5.17: Cross-section drawn across Steenbok prospect. The prospect is located on the SE limb of the Navachab synform and the zone of mineralisation is located on the NW limb of a fifth-order antiform. Due to the lack of the well-developed subdivision of unit 5, there is only one zone of mineralisation at Steenbok prospect corresponding to the unit 5e and unit 6 contact.

Chapter 6 Quartz Veins in the Zoo Prospects

Gold mineralisation at the zoo prospects is hosted in hydrothermal quartz veins. Five main and distinct sets of quartz veins can be identified in the zoo prospects. The formation of the quartz veins is obviously structurally controlled, but, as evident from the previous chapters, there is clear lithological control exerted by the dolomitic unit 5 of the Karibib Formation, its contacts with adjoining calcareous marbles and more subtle variations of lithological subunits within the unit. Factors that control quartz veining and, thus, mineralisation will be developed in this chapter.

The highest density of quartz veins is observed near the contact between unit 5e and unit 6, as well as near the contact between unit 5c and unit 5d. The unit 5e and unit 6 contact represents the sharpest competency contrast controlling the bulk of the auriferous quartz veins and is, as such, the primary target of exploration. Importantly, the unit 5e and unit 6 zone of vein-hosted mineralisation is continuous through the prospects and can be followed from e.g. Gecko in the south to Klipspringer in the north on the NW limb of the Navachab synform. The Steenbok prospect is located in exactly the same stratigraphic position on the SE limb of the synform. In contrast, quartz veining and mineralisation associated with the contact between units 5c and unit 5d zone is only intermittently developed, forming pods of 20-50 m length. This mineralisation is not developed in Steenbok, where unit 5 is massive and homogeneous (see chapter 5.5).

Quartz in the auriferous quartz veins has a milky or greyish-smoky appearance. Primary, macroscopic growth textures of quartz have not been observed and the veins are massive and largely recrystallized. Microcracks in the quartz veins are not uncommon and are typically filled with sulphides. On a macroscale, the vein walls are generally sharp and parallel-sided and commonly surrounded by alteration halos consisting of mainly tremolite. A more detailed characterization of each quartz-vein set is given in the following section.

6.1. S₂ Parallel Veins (S₂P)

S₂ foliation-parallel veins (S₂P) occur in all of the prospects. The veins trend NE and have steep dips to both the NW and SE (Fig. 6.1a-d). S₂P veins show a large range in thickness and isolated veins can be up to 10 cm thick. More commonly, the veins form up to 1 m wide clusters of thin (1-2 mm), closely-spaced (1-5 mm) veins. In places, several of these clusters occur, separated by wall-rock with only minor veining. These clusters of closely-spaced veins may be several metres wide (refer to Appendix IIa, 0-4 m; Appendix II d, 7-10 m). Along strike, the extent of the S₂P veins can be several metres and reach up to 10 m long in places. In some cases, the veins have small (up to 5 cm) blows where the thickness of the vein increases.

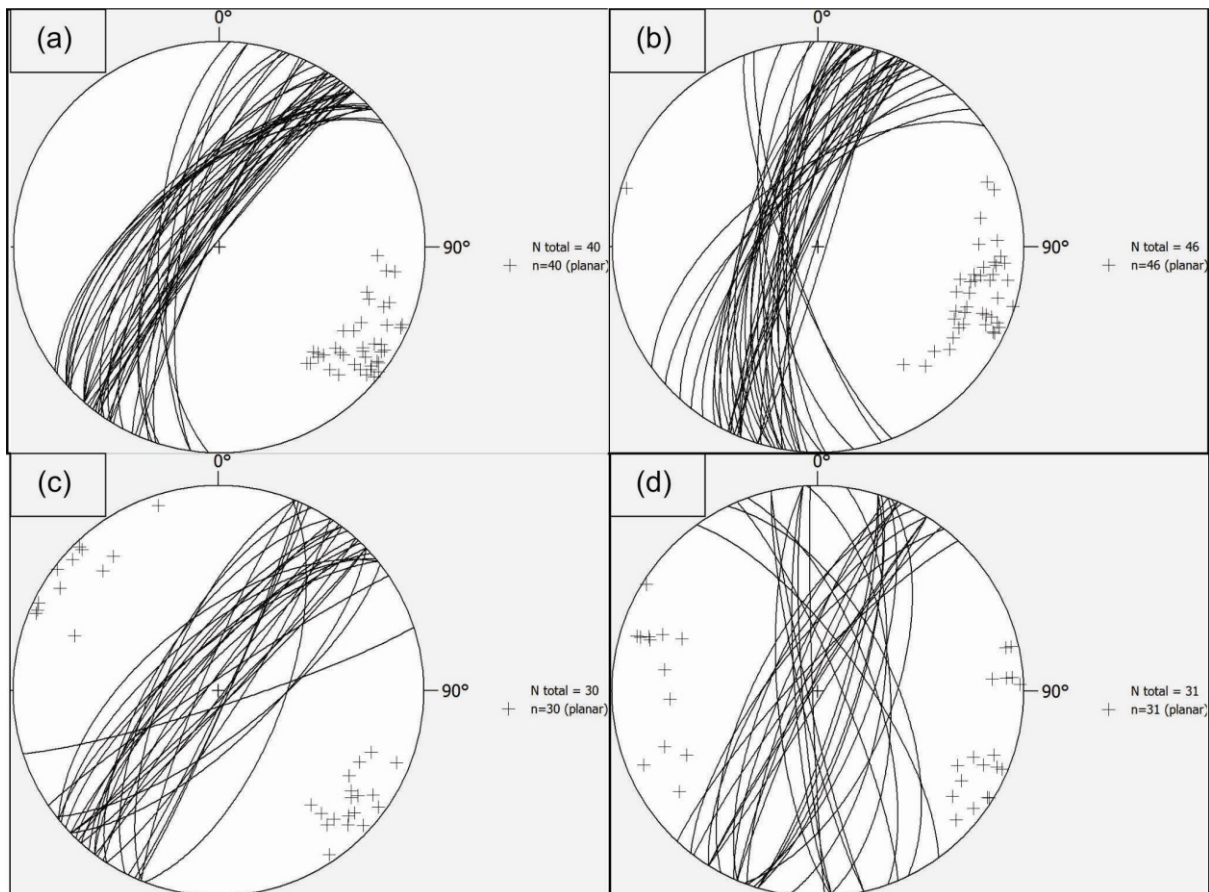


Figure 6.1: Stereonet for S₂P veins showing NE to NNE trends and steep dips. Most of the dips are to the NW, but SE dips also occur. (a) Gecko. (b) Grid A. (c) Klipspringer. (d) Steenbok

S₂P veins are commonly deformed. Deformation of the S₂P veins is particularly pronounced for the thicker (>2 cm) veins that have commonly undergone boudinage (Fig. 6.2a). The separation of the boudins suggests a maximum stretch (X) parallel to L₂ and F₂ fold axes, with a minor component of stretch (Y) in the vertical. This results in overall a chocolate-tablet boudinage of the veins. On weathered surfaces, iron hydroxides are enriched in boudin necks and along the high-angle extension fractures within the boudins. This may suggest a remobilization of original sulphides into the extensional sites during boudinage. Tremolite alteration is also very prominent in the necks of the boudins. Thin S₂P veins in vein clusters are locally folded (Fig. 5.2b). The folds show shallow plunges, parallel to F₂ folds and the asymmetry of folds also points to an origin of the folding during F₂.



Figure 6.2: Deformation characteristics of S₂P veins. (a) Photo with view to the east showing S₂P veins at Steenbok. The geological hammer is placed on a cluster of thin, closely-spaced S₂P veins. Note the thick vein to the right-hand side of the hammer that has undergone boudinage with complete separation of some blocks. Note also the concentration of Fe hydroxides in boudin necks that suggests migration of hydrothermal sulphides into the boudin interpartitions. (b) Cluster of thin, closely-spaced S₂P veins showing folding. The red arrow shows the axial trace of the folds. The small-scale folds are parallel to the regional F₂ folds. View to the NE, Gecko.

6.2. ac Veins

A prominent set of NW- to WNW-trending, subvertical- to steep NE-dipping veins is developed throughout the zoo prospects (Fig 6.3a-d). This orientation is normal to the plunge-direction of F_2 folds, so that these veins are henceforth referred to as ac veins, which represent the second-most prominent veins set in the zoo prospects. Ac veins are generally thicker than S_2P veins, ranging in thickness from ca. 5 mm to 10 cm, with an average thickness of 2-5 cm. The veins are characterized by a commonly massive core of quartz, surrounded by a prominent alteration halo of centimetre-large tremolite needles intergrown with carbonate and quartz. The tremolite either forms radial aggregates, or more commonly, the tremolite grows normal to the vein walls (Fig. 6.4a).

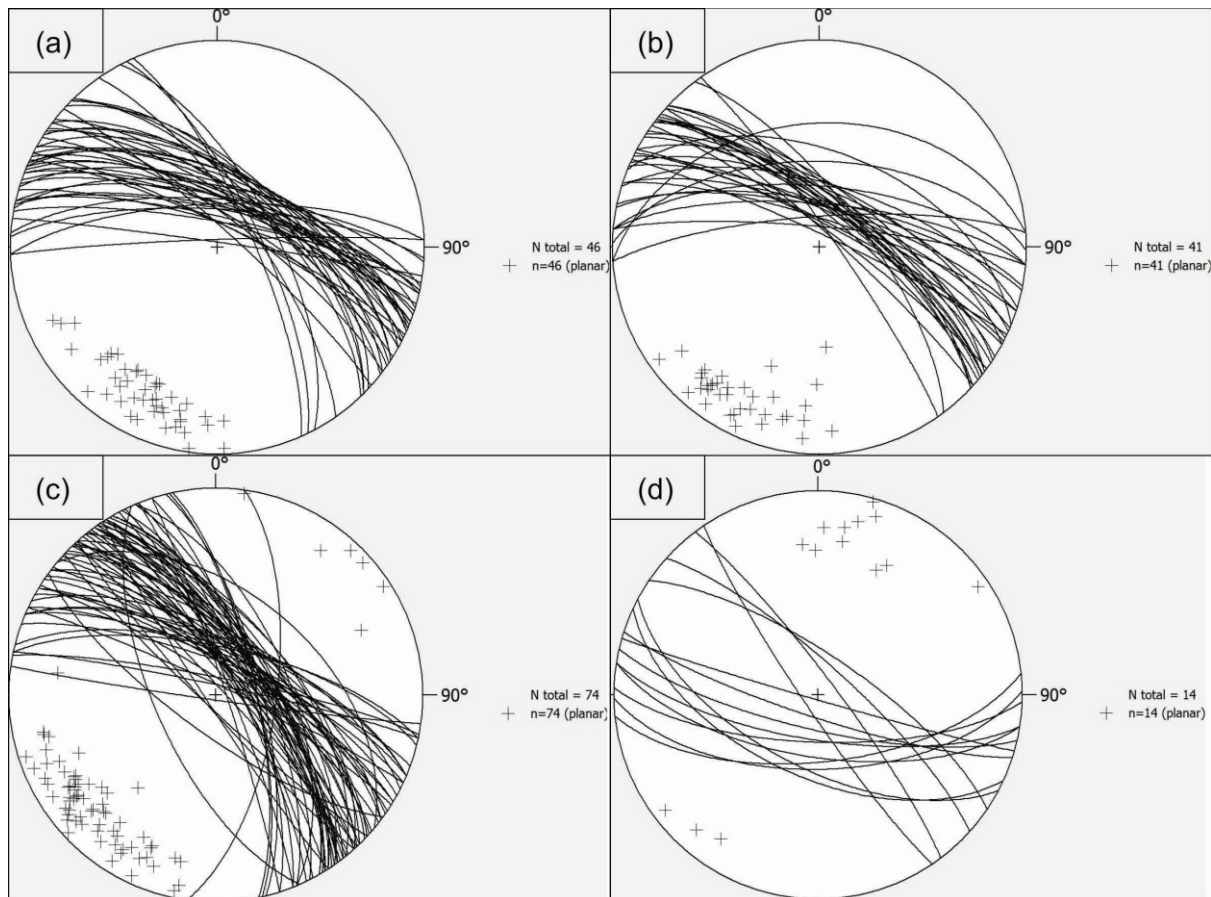


Figure 6.3: Stereonet of ac veins showing NW trends and subvertical- to steep dips. The dips are mostly to the NE, but SW dips also occur. (a) Gecko. (b) Grid A. (c) Klipspringer. (d) Steenbok. The veins at Steenbok show a 20-30° anticlockwise rotation of the veins. The strike of the bedding at Steenbok is slightly more northerly when compared to the other prospects, which may explain the slight rotation of the veins.

Given that the growth of the tremolite provides an indication of the opening vector of the veins, this indicates the quartz veins to represent mode I, extensional veins (Fig. 6.4a). This corresponds to the direction of the sub-horizontal NE-SW D_2 stretch, parallel to the L_2 lineation and F_2 hinges (Chapter 4). Figure 4.5b shows that the F_2 hinge-parallel stretch is not only confined to dolomitic marble, but occurs throughout the study area and on all scales. The ac veins are particularly abundant in dolomitic units of units 5c, 5d and 5e. Here, they show a relatively regular spacing of 0.5-1 m. The veins are typically lensoid in plan view and cross-sections, being thicker in their centre and tapering towards their termination. The termination of the veins commonly coincides with bedding contacts of prominent dolomitic units and the veins rarely extend beyond the competent dolomites. As a result, ac veins are rarely longer than 5 m, the width of the most prominent dolomitic beds. Overlapping vein terminations are often observed and are characterized by a thinning of the vein over a few centimetres.

The intersection of ac veins with S_2P veins is commonly characterized by intense wall-rock alteration and, thus, the potential for high grades of gold. The age relationship of ac veins vs. S_2P cannot be determined by cross-cutting relationships due to the lack of displacement of either set. In addition, the increased wall-rock alteration makes it hard to determine cross-cutting relationships. The intensification of alteration around the intersections of vein sets suggest some degree of contemporaneity. In places, ac veins have undergone gentle folding about steep NE-plunging, NW-trending fold axes (Fig. 6.4c), corresponding to the orientation of regional F_2 folds, albeit with steeper plunges. However, ac veins may also appear undeformed. The presence of folded and undeformed ac veins is even developed in individual outcrops suggesting that vein emplacement occurred during the waning stages of D_2 .

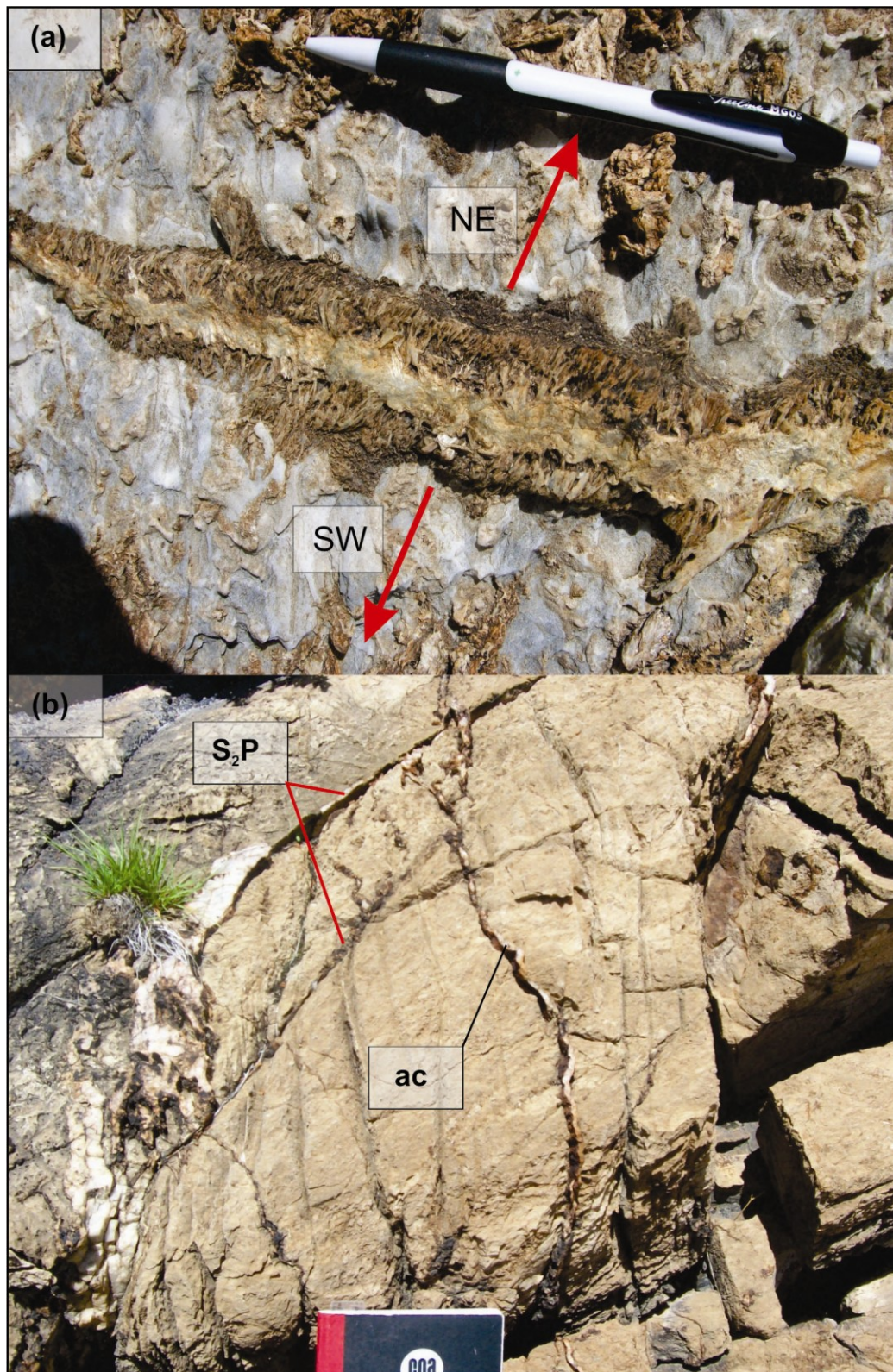


Figure 6.4: (a) Photo showing growth of tremolite needles normal to the vein wall, illustrating the extensional origin for the formation of ac veins and corresponds to the direction of subhorizontal NE-SW D_2 stretch. Plan view, Klipspringer; (b) Photo showing gentle folding of ac vein. Oblique plan view to the SW, Steenbok.

6.3. Shallow, Sheeted Quartz Veins (SSQ)

Shallowly-dipping veins are rather localized and could only be identified at a few localities at e.g. the Gecko prospect. The shallow veins have a similar orientation to the main swarm of sheeted quartz veins in the main pit of the Navachab Gold Mine to the immediate east, showing W- to NW-trends with shallow northerly dips (Fig. 6.5a). The veins are generally thin (mm-scale) and closely-spaced (Fig. 6.5b), forming up to 2-3 m wide clusters. Gentle folding of the veins is common, and fold plunges are shallowly to the NE, parallel to F_2 folds. The SSQ occur near to the contacts of competent units, i.e. the contacts of unit 5c/5d and unit 5e/6.

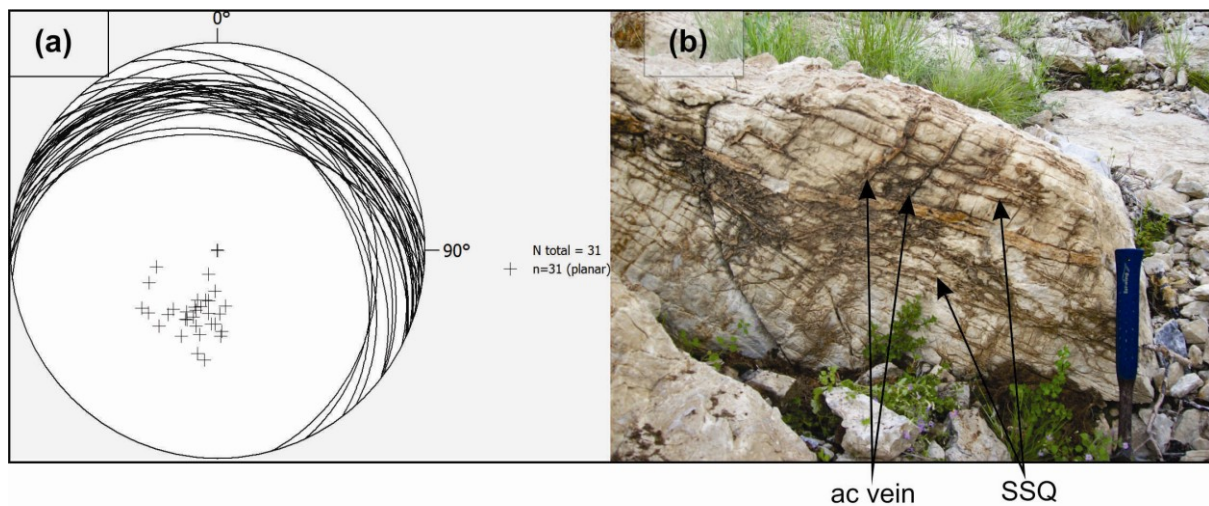


Figure 6.5: (a) Stereoplot of shallow, sheeted quartz veins recorded at Gecko prospect showing W- to NW-trending veins with shallow dips. (b) Photo showing the shallow dipping SSQ as well as high-angle ac veins in dolomitic marble of unit 5e. Photo looking onto the bedding plane with a view to the NW, Gecko prospect.

6.4. Shear Veins

Shear veins are only very locally developed, but good examples are found e.g. at the Klipspringer prospect between unit 5c and unit 5d. The veins are NNE-trending with moderate W- to NW- dips (Fig. 6.6a). The veins are short and stubby and individual veinlets commonly show a sigmoidal shape. The thickness of shear veins rarely exceeds several millimetres and veins are no longer than 10 cm. These thinner, sigmoidal veins tend to form en-echelon arrays, whereas thicker, centimetre-wide veins are rather isolated. The en-

echelon arrangement and their occurrence in NW-dipping arrays suggest that the veins formed along shear fractures. The sigmoidal geometry and NW dips of veins in the vein clusters indicate a top-to-the-SE movement (Fig. 6.6b), and formed in response to NW-SE directed shortening during vertical extension of rhombic boudins of competent dolomitic marble (Fig. 6.7). As mentioned above, shear veins are only of local significance at e.g. the Klipspringer prospect.

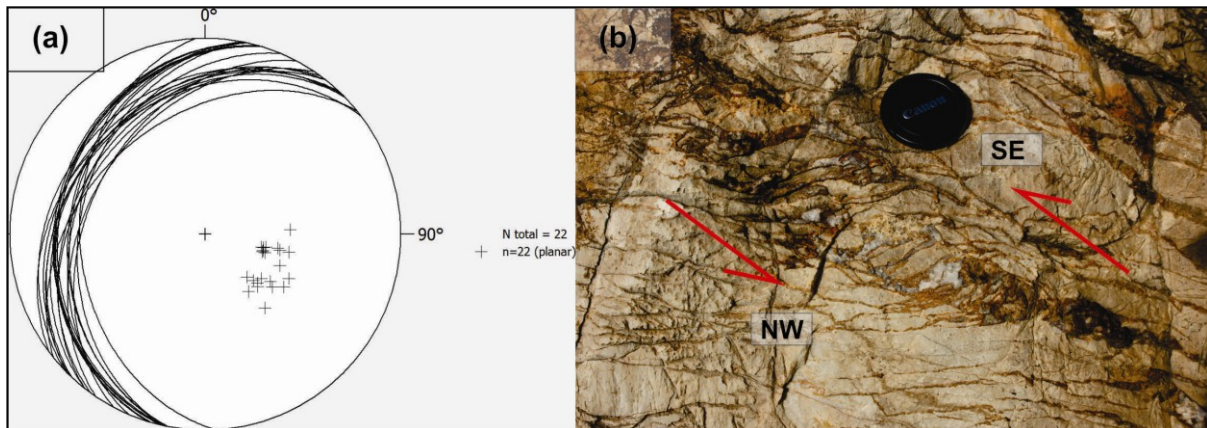


Figure 6.6: (a) Stereoplot of shear veins recorded at Klipspringer prospect showing NNE-trending veins with moderate dips. (b) Photo showing sigmoidal shear veins (cross-sectional view) with view to the SW. Note the thickening of veins in their central parts tapering towards their lateral terminations.

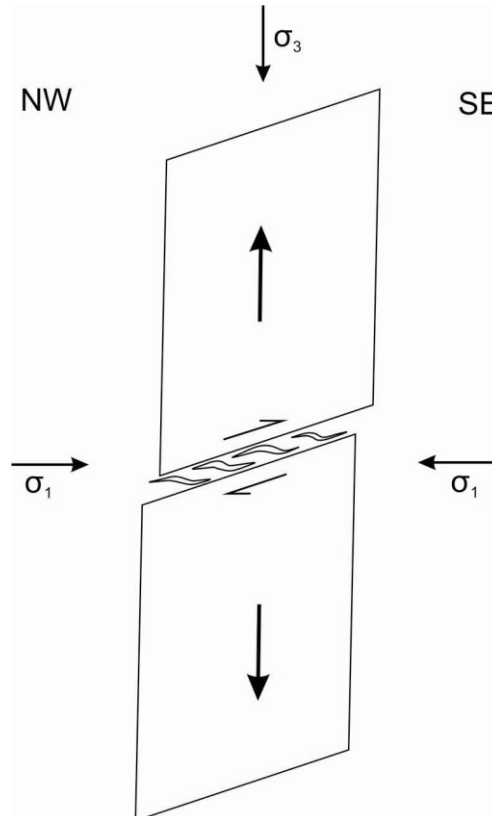


Figure 6.7: Simplified diagram illustrating how shear veins formed in response to NW-SE directed shortening. The vertical extension of competent dolomitic marble formed rhombic blocks that produce a component of pure shear and resulted in the formation of shear veins with a typical sigmoidal geometry.

6.5. Conjugate Set

This set forms a conjugate set with the ac veins (Fig. 6.8a). The veins are N- to NNE-trending with steep dips (Fig. 6.8b) The veins have a regular spacing of 0.5-1 m and are thin (mm scale). These veins represent a minor vein set when compared to the widespread ac veins and has only been observed at the Gecko and Klipspringer prospects. Cross-cutting relationships between this vein set and the S_2P veins are common and invariably indicate the S_2P veins to be older (Fig. 6.8c).

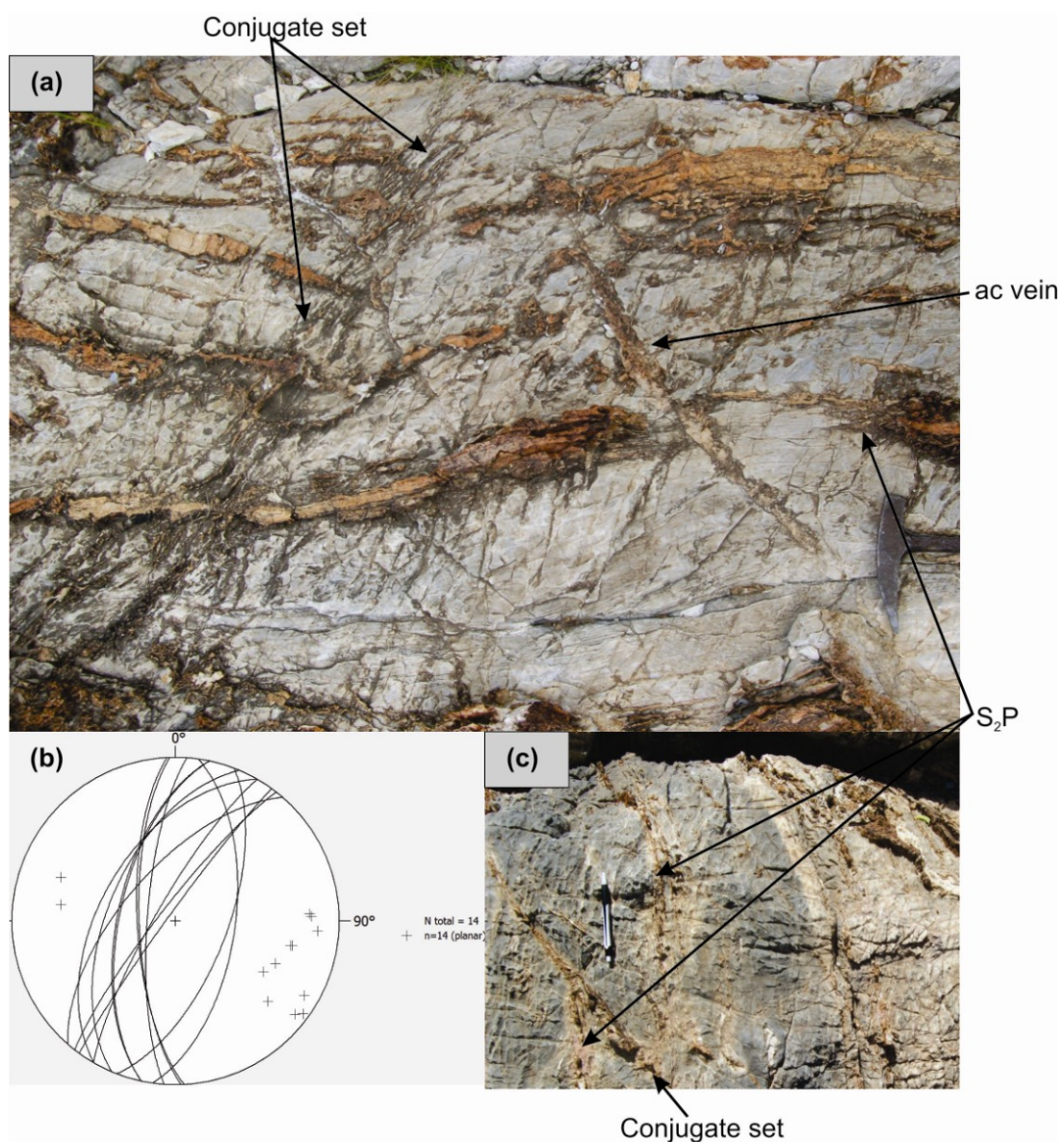


Figure 6.8: (a) Photo showing conjugate set (veins are delineated by reddish and positive weathering in the grey-beige marble), ac vein and S_2P vein. Hammer for scale at bottom right of photo. View to the SW, Gecko prospect. (b) Stereoplot for conjugate set recorded at Klipspringer and Gecko prospects showing N- to NNE-trends and steep dips. (c) Cross-cutting relationship between the younger conjugate set and the older S_2P vein set. View to the NE, Klipspringer prospect.

6.6. Vein Stockworks in Dilational Sites

Quartz-vein stockworks and pods of massive silicification are distinct from the discrete vein geometries described above. This type of quartz veining occurs locally in the unit 5e dolomitic marbles, confined to metre-wide zones particularly along the contacts of unit 5e with the overlying calcareous marbles of unit 6. Quartz veining is associated with a prominent tremolite alteration and sulphide mineralisation, all testifying to the increased fluid-flow in these dilational zones.

Stockwork veining involving the boudinage of competent rock with subsequent stockwork veining in the necks of the boudins is common at Grid A and Klipspringer (Fig. 6.9a). This type of mineralisation was first observed at Klipspringer and hence, is referred to as Klipspringer-type mineralisation. This type of mineralisation is very localized and somewhat erratic and depends on the spacing and geometry of boudin structures (Fig. 6.9b).

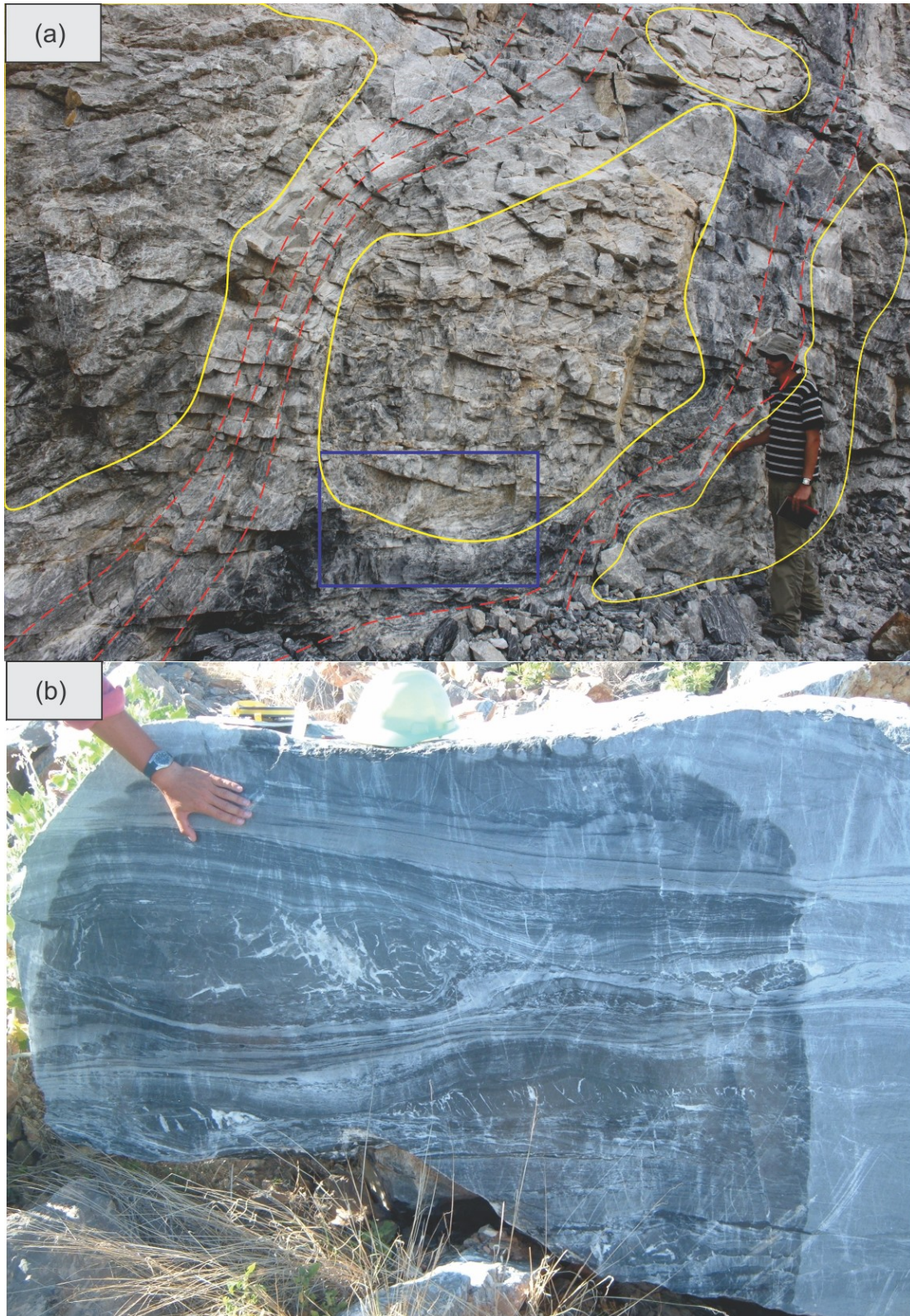


Figure 6.9:(a) Photo showing an example of stockwork veining involving the boudinage of competent dolomitic marble (Klipspringer-type mineralisation). Klipspringer-type mineralisation involves the boudinage of competent rock (here dolomitic marble outlined by yellow polygons) with subsequent stockwork veining in the necks of boudins (indicated by purple box). S_2 (red, dashed line) often wraps around blocks that have been separated. The photo is an oblique view to the N, Grid A (b) Photo of stockwork veining in the neck of a boudin. In this case the boudin occurs within unit 6. View to the SE.

Quartz vein stockworks are particularly pronounced in dilational jog geometries. Figure 6.10 is a simplified diagram of Domain B of Figure 5.9 and shows how the (1) geometry of the anastomosing shear zones, and (2) their kinematics can result in both compressional and dilational jog geometries. Quartz veining may take the form of stockworks, in which a multitude of cross-cutting quartz veins make up to 60 % of the rock. In zones of massive silicification, vein-hosted breccias have developed where earlier stockwork veins are preserved in angular and seemingly rotated wall rocks cemented by milky quartz and associated tremolite and sulphides that form the matrix of the breccias. The overprint of earlier stockworks by later massive silicification also emphasizes the progressive development of the quartz veining and fluid pumping through these zones. The boundaries of these zones of intense quartz veining are mainly sharp and determined by the presence of narrow, S_2 -parallel shear zones. The largest of these stockworks can be mapped along the NE wall of the Grid A open-pit, where the dolomitic marbles are in contact with calcareous marbles of unit 6. The exposed stockwork has a bell-shaped geometry (Fig. 6.11). This geometry is the result of the orientation of the two bounding high-strain zones represented by the sheared contact between unit 5b and unit 6 in the east and a S_2 -parallel shear zone in the west.

Dilational jogs show abundant quartz veining and near-massive silicification, in places, pronounced tremolite alteration and sulphide mineralisation (Fig. 6.11). Brecciation of the wall-rock in the dilational sites is common (Fig. 6.12). Brecciation resulting from the collapse of wall-rock into dilational sites opened during shearing/slip in moderately dipping veins is observed in the prospects (Fig. 6.13b). The mosaic breccia typically consists of angular dolomitic marble fragments cemented by quartz-tremolite and represent small pods of high-grade mineralisation.

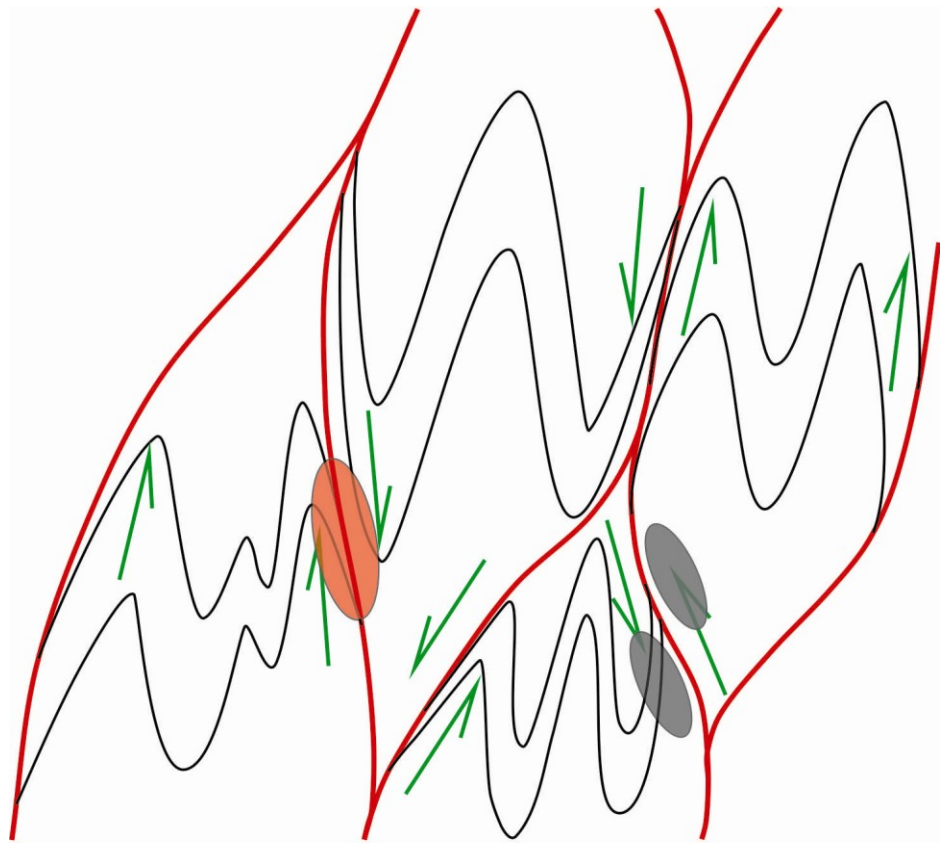


Figure 6.10: Simplified diagram of Domain B of (Fig. 5.9). Depending on the geometry and kinematics, low-displacement, anastomosing shear zones (S_2 parallel) on the limbs of folds can create space by means of dilational jogs (grey ellipses) into which fluid can enter and result in mineralisation. This scenario results in massive silicification, alteration and mineralisation, shown in (Fig. 6.11). Compressional jogs (red ellipses), in contrast, are not mineralized.

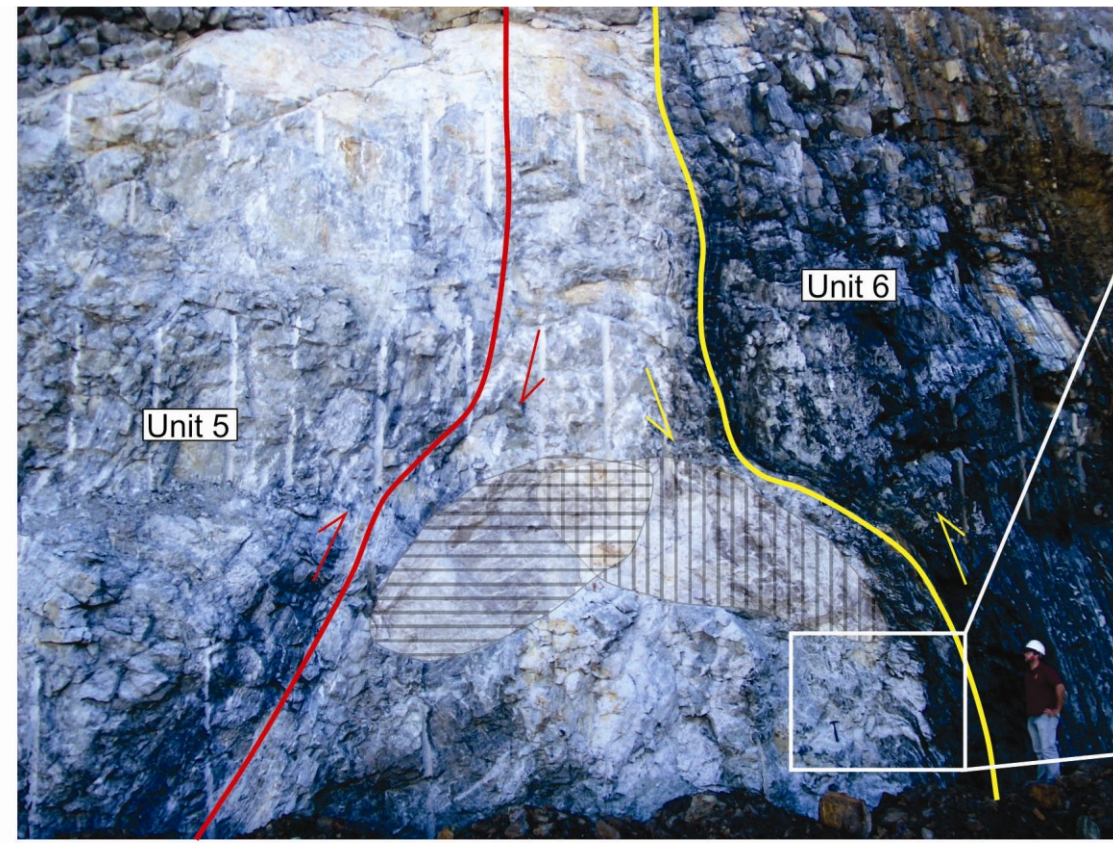


Figure 6.11: Enlarged photo of Domain C of (Fig. 5.9). The photo shows how space is created by means of shearing and folding to create dilational jogs. In this case the spaces created are close enough to have overlapped and resulted in high grades of mineralisation.

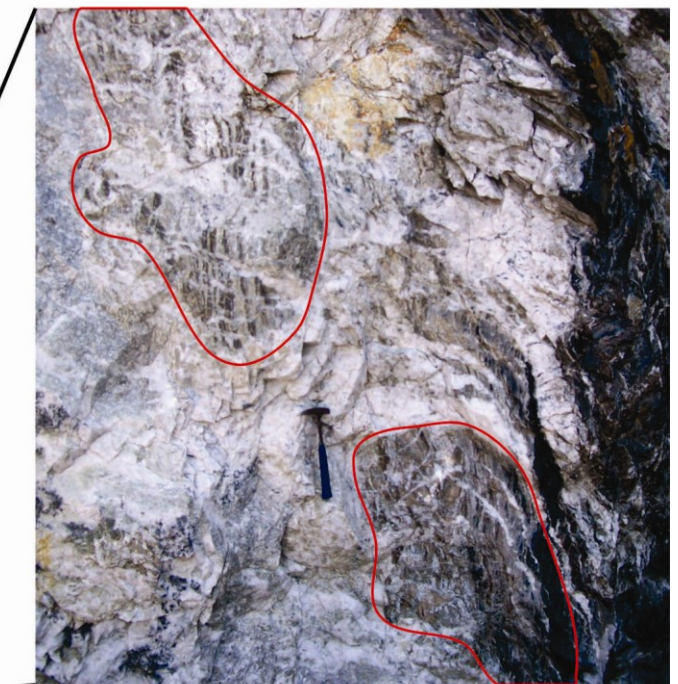


Figure 6.12: Enclosed in the red polygons are two dilational sites that have undergone brecciation of the dolomitic marble. The breccia typically consists of angular dolomitic fragments that have been cemented by quartz-tremolite.

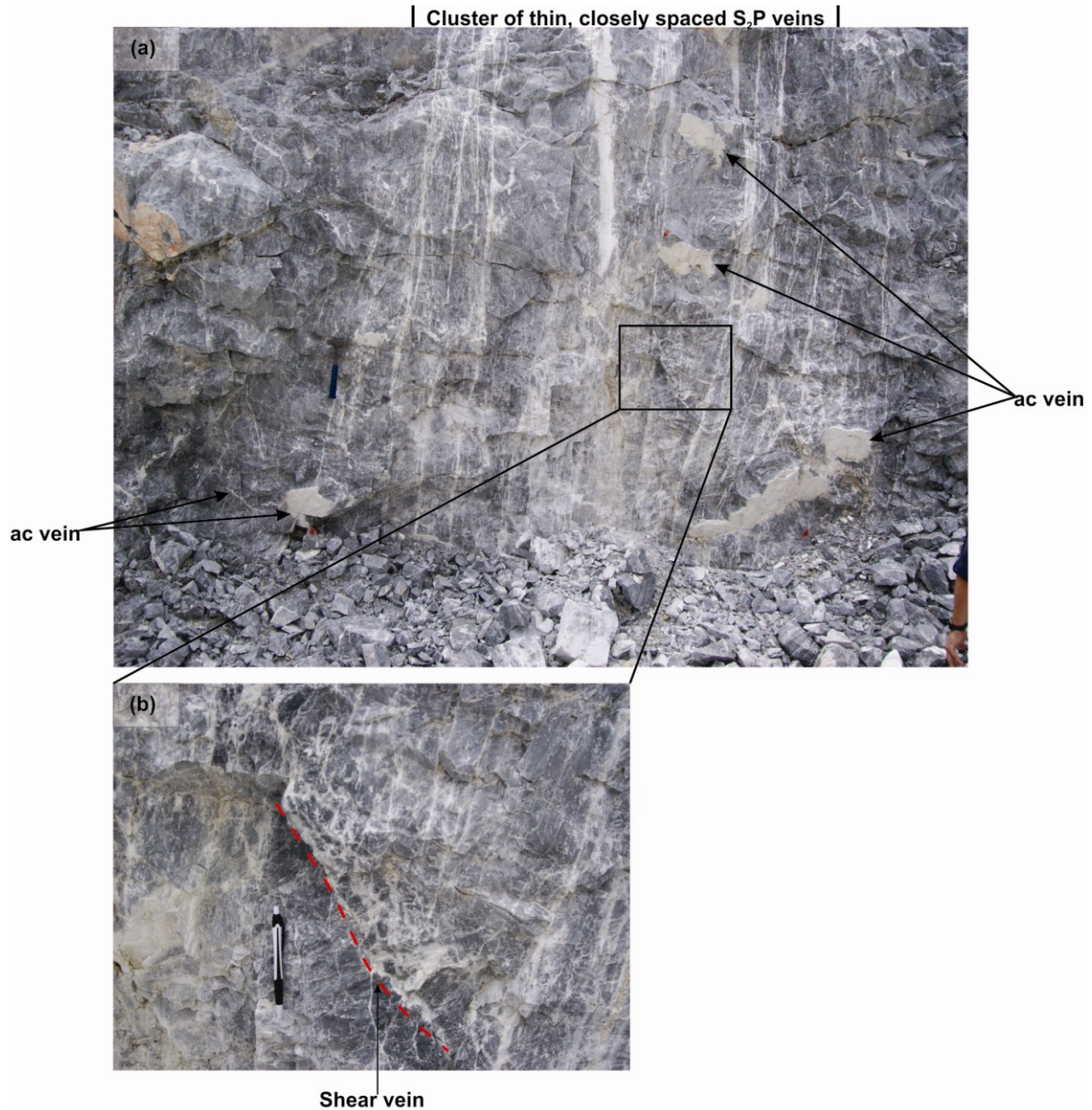


Figure 6.13: (a) Cross-sectional photo with a view to the NE of Pit 2 at Gecko. The photo shows the several metre vertical extent of the S₂P veins and the typical cluster style of veining of the thin, closely-spaced veins. The pit wall is subparallel to the strike of the ac veins and remnants of the veins are found as patches on the cut (annotated). In this case, ac veins cross-cut S₂P veins. S₀ is ca. 136/74°. Geological hammer in the middle left of photo for scale. (b) Mosaic breccia with angular dolomitic marble fragments (dark-grey) cemented by quartz/tremolite (white). The texture indicates that the brecciation occurred during the collapse of the wall rocks into dilational sites opened during shearing/slip along a shear vein. Note the relatively sharp footwall contact of the breccia, but the gradual disintegration of wall rocks and earlier veins in the hangingwall.

6.7. Quantitative Analysis of Quartz Veins in Borehole and Panels

For a more quantitative analysis of quartz veining, the quartz veins were mapped in detail along panels at all four prospects. Sample lines were drawn at a height of 1 m and veins thicker and including 2 mm were recorded for vein thickness, orientation and spacing. In addition, seven diamond drillcores were analysed for vein characteristics in the subsurface. The logging of borehole cores was intended to demonstrate the continuation of surface features and to verify the controls of the mineralisation identified during surface mapping. The orientation of the veins in the drillcore could not be established because the holes were not orientated at the time of drilling. As a result only features such as lithology, mineralogy, wall-rock alteration, vein density and deformation were noted. Table 6.1 is a summary of vein data from sampling lines and borehole cores. At the Gecko prospect, two trial pits were available for analysis and five boreholes. The raw data and panels mapped for Gecko is shown in Appendix II. At Grid A, two benches were mapped and two boreholes were analysed. The raw data and panels mapped for Grid A are shown in Appendix III. At the Klipspringer and Steenbok prospects, the road cuts constructed for the access of the drill rigs were analysed. The raw data for Klipspringer and Steenbok is shown in Appendix IV and V respectively.

Table 6.1: Summary of the raw data for veins of panels mapped at the prospects and borehole cores logged from Gecko and Grid A. Raw data can be found in Appendices II-V.

Prospect	Panel	Line Length (m)	Total No. of Veins	Vein Thickness (mm)		
				Min.	Max.	Ave.
Gecko	Pit 1 Panel 1	20	40	2	110	6.2
Gecko	Pit 1 Panel 2	20	30	2	10	3.5
Gecko	Pit 2 Panel 1	20	18	2	3.5	2.5
Gecko	Pit 2 Panel 2	10	22	2	17	4.8
Grid A	1105m Panel 1	15	10	2	4	2.9
Grid A	1105m Panel 2	25	23	2	12	4.3
Grid A	1105m Panel 3	10	15	2	10	5.2
Grid A	1125m Panel 1	20	24	2	9	4
Grid A	1125m Panel 2	30	39	2	46	9.0
Klipspringer	Road cut	300	57	2	40	7.4
Steenbok	Road cut	150	22	2	35	7
Prospect	Borehole	Length of core (m)	Total No. of Veins	Vein Thickness (mm)		
				Min.	Max.	Ave.
Gecko	AD-128	34.08	52	2	10.2	4.5
Gecko	AD-129	80.36	90	2	21	4.1
Gecko	AD-130	15.33	49	2	19	4.3
Gecko	AWD-3	111.0	23	2	51	9
Gecko	AWD-4	68.5	15	2	76	18
Grid A	AD-122	21.60	55	2	19.3	5.7
Grid A	AD-123	61.79	93	2	22.2	4.8

6.7.1. Gecko Prospect

Panels

In total, four panels were mapped at Gecko and five borehole cores logged. The location of the panels and boreholes is shown on Figure 6.14.

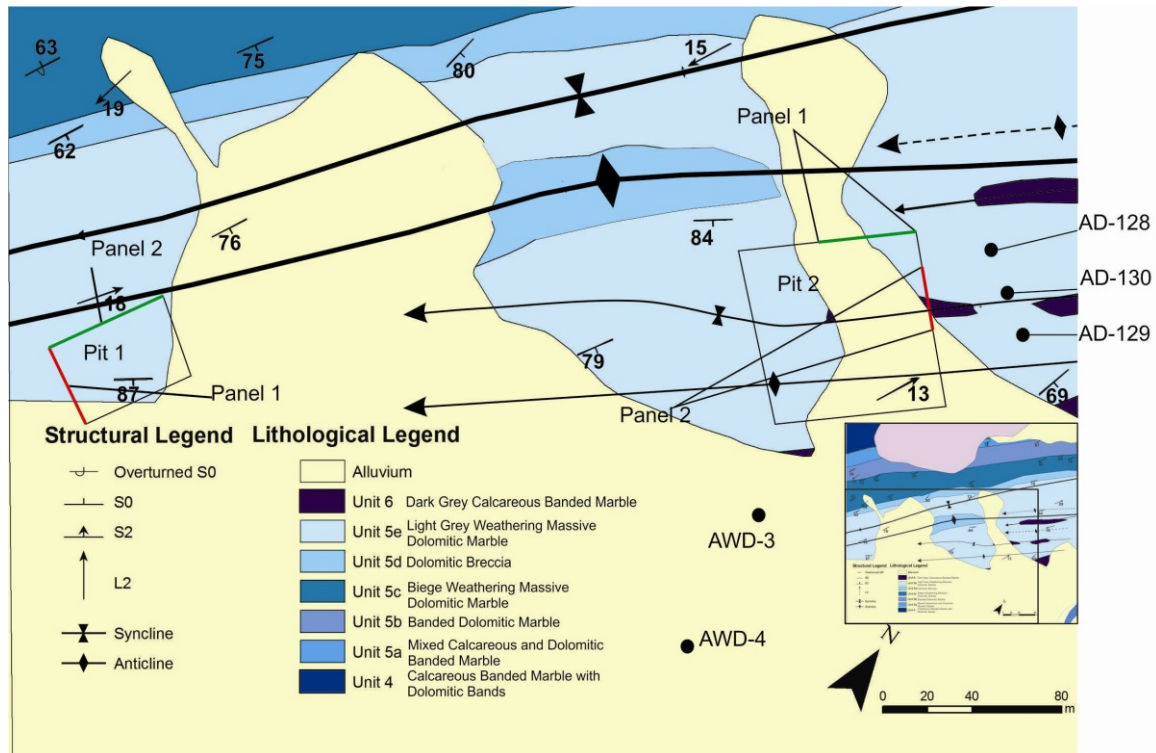


Figure 6.14: Geological map of the Gecko prospect showing the location of boreholes (black dots) and panels mapped. Red lines represent cross-sectional panels and green lines represent longitudinal sections. Insert shows the location of the map with regards to geological of map Gecko. Note the location of the trail pits near the contact of unit 5e and unit 6.

Pit 1 Panel 1 (Appendix IIa) is a cross-sectional panel that occurs near the contact of unit 5e and unit 6 and the start of the panel is ca. 15 m from unit 6. A total of 40 veins were recorded over 20 m with the majority of the veins having the orientation of the S₂P veins. The thickness of the veins varies from <2 mm to 110 mm, with an average thickness of 6.2 mm. The S₂P veins in the panel show a good clustering of veins, especially the first 5 m of the panel with the abundance of the veins decreasing away from the contact. The spacing between clusters of S₂P veins is generally ca. 0.5 m and the average spacing between veins is 40 cm.

Pit 1 Panel 2 (Appendix IIb) is a longitudinal section that occurs ca. 40 m from the contact of unit 5e and unit 6. In total 30 veins were recorded over 20 m with the majority of the veins having an S_2P vein orientation. The thickness of the veins varies from <2 mm to 10 mm with an average thickness of 3.5 mm. Given that the panel is a longitudinal section and as such does not cross as many S_2P veins as Panel 1, the clustering effect shown in Panel 1 is not clearly shown here. However, the Panel does show the conjugate nature of the S_2P and ac veins (8-9 m, Appendix IIb). The spacing between veins is on average 60 cm.

Pit 2 Panel 1 (appendix IIc) is a longitudinal section that occurs ca. 45 m from the contact of unit 5e and unit 6. In total 18 veins were recorded over 20 m with a thickness variation of <2 mm to 3.5 mm and an average thickness of the veins of 2.5 mm. The average spacing of veins in this panel is 113 cm. The clustering effect of the S_2P veins is illustrated in this panel.

Pit 2 Panel 2 (Appendix II d) is a cross-sectional panel that starts ca. 15 m from the contact of unit 5e and unit 6. In total 22 veins were recorded over 10 m with a majority of the veins having a S_2P orientation. The thickness of the veins varies from <2 mm to 17 mm with an average thickness of 4.7 mm. The panel shows clustering of the S_2P veins and in general the spacing between clusters is 0.5- 1 m. The average spacing between veins in this panel is 40 cm.

Borehole Cores

Only three (AD-128, 129, 130) of the five boreholes at Gecko prospect were analysed for the thickness and spacing of the veins. Boreholes AWD-3 and AWD-4 were only analysed for mineralogy and wall-rock alteration.

AWD-3 has an inclination of 65° to the NW. The borehole starts in unit 6 and intersects unit 5e after 81.2 m. Appendix IIe shows the raw data for the borehole. The borehole has few measurable veins, but shows two distinct zones of mineralisation with a marked clustering of thin veins (stockwork). A total of 23 veins occur over 111 m with a minimum thickness of 2 mm, a maximum thickness of 51 mm and an average thickness of 8 mm. Spacing of the veins in this borehole was not recorded due to the sparse nature of recordable veins, i.e. most of the veins are veinlets and represent stockworks that coincide with zones of

alteration. In the boreholes, the zones of wall-rock alteration are clearly distinguishable from the unmineralized dolomitic marble. Figure 6.15a is a simplified log of borehole AWD-3 and shows the location of two zones of mineralisation that coincide with the wall-rock contacts within unit 5 (unit 5d and e), and between unit 5 and unit 6. The first zone of mineralisation, at a depth of 86.52 m in borehole AWD-3, occurs near the contact of unit 5e and unit 6. The second zone of mineralisation is encountered at a depth of 151.15 m and coincides with the contact between unit 5d and unit 5e. This agrees with the observations made at surface and indicates the continuity of the mineralized zones along these lithological contacts (chapter 5.2). Small pods of wall-rock alteration do occur between the two zones of mineralisation but do not exceed 5 m in width. Wall-rock alteration typically shows light- to dark green and creamy white colour (Fig 6.15b). Within and proximal to zones of alteration, abundant quartz veins and tremolite, oxides and sulphides (pyrite, chalcopyrite and bornite) occur, but visible gold is rare (Fig. 6.15c). The dolomitic marble bordering around zones of alteration has a light-brown colour and contains tremolite needles (Fig. 6.15d). Except for the occurrence of sporadic tremolite, the barren dolomitic marble is devoid of any of alteration features. Figure 6.15e is an example of how the intraformational dolomitic breccia (unit 5d) appears in a diamond drillcore. The white- to light-green quartz veins are usually surrounded by alteration halos of tremolite (Fig 6.16a). Where veins are boudinaged, the wall-rock alteration and intergrown sulphides often fill the boudin interpartitions (Fig 6.16b).

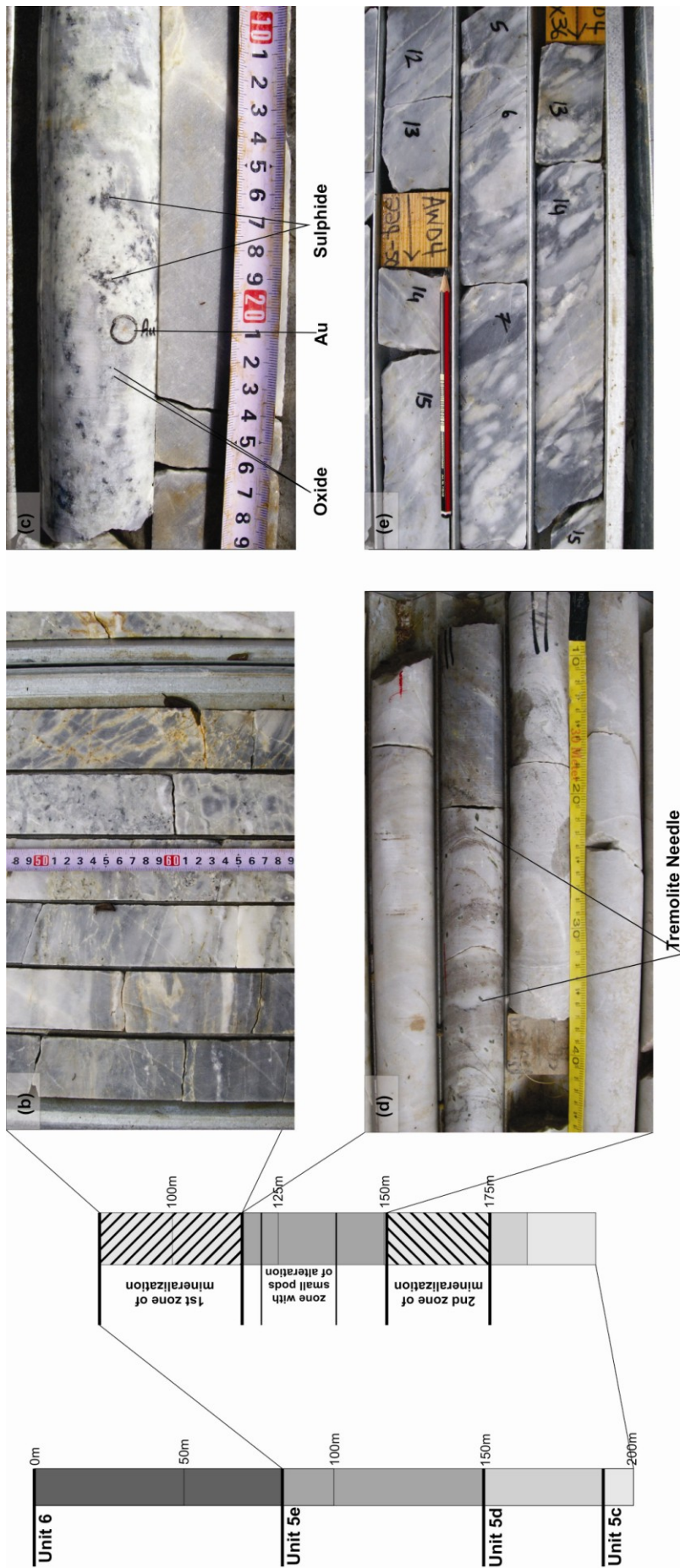


Figure 6.15: (a) Simplified stratigraphic column of borehole AWD-3. The column shows the locality of the zones of mineralisation. The first and larger zone occurs near the contact of unit 5e and unit 6, and the second zone occurs at the contact of unit 5d and unit 5e. Small pods of wall-rock alteration occur between the two zones but seldom exceed 5 m in width. (b) Typical light- to dark green and creamy white wall-rock alteration of the dolomitic marble. Note the stockwork to the right of the tape measure. (c) Oxides and sulphides typically occur in the zones of mineralisation, and rarely free gold is found in these zones. (d) Light-brown wall-rock alteration of dolomitic marble surrounding the zone of mineralisation with numerous tremolite needles. (e) Appearance of a dolomitic breccia (unit 5d) in borehole AWD-3.

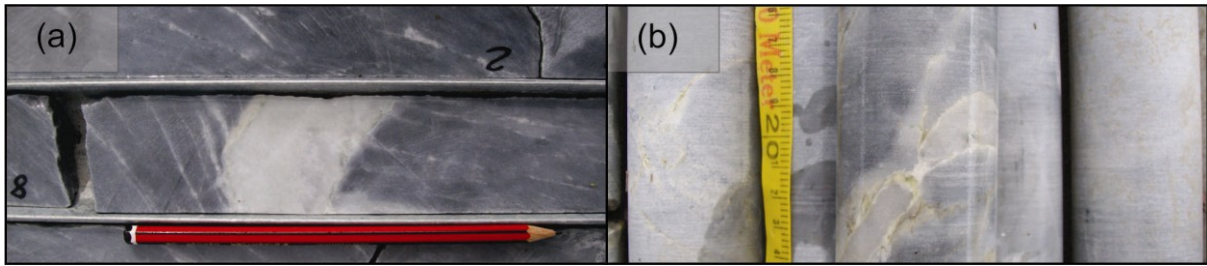


Figure 6.16: (a) Alteration halo surrounding a quartz vein. (b) Tremolite alteration halo around a boudinaged quartz vein and alteration has filled the space created in the neck of the boudin.

Borehole AWD-4 has an inclination of 60° to the NW. The borehole starts in unit 6 and intersects unit 5e at 161.50 m. The raw data for the borehole is shown in Appendix II f. As with AWD-3, borehole AWD-4 has markedly fewer veins than boreholes AD-128 to 130, but also shows two distinct zones of mineralisation: one at the contact of unit 5e and unit 6 (at a depth of 165.09 m) and the other at the contact of unit 5c and unit 5d (at a depth of 202.95 m). This borehole, however, has patches of alteration that range from <1 m to 5 m in width. The borehole ends in the second zone of mineralisation. As with borehole AWD-3, the spacing of veins was not recorded due to the sparse nature of the measurable veins and the fact that most veins are part of stockworks that occur within the zones of alteration around lithological contacts.

AD-128 has an inclination of 55° and an azimuth to the SSE. The borehole only occurs within dolomitic marble (unit 5e) and does not intersect the contact between unit 5 and unit 6. The distance to the contact with unit 6 is unknown. Appendix II g shows the raw data for borehole AD-128. A total of 52 veins were recorded over 34.1 m. The thickness of the veins ranges from 2 mm to 10 mm with average vein thickness of 4.5 mm. Zones of intense wall-rock alteration are shown and in general occur regularly with a spacing of 4 m to 6 m. The average spacing of recorded veins is 67 cm.

AD-129 has an inclination of 54° with an azimuth to the WSW. The borehole starts in unit 6 and the contact with unit 5e is made after 11.56 m. Thus the borehole intersects the unit 5e and unit 6 zone of mineralisation identified on surface.. Veining does occur in the contact zone. The raw data for borehole AD-129 is shown in Appendix II h. A total of 90 veins were recorded over 80.36 m. The thickness of the veins ranges from 2 mm to 21 mm with many of the thicker veins showing boudinage. This indicates that most of these veins are S_2P veins.

The average thickness of the veins is 4.1 mm. Numerous stockworks occur within the borehole in which veinlets show a somewhat scattered orientation in the borehole. The stockworks coincide with zones of intense wall-rock alteration and could represent dilational sites such as those observed at Grid A (Chapter 6.6; Figs. 6.11 and 6.12). The spacing of the stockworks is close (1-3 m) in the upper parts of the borehole, and increases markedly towards the bottom of the hole. The average spacing of the recorded veins in the hole is 79 cm.

AD-130 is a vertical hole that is collared in unit 6. The borehole has a length of 50 m and only intersects the unit 5e and unit 6 zone of mineralisation. The raw data for the borehole is shown in Appendix Iii. A total of 49 veins were recorded over 17.41 m, after which only barren dolomitic marble (unit 5e) is observed. The contact between unit 5d and unit 5e was not reached. The thickness of the veins ranges from 2 mm to 19 mm with an average vein thickness of 4.3 mm. The contact between unit 5e and unit 6 is the only zone in which intense wall-rock alteration occurs. The average spacing of the recorded veins in the borehole is 32 cm.

6.7.2. Grid A Open-Pit

At Grid A, five panels were mapped on two levels. This included three panels at an elevation of 1105 m and two at an elevation of 1125 m. The location of the panels is shown on Figure 6.17.

As mentioned in chapter 5.2, the subdivision of unit 5 at Grid A is not as straightforward as in other prospects, due to the intense folding and structural disruption of the sequence. The main marble at Grid A is a banded dolomitic-calcareous marble (unit 5b), interlayered with more massive dolomitic marble. This marble package is in contact with the overlying calcareous marble of unit 6 and veining is spatially closely associated with this contact due to the likely competence contrasts across this contact.



Figure 6.17: Photo of the open pit at Grid A, view to the north. The photo shows the location of the five panels mapped at Grid A.

Panels

Two cross-section and one longitudinal section were mapped on the bench at the 1105 m elevation. The first cross-section (ML Panel 1; Appendix IIIa) has a width of 15 m. The panel includes both dolomitic and calcareous marble. In the middle of the panel is a folded domain that includes a high-strain zone. In total, 10 veins were recorded with a minimum thickness of 2 mm, a maximum of 4 mm and an average thickness of 2.8 mm. Conjugate sets of ac and S_2P veins occur within unit 5b with stockworks of veining occurring near the contact of massive dolomitic marble and calcareous marble in a folded domain (at 5 to 8 m).

The second cross-section (ML Panel 2; Appendix IIIb) occurs 15 m to the NW of the panel above and has a width of 25 m. A total of 23 veins were recorded. The minimum vein thickness is 2 mm, the maximum 12 mm and the average thickness is 4.3 mm. The panel has numerous coarse-grained calcite veins near the contact of the dolomitic marble and calcareous marble. The majority of the veins are located within dolomitic marble with

several veins extending from the dolomitic marble into the calcareous marble. Several refolded boudins capped with calcite, and pinch and swell structures occur in the panel.

The longitudinal section (ML Panel 3; Appendix IIIc) has a width of 10 m. A total of 15 veins were recorded with a minimum thickness of 2 mm, a maximum of 10 mm and an average thickness of 5.2 mm. The panel occurs only in banded dolomitic marble (unit 5b). The majority of the veins recorded are ac- and conjugate-set veins, which is to be expected as the panel is a longitudinal section so that S_2P veins run parallel to the panel.

On the bench of elevation 1125 m, a cross-sectional panel and longitudinal section were mapped. The cross-section (UL Panel 1; Appendix III d) occurs within banded dolomitic marble (unit 5b) with the end (SE) of the panel occurring 5 m from the contact of unit 5b and unit 6. The abundance of veins increases towards the contact. A total of 39 veins were recorded over 30 m with a minimum thickness of 2 mm, a maximum of 46 mm and an average thickness of 9 mm. The panel contains ac-, conjugate-set and S_2P veins. The majority of the veins recorded are S_2P veins.

The longitudinal section (UL Panel 2; Appendix III e) has a width of 20 m. The panels occur near a contact of banded dolomitic marble and calcareous marble. Bedding is indicated where it was visible. The section contains two refolded boudins, one that is capped with calcite (at 12 m) and the other capped with quartz-vein stockworks (at 18 m). A total of 24 veins were recorded with a minimum thickness of 2 mm, a maximum of 9 mm and an average thickness of 4 mm. The majority of the veins are S_2P veins.

Borehole Cores

Two boreholes were analysed at Grid A. Borehole AD-122 has an inclination of 59° (Appendix III f). The borehole starts in dolomitic marble and cuts calcareous marble at the end of the hole (in fold of unit 6, refer to Fig. 5.8). A total of 55 veins were recorded over 21.60 m with a minimum thickness of 2 mm, a maximum of 19.3 mm and an average thickness of 5.7 mm. The average spacing of the veins is 39 cm. Wall-rock alteration is rarely

observed in the borehole, except for the last 4 m of the hole at the contact of calcareous marble and dolomitic marble.

Borehole AD-123 has an inclination of 55° (Appendix IIIg). The borehole only occurs within dolomitic marble. A total of 93 veins were recorded over 61.8 m with a minimum thickness of 2 mm, a maximum of 22.2 mm and an average thickness of 4.8 mm. The average spacing of the veins is 0.67 m. As with borehole AD-122, wall-rock alteration is rarely observed.

6.7.3. Klipspringer Prospect

A 300 m section of the road cut at Klipspringer was analysed for its quartz-vein inventory (Appendix IV). The location of the road cut is shown on Figure 6.18. The road cut is a longitudinal section and runs near the zone of mineralisation that occurs at the contact of unit 5e and unit 6. A total of 57 veins were recorded with a minimum thickness of 2 mm, a maximum of 40 mm and an average thickness of 7.4 mm. Spacing of veins at Klipspringer could not be considered due to the often collapsed road cut walls.

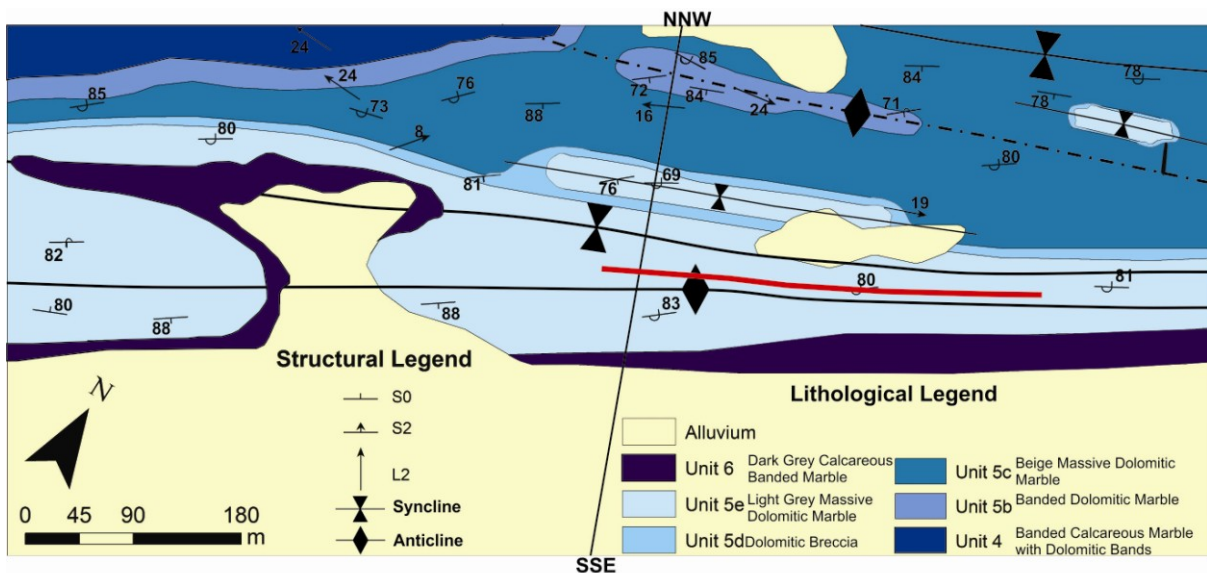


Figure 6.18: Geological map of Klipspringer that shows the location of the road cut analysed for its quartz vein inventory. The road cut runs subparallel to the plunge of the folds.

6.7.4. Steenbok

A 150 m section of the road cut was analysed for its quartz vein inventory (Appendix V). The road cut is an oblique section and occurs at the unit 5e and unit 6 zone of mineralisation (Fig. 6.19). A total of 22 veins were recorded with a minimum thickness of 2 mm, a maximum of 35 mm and an average thickness of 7 mm. As with Klipspringer the walls of the road cut at Steenbok has in places collapsed. The number of measurable veins at Steenbok is notably less than at the other three prospects.

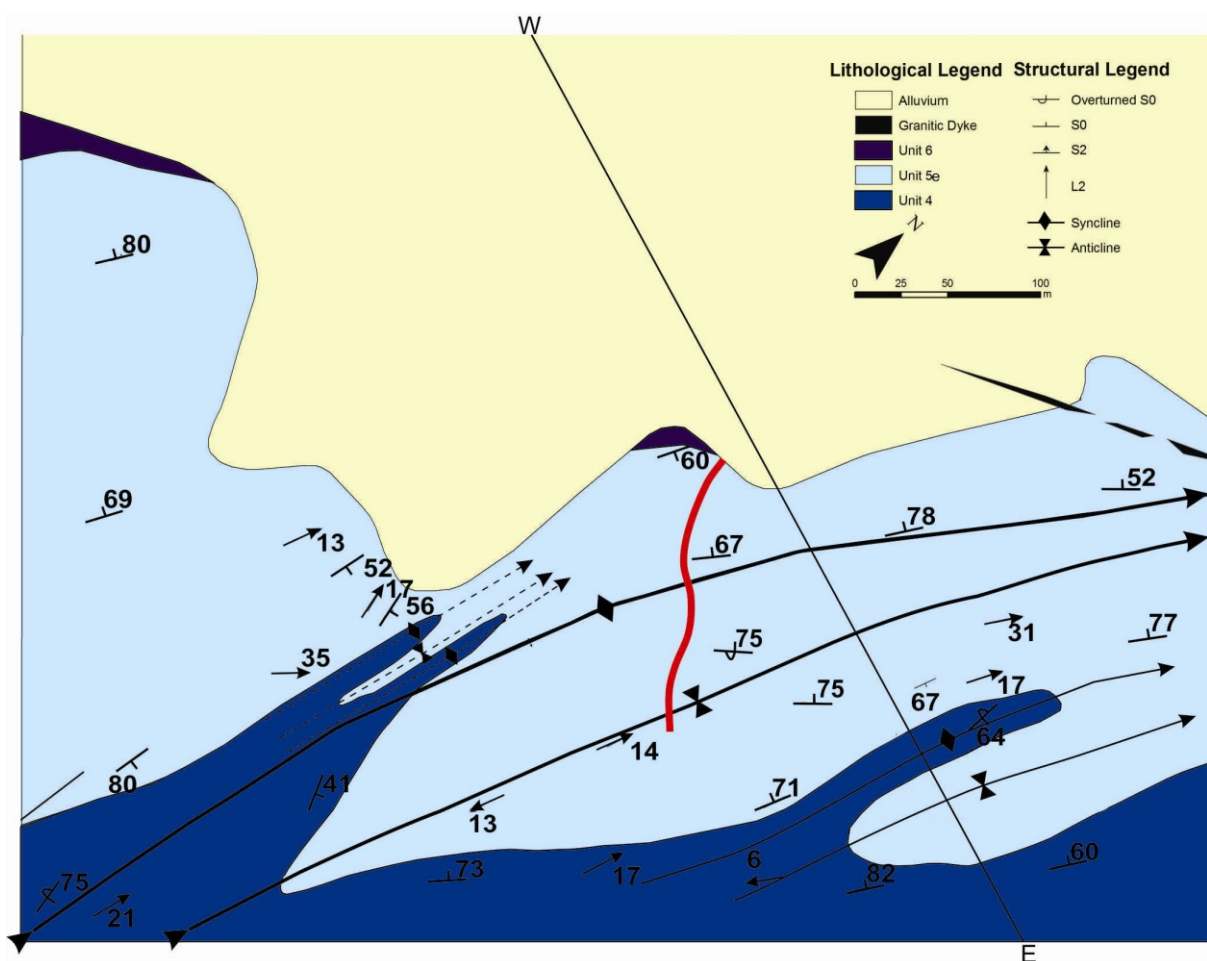


Figure 6.19: Geological map of Steenbok showing the location of the road cut analysed. The road cut (red line) runs oblique to the plunge of the folds at Steenbok.

Chapter 7 Discussion

7.1. Karibib Formation

The Karibib Formation was mapped in order to allow for a better correlation of lithostratigraphic units within the Navachab synform so as to identify the main rock units hosting the hydrothermal mineralisation. Previously, the identification of marble units was mainly of a descriptive nature (e.g. banded dolomitic marble, grey calcareous marble, etc.), but with only limited correlation between different parts of the synform. In addition, lithologies exert an important control on the mineralisation and the correlation of marble units and lithological packages would help to delineate zones of increased mineralisation potential.

7.1.1. Depositional Environment

A detailed discussion of the depositional environment and sedimentation of the Karibib Formation is beyond the scope of this study. However, the detailed subdivision of the Karibib Formation highlights a few aspects.

The Karibib Formation is a heterogeneous sequence in that it contains beds with varied composition, dolomitic vs. calcareous, and grain size, intraformational breccia vs. fine-grained laminated beds. Compositional cycles are observed on all scales from alternating packages of calcareous marble (units 1-4, 6) and dolomitic marble (unit 5), to alternating beds of calcareous and dolomitic marble and calc-silicate felsites. The fine-grained laminated marble is interrupted periodically by high-energy, mass-flow breccias.

Badenhorst (1992) suggests a platform, slope and basin configuration for the origin of the Karibib Formation with the platform situated to the north of Karibib (the "Otavi shelf") and the platform terminated in a NW inclined slope in the area of the Navachab synform with outer ramp facies to the far north in Okakango. Upper slope sediments in the Navachab

synform are covered by intertidal and supratidal carbonates (Badenhorst, op cit.) The slope origin of the Karibib Formation in the Navachab synform accounts for the abundance of high-energy mass flow breccias in the Karibib Formation, particularly in units 1-3, where breccias constitute up to 25% of the marble sequence. The thickness variations and, in fact, complete pinching of several metre thick breccia horizons as well as the thickness variations of the individual units possibly indicates the origin of the mass flows in channels created in the upper slope regions of the carbonate shelf at the time of sedimentation. This agrees with the erosional surfaces (e.g. Fig. 3.1b) observed in the Karibib Formation and underlines the turbiditic origin of the Karibib Formation as suggested by previous workers (e.g. Badenhorst, 1992; Miller, 2008).

7.1.2. Lithological controls on mineralisation

Lithological mapping of the Navachab synform has shown that all of the zoo prospects are centred around and within the thick package of dolomitic marble of unit 5 sandwiched by calcareous marbles of unit 4 and unit 6. There are two zones within and around unit 5 in which quartz veins are particularly abundant. This includes (1) the contact between unit 5e and the overlying calcareous marbles of unit 6, and (2) the dolomitic intraformational breccia of unit 5d, particularly the contact zone between the marble breccias (unit 5d) with the underlying massive dolomite of unit 5c. This highlights the significance of contacts between lithologies of different competencies for veining and, therefore, mineralisation.

During deformation, the interface between lithologies of varying competencies records prominent strain-rate gradients. In the case of the Navachab synform, the relatively incompetent calcareous marbles are able to accommodate deformation by ductile flow. This is clearly evidenced by the pervasive fabric development in the calcareous compared to dolomitic marbles and the strongly disharmonic folding in the calcareous marbles. The rheological stiffer dolomitic marbles, in contrast, show slower flow rates. Combined with lower tensile strengths of the competent dolomitic marble units, these marbles are prone to fracturing in order to accommodate the strain rate of the surrounding calcareous marble. In fact, veining (S_2P veins) and also the development of high-strain zones along the contact

zones indicate that e.g. flexural-slip during F_2 folding was localized along these zones. Strain localization, and associated veining and focusing of fluid-flow along lithological contacts is a commonly observed feature in many lode-gold deposits. Mineralized zones are preferentially concentrated along e.g. granite-greenstone contacts (e.g. Card, 1992; Robert and Poulsen, 2001; Cassidy et al., 1998; Peschler et al., 2006), massive BIF horizons enveloped by mafic and commonly chloritized metamafigs, or along the interface of ultramafic and mafic rocks (e.g. Vielreicher et al., 1994; Junqueira et al., 2007). In the Karibib district, the significance of rheological contrasts for fluid-flow and mineralisation is emphasized by the MC-type mineralisation of the main pit, but also Anomaly 16 in the hinge of the Usakos dome, to the SW of the study area. In both cases, mineralisation is confined to the contact between the siliciclastic Spes Bona Member and the stratigraphically lowest marble unit of the Damara Supergroup, the Okawayo Member. This aspect will be further discussed in chapter 7.3.

7.2. Structural Geology of the Navachab Synform

7.2.1. Structural Geometry of the Navachab synform

The Navachab synform shows a strongly non-cylindrical geometry, characterized by:

(1) variable plunges, both to the NE and SW and both for the first-order synform, as well as parasitic folds. In fact, numerous fourth- and fifth-order folds that determine the geology of the prospects are doubly plunging, although plunges remain predominantly shallow;

(2) highly variable interlimb angles. In the SW of the Navachab synform, dips are moderately to the east on the western limb and steep- to overturned on the eastern limb. Interlimb angles of second- and lower-order folds are open- to close. Towards the NE and along the axial trace of the synform, the interlimb angles of the first-, second-, and third-order folds are tight- to isoclinal. This tightening is the result of the progressive steeping of the bedding on the western limb of the Navachab synform. For example, at the Gecko prospect the dip of bedding is steep to the SW and further to the NE, in the Dernberg anticlinorium, dips are

steep- to overturned. For the eastern limb, the dips of bedding decrease from subvertical- to overturned to steep- to moderate dips, resulting in a slight SE vergence of the Navachab synform in the NE part of the study area. This also results in the more symmetrical shape of the Navachab synform in the NE compared to the SW, where the fold shows a pronounced NW vergence.

The steepening of bedding towards the NE of the Navachab synform is of paramount importance to the location of the mineralisation. All prospects are located on the steep- to subvertical limbs of fourth- and fifth-order folds in the upright, NE parts of the Navachab synform. In contrast, mineralisation is not developed in the SW and more open parts of the synform, despite the presence of the lithologically favourable unit 5.

7.2.2. Strain in the Navachab synform

The steepening of the fold limbs and systematic decrease in interlimb angle is associated with a distinct variation in strain from NE to SW and along the axial trace of the synform (chapter 5). Strain intensities in the SW parts of the Navachab synform are markedly lower indicated by the relatively open fold shapes of F_2 folds and the spaced nature of the SE-dipping S_2 foliation. The reason for this is probably related to the proximity of the broad hinge of the Usakos dome. The core of the hinge consists of the > 600 m thick succession of metapsammities, schists and calc-silicate felses of the Spes Bona Member. These rocks preserve internal structures very well, indicating relatively low-strain intensities. Given the competent nature of this thick package, regional shortening has resulted in only open- to close F_2 fold geometries. The underlying competent rock units have effectively prevented the tightening of folds in the directly overlying, incompetent marbles of the Karibib Formation. The effects of this basal strength beam is much less pronounced in the stratigraphically higher marble units away from the hinge and finds its expression in tighter fold shapes and upright fold geometries. This also implies the presence of detachment horizons within the Karibib Formation, since fold profiles in, at least, the first- and second-order folds are likely to be highly variable in a single fold. Detachment folding is clearly

evident in lower-order (fifth- and sixth) folds (e.g. Fig. 4.7a), but cannot be readily identified on a regional-scale.

Strain intensities in the NE-parts of the Navachab synform, corresponding to the steep- to vertical strata, are markedly higher. The steep limbs record a pronounced co-axial, NW-SE-directed, subhorizontal flattening strain. This is indicated by (1) the symmetrical and often chocolate-tablet type boudinage (both extension in the vertical and horizontal directions) of competent horizons (Fig. 4.4), (2) the symmetrical and prominent fold-axis parallel stretch (Fig. 4.5b), and (3) the near upright, steep SW and NE dipping S_2 (Domain B, Fig. 5.9) and associated bivergent folds resulting in e.g. the formation of the positive flower structure represented by the doubly-verging Dernberg anticlinorium (cross-section I-J, Fig. 4.6). All this indicates a geometrical hardening during folding in which the strata on the steepened limbs is rotated to subvertical attitudes and, hence, at right angles to the regional, NW-SE directed subhorizontal shortening strain. In this orientation, the strata cannot accommodate further shortening by e.g. further fold amplification and associated flexural-slip. Progressive shortening is rather accommodated by internal shortening and lateral or vertical flow. This internal shortening following the lock up of folds for flexural-slip is, in particular, illustrated by the S_2 development in the steep NE parts of the synform. This also has direct implications for the location of the mineralisation:

1. The S_2 foliation records a strain localization, resulting in the formation of anastomosing, small-scale, S_2 -parallel shear zones (Fig. 5.9). These shear zones nucleate preferentially along limbs of F_2 folds. The geometry and shear sense is of paramount importance (Fig. 6.10) since dilational jogs that form in bends of shear zones create areas of low-mean rock stress and form sinks into which fluid can enter and cause fracturing of the rock and subsequent veining (Fig. 6.11). Compressional jogs, in contrast, are sites of high-mean rock stress and rather forces fluid out. Inconsistent shear sense (NW and/or SE up and a variable strike-slip component, Fig. 5.8) indicates that the shear zones are not part of e.g. larger wrench tectonics, but really part of S_2 and forming conjugates that accommodate subhorizontal shortening and lateral and vertical extrusion of the rocks. This type of foliation development is not present in the SW and broader hinge of the synform.

2. In cases of pronounced rheological contrasts between units, and particularly along lithological contacts such as unit 5 and unit 6, parasitic folds may be sheared off along their limbs (Domain B, Fig. 5.9). Incompetent calcareous marbles form mullion-type structures that are able to pierce through and dismember limbs of dolomitic marbles. This scenario of dismembered folds of dolomitic marbles is illustrated in the NE panels of Grid A (Appendix IIIe, at 12 m and 18 m). Strain incompatibilities arising during the often detachment-type folding (refer to Fig. 4.7a) seem pertinent for the mineralisation, providing localized areas of dilation and increased veining leading to, in places, massively silicified and mineralized pods. This case is documented in Figure 6.11 and 6.12 which is located along the contact zone between unit 5e and unit 6 and exposed in the NE panels of Grid A. Similar zones of stockwork-type veining can be logged in core (e.g. borehole AWD-3, between metre 86.52 and 90.60; refer to Fig. 6.15b) along the same contact. Given the (1) shallow fold plunges, and (2) shallowly-plunging intersection between S_2 domains and bedding contacts, the mineralized shoots are expected to show shallow plunges, subparallel to F_2 fold hinges. However, given the irregular, anastomosing pattern of S_2 domains (e.g. documented in panels of Grid A, Fig. 5.9), ore shoots are most likely discontinuous on the scale of tens of metres, despite similar plunge directions.

In shallowly-dipping strata of the SW hinge, in contrast, shortening and folding can still be accommodated by flexural-slip accompanying the steepening of the fold limbs. This is the main structural difference between southern and northern extent of the Navachab synform, which bears directly on the localization of the mineralisation, i.e. all prospects and also the Navachab main pit are located in subvertical, highly-strained strata.

This structural control, i.e. the formation of high-strain domains superimposed on suitable lithological contacts seems pertinent for the formation of economically viable quartz veining, also highlighted by the lack of veining in unit 5 dolomitic marbles found in the low-strain hinge of the Usakos dome.

7.2.3. High-strain zones

The previous paragraphs highlight the significance of the spatial relationship between unit 5 and D_2 -related high-strain fabrics for quartz veining. In the study area, there are two distinct high-strain zones of regional extent (Fig. 4.6), located on the steep- to overturned NW limbs of first-order antiforms (Karibib and Usakos domes). The high-strain zones converge in the NE of the Navachab synform, but die out along strike. The often chocolate-tablet boudinage of competent rock in the high-strain zones indicates a pronounced co-axial shortening strain (D_2) and coincides with the tightening of the Navachab synform in the NE. However, both the NW and SE high-strain zone only affect the lower, mainly calcareous units of the Karibib Formation. The along-strike projection of the NW high-strain zone towards the NE only straddles the western limb of the Dernberg anticlinorium, where the Grid A and Klipspringer prospects are situated around unit 5 on the eastern limb of the first-order fold. The SE high-strain zone, identified by Kitt (2008), may link up with the shear zone excising units 1-3 along the SE limb of the Navachab synform in the NE of the study area. The open pit may therefore represent a right stepover with a dextral sense of shear for the high-strain zone and the shear zone (Fig. 7.1), and provide the structural dilatancy for the mineralisation.

Near the bifurcation of the Navachab synform near Gecko, a several metre wide zone of mylonites is developed along the contact of unit 5 and unit 6. Along strike, but below alluvial cover, the mylonites can be projected to join up at the Gecko prospect and further on to Grid A and Klipspringer. Given the close proximity of the high-strain zone to the hinge of the Navachab synform it is inferred that the high-strain zone may in fact turn around in the hinge and join up with Steenbok on the southern limb of the Navachab synform and continue along strike towards the NE.

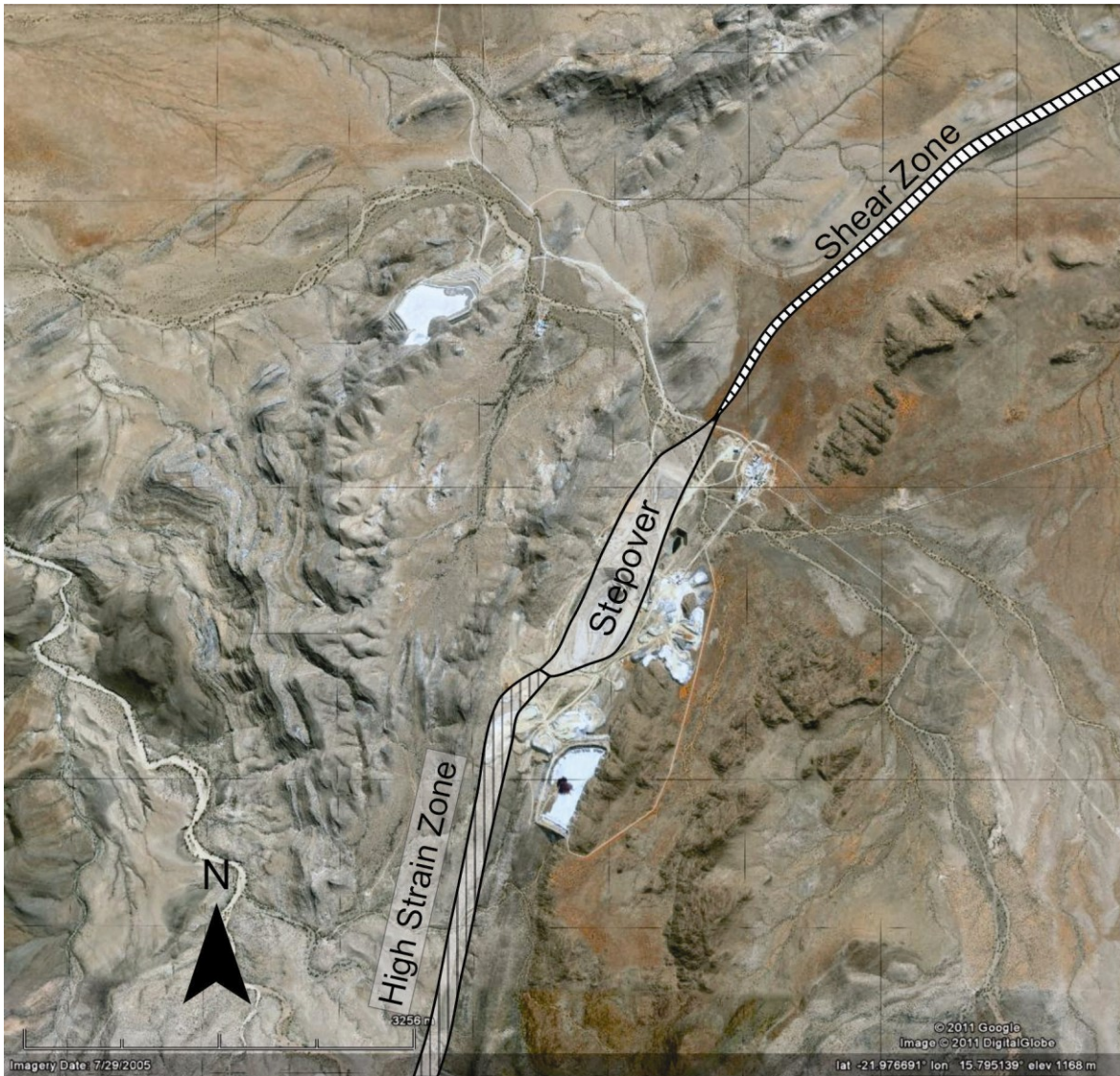


Figure 7.1: Schematic diagram showing the formation of a stepover in which the main pit at Navachab Gold Mine is hosted. The stepover has a dextral sense of shear. The SE high-strain zone links up with the shear zone identified in this study by means of the stepover. Google Earth image.

7.3. Quartz Veins

The Mohr-Coulomb theory of rock failure predicts the formation of extensional (mode I), extensional-shear, and shear fractures (mode II and III) in relationship to the orientation and magnitude of regional stresses, but also critically depending on fluid pressure (e.g. Sibson, 1996; Robert and Poulsen, 2001). Fluid pressure (P_f) counteracts normal stresses (σ_n) so that the effective normal stress (σ_n') acting on a plane is defined as $\sigma_n' = \sigma_n - P_f$ and fracturing of a rock mass is governed by the effective principle stresses defined as $\sigma_{1,2,3}' = \sigma_{1,2,3} - P_f$

(Robert and Poulsen, op cit.). Extensional fractures typically develop parallel to σ_1 when σ_3' equals or exceeds the tensile strength (T) of the rock, which is only possible under conditions of low differential stress, where $\sigma_3' \geq -T$ and $\sigma_1' - \sigma_3' \leq 4T$ (Robert and Poulsen, op cit.). Extensional fracturing, thus, only occurs for negative values of σ_3' . At the relatively high confining lithostatic pressures that prevail at the crustal levels inferred for the formation of lode gold deposits (> 2 kbars), this condition is only possible in the presence of elevated fluid pressure (e.g. Etheridge et al., 1983; Sibson et al., 1988; McCuaig and Kerrich, 1998). In fact, suprahydrostatic levels of lithostatic fluid pressures must be assumed for metamorphic terrains (greenschist-facies and above) recording deformation and associated quartz veining to allow for the formation of extensional fracturing (Etheridge et al., 1984; Cox et al., 1995). Shear fractures form when $\sigma_1' - \sigma_3' > 5.66T$ (Sibson, 2001). Thus extensional fractures are favoured in rocks of low tensile strength (here: dolomitic marbles) and/or at low differential stresses, and shear fractures form in rocks of higher tensile strength (here: calcareous marbles) and/or at higher differential stresses.

The quartz veins in the zoo prospects can be classified as shear- or extensional veins. The S₂P veins and the shear veins are shear fractures (veins), and the SSQ, ac- and conjugate vein sets occupy extensional fractures. Competency contrasts between the subunits has resulted in minor (10-20°) refraction of quartz veins and, in particular, ac veins. At the Steenbok prospect, the quartz veins have undergone an anticlockwise rotation by ca. 20-30 degrees when compared to the sets developed on the opposite limb of the Navachab synform. The strike of the bedding at Steenbok is more northerly when compared to the prospects on the NW limb of the Navachab synform, which may point to a post-emplacement rotation of the quartz veins and wall rocks to a more northerly strike.

The concentration of extensional veins in and around the dolomitic units 5d and unit 5e illustrates the theoretical relationships between rock competencies (tensile strengths), fluid pressures and mode of fracturing very well. For example, SSQ and, in particular, ac veins are almost exclusively found in unit 5d and, to a lesser extent unit 5e. The competent marble breccias of unit 5d must be considered to have been the lithology with the lowest tensile strength, so that extensional failure and veining during deformation is localized in and around these marble units. The orientation of the veins document the bulk shortening strain and the failure of the marbles normal to the local stretch (X, with $X \geq Y \geq Z$), i.e. both

subvertical (SSQ veins) and subhorizontal, fold (F_2)-axis parallel (ac veins). The presence of both vertical and horizontal veins indicate either alternating directions of the principal stretch or the fact, that the principal (X) and intermediate (Y) axes of stretch were very similar in magnitude ($X \approx Y \gg Z$, see also chapters 4.2 and 4.3).

S_2P veins, in contrast, are shear veins and mainly localized along the contacts between the dolomitic unit 5e and the incompetent calcareous unit 6. The veins are commonly folded (F_2), suggesting a bedding-parallel simple-shear component during and after their formation. The intense fabric development and parasitic folding most likely records the localization of the flexural-slip component along this contact during progressive F_2 folding and fold amplification. The veins form in the unit with the lower tensile strength, i.e. unit 5e, but stay close to the contact along which the shear has been resolved. The (1) abundance of S_2P veins along prominent lithological contacts (e.g. between units 5e and 6) and (2) folding of S_2P veins and vein clusters into F_2 -parallel folds further suggest an origin of the veins during F_2 folding and associated flexural-slip, particularly along prominent bedding anisotropies. Moreover, the commonly observed boudinage of S_2P veins also agrees with their orientation along or close to the S_2 foliation, i.e. the finite plane of shortening during D_2 .

It follows that although up to five different vein sets can be distinguished in each of the prospects, individual vein sets can be shown to be controlled by slightly different structural and lithological sites within and adjacent to the dolomitic units 5d and unit 5e. This highlights the subtle lithological controls of veining and vein geometries in addition to the structural controls during fluid-flow. The occurrence of individual vein sets is unlikely to have contributed to economic-grade mineralisation. It is rather the co-existence and intersection of two or more vein sets that account for a more significant fluid throughput and, thus, mineralisation. The significance of the intersection of vein sets for fluid and more pervasive throughput is also illustrated by the concentration of alteration in sites where two or more vein sets intersect (Fig. 7.2). In addition, localized, but pervasively silicified areas such as dilational jogs (Fig. 6.11) or boudin necks (Fig. 6.9) delineate zones of very high fluid throughput and mineralisation that are superimposed onto the more regional veining.

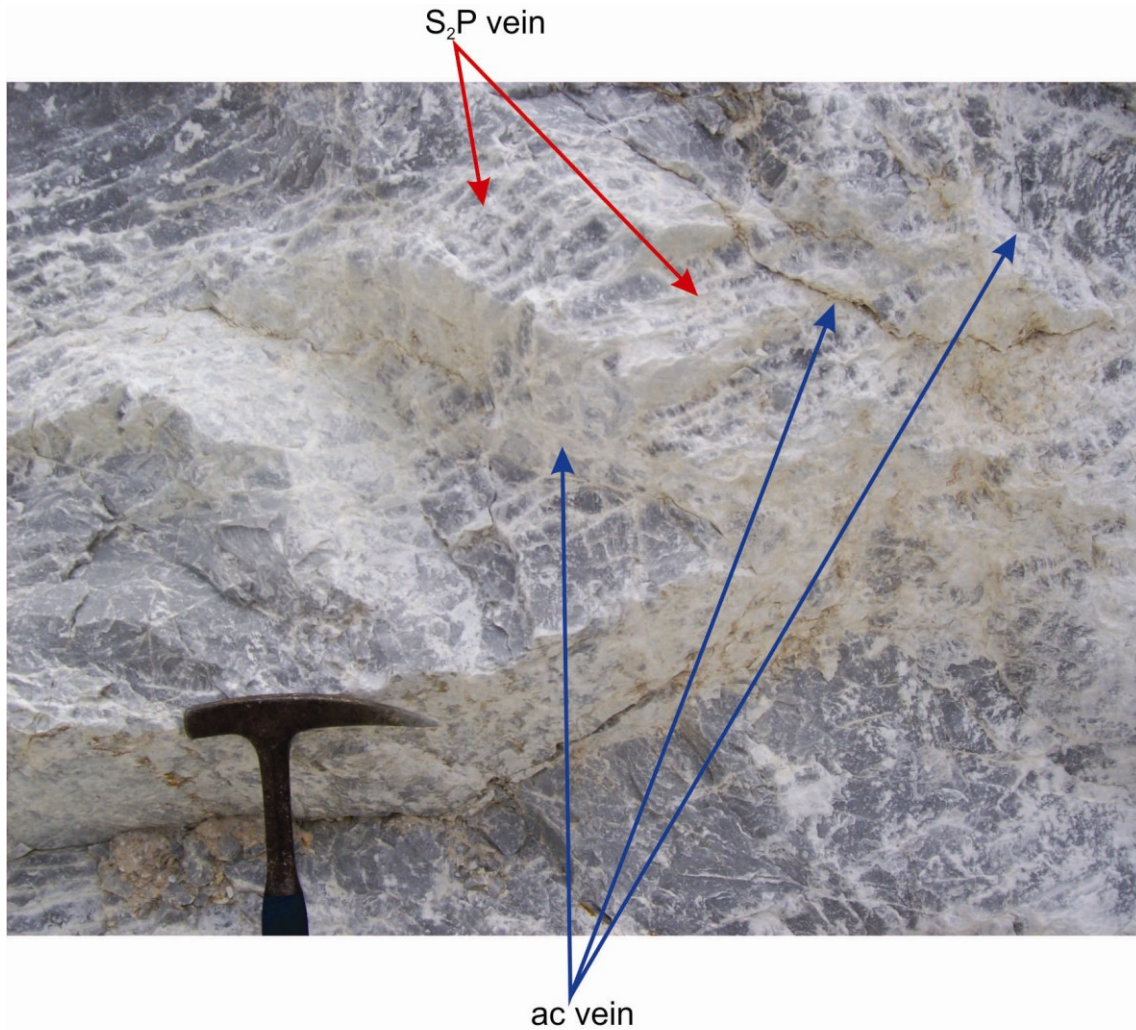


Figure 7.2: The intersection of two or more vein sets indicates the presence of increased fracture permeability required for increased fluid throughput and, hence, the potential for gold mineralisation. Here, the photo shows the intersection of a prominent set of S₂P veins (orientation annotated by red line) and high-angle ac veins (annotated by blue line).

7.3.1. Progressive Development of Quartz Veins

The relative timing of quartz-vein sets can be established based on cross-cutting relationships, deformation of the quartz veins and, also, the geometry of the quartz veins. S₂P veins are the first veins to form. The cross-cutting relationship of S₂P veins and ac veins is difficult to establish due to the often intense wall-rock alteration observed at the intersection of the two vein sets which masks any displacement of S₂P veins by ac veins. The later timing of ac veins is suggested by their only gentle folding, compared to the, in places, tightly folded and/or boudinaged S₂P veins. Cross-cutting relationships and deformation do

not allow to distinguish the relative timing between ac veins and sheeted quartz veins, and the two sets are considered to have formed largely contemporaneous. Conjugate and shear veins, in contrast, seem to have formed last as they appear largely undeformed. Cross-cutting relationships between conjugate veins and S_2P veins are often observed with the latter being displaced by the conjugate veins (Fig. 6.8c). The progressive deformation of S_2P veins during the steepening of fold limbs and the emplacement of e.g. ac-, SSQ- and conjugate veins into vertical limbs indicates that veining and fluid-flow were active over a protracted period of time. Given that normal strain rates are 10^{-13} to 10^{-15} s^{-1} , fluid-flow must be assumed to have occurred over at least 10^4 and possibly 10^5 years. The higher estimate takes into account that veining evidently occurred during the waning stages of deformation and, thus, slower strain rates.

Based on cross-cutting relationships and the overall structural evolution of prospects, quartz veining and mineralisation at the four prospects can be described as a two-stage process.

Stage 1

The first stage involves the development of early S_2P veins during flexural-slip (Fig. 7.3). The folding of the S_2P veins, when compared to the other four vein sets, indicates that (1) the veins must have been emplaced at an early stage, and (2) during fold amplification and steepening of F_2 fold limbs. The subsequent boudinage records the rotation of the veins into an S_2 -parallel orientation as a result of the steepening of the limbs, here undergoing layer-parallel stretch and chocolate-tablet type boudinage as it is recorded for competent units of the wall rocks (Fig. 6.2a). Flexural-slip on fold limbs reaches a maximum when the dip of fold limbs reaches $\sim 60^\circ$. This agrees with the general observation that shear veins occur predominantly in moderate- to steeply- dipping strata ($>45^\circ$) (Robert and Poulsen, 2001). This scenario is also realized in the zoo prospects, where S_2P clusters occur in steep strata and have an axial planar orientation. Similarly, this also accounts for the lack of quartz veining in the unit 5 dolomitic marbles in the hinge of the Usakos dome, where dips rarely exceed 30° . The theory predicts (Tanner, 1989) that flexural-slip and associated bedding-parallel veining cease to operate at dip angles of above $60 - 65^\circ$ due to the increase of the normal stress on the steepened bedding planes. At these dip angles, folding is no longer

associated with flexural-slip. The fold locks up and other fold mechanisms must accommodate further shortening of the fold (Tanner, 1989). In the Navachab synform this was achieved through co-axial flattening (layer-normal shortening and layer-parallel extension) of the competent units resulting in layer-parallel stretch in the form of boudinage of competent units and the second stage of mineralisation.

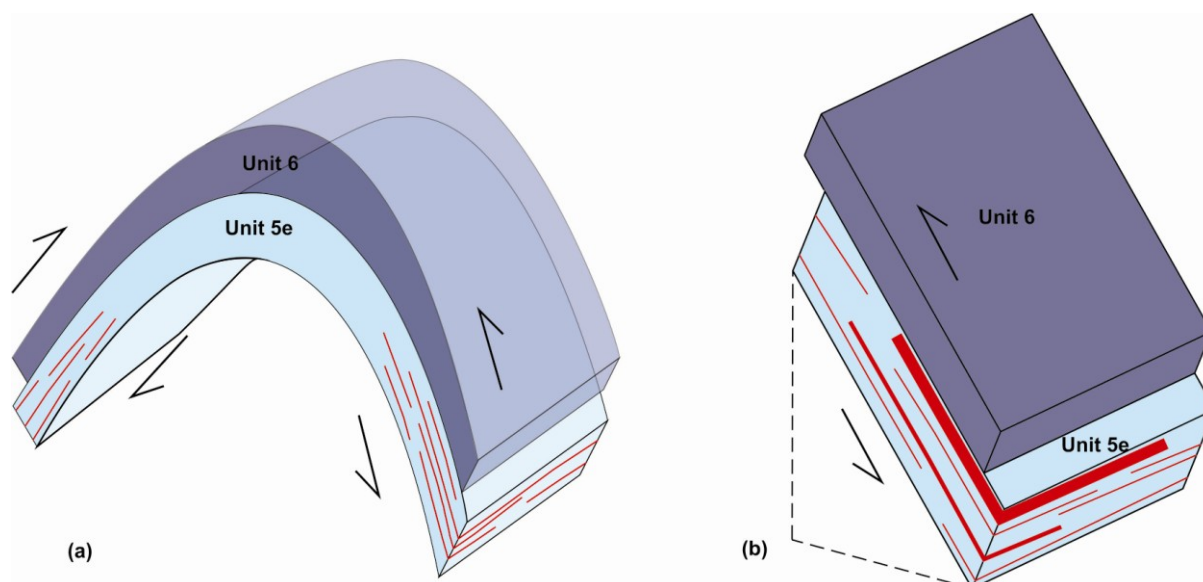


Figure 7.3: Stage 1 of mineralisation. (a) Illustration of the formation of S₂P veins (red lines) as a result of flexural-slip along the limb of an anticline. Flexural-slip is particularly localized along bedding contacts with pronounced rheological differences (e.g. unit 5e and unit 6). At this stage, the dip of the limbs is <65°. **(b)** Block diagram showing S₂P veins which form in response to flexural-slip when the dip of the limbs of folds is <65°. The formation of S₂P veins is confined to the competent dolomitic marbles of unit 5e.

Stage 2

The second stage of mineralisation occurred when further NW-SE directed shortening could no longer be accommodated by fold amplification and the fold locked up. At this stage, strain is accommodated by internal shortening of the strata. In the wall rocks, the stretch is indicated by predominantly subhorizontal, F₂ fold-axis parallel stretch and boudinage of competent horizons (Fig. 6.9) and a component of steep stretch and associated boudinage (Fig. 4.4) This enables the formation of (1) vertical, F₂ fold-axis normal fractures and veins (here: ac veins and conjugate set), and (2) subhorizontal veins (SSQ) that accompany the stretch and internal deformation of the wall-rock strata (Fig. 7.4). During this stage, boudinage of competent wall rocks and S₂P veins occurs. The presence of both horizontal (SSQ) and vertical (ac) vein sets and the inconsistent cross-cutting relationships between the

veins indicates that they formed at the same time. The orientation and co-existence of the quartz veins points to a largely co-axial, NW-SE-directed, subhorizontal layer-normal shortening strain during vein emplacement. This is further evidenced by the chocolate-tablet-type boudinage displayed by competent wall-rocks and the symmetrical folding of e.g. ac- and SSQ veins. The symmetrical folding of the vein sets also suggests that bedding-parallel flexural-slip had ceased to operate and that extensional veins were emplaced during the lock-up stage of F_2 folds, when limbs had rotated to steep ($>65^\circ$) attitudes.

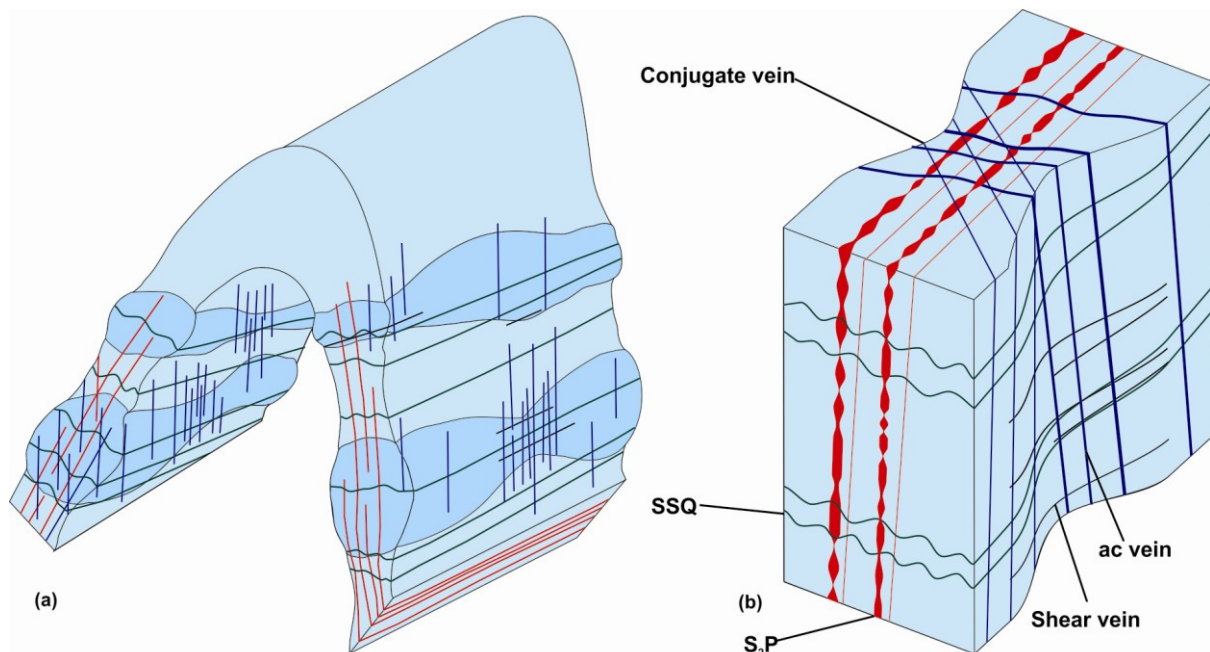


Figure 7.4: Stage 2 of mineralisation. When NW-SE directed shortening can no longer be accommodated by fold amplification, fold lock-up occurs and strain is accommodated by internal shortening of the strata and both vertical and horizontal extension. In the wall rocks, the stretch is indicated by predominantly subhorizontal, F_2 fold-axis parallel stretch and minor component of steep stretch along bedding planes and folded bedding. This enables the formation of (1) vertical, F_2 fold-axis normal fractures and veins (here: ac veins and conjugate set, purple lines), and (2) subhorizontal veins (SSQ, green lines) that accompany the stretch and internal deformation of the wall-rock strata. (a) Illustration of an anticline with dip of limbs $\geq 65^\circ$. SSQ veins formed as a result of early fracturing of the dolomitic marble. Layer-parallel stretch of competent rock causes boudinage and in the necks of boudins steep veins formed. Shear veins formed in the necks of boudins where NW-SE directed shortening resulted in a component of pure shear at 45° to shearing. (b) Block diagram showing the formation of SSQ veins as a result of subhorizontal fracturing, and subvertical fracturing in the necks of boudins resulted in the formation of ac- and conjugate set. The ac- and conjugate set of veins mainly form in the necks of boudins, but do occur outside of the necks. The diagram also shows the boudinage of the S_2P veins (red lines) and the folding of SSQ and ac veins.

In addition to the regular vein sets, localized dilational sites represent zones of massive fluid ingress as evidenced by the degree of silicification. Dilational jogs form as a consequence of the geometry and kinematics of S_2 -parallel, anastomosing shear zones that develop in

response to fold tightening and internal shortening of the rocks (Fig. 6.11). The Klipspringer-type mineralisation also forms during this stage, characterized by the localized fluid-flow into boudin necks of disrupted competent marble enveloped by calcareous marble (Fig. 6.9a). This type of mineralisation is localized to specific structural sites, but significant, given the sheer throughput of hydrothermal fluid these sites have evidently focussed.

The superimposition of the localized, dilational sites with the more regular vein sets clearly constitutes prime targets for exploration. This scenario is realized at Grid A where (a) rheological contrast in form of the contact between unit 5 and unit 6, (b) strain incompatibilities in the form of lower-order and detachment folding and S_2 -parallel, anastomosing shear zones, and (c) the presence of regular vein sets coincide. This scenario is less pronounced at the Gecko and Klipspringer prospects where rheological contrasts and regular vein sets are present, but strain incompatibilities that would have led to the formation of dilational sites are not that well developed. This scenario of spatially and temporally coinciding structural and/or lithological factors is even less pronounced at Steenbok, where (a) dolomitic marbles of unit 5 lack internal heterogeneities, (b) lower-order folding does not affect lithological contacts, and (c) regular vein sets are developed, but volumetrically subordinate.

These structural and lithological criteria allow to establish a broad hierarchy for the characterization of the mineralisation potential of the zoo prospects.

7.4. Fluid-flow in the Navachab Synform

The mineralizing fluid of the Navachab Gold Mine is suggested to be of metamorphic origin (Dziggel et al., 2009; Wulff et al., 2010) consistent with the geological, structural, and geochemical characteristics of the deposit (Wulff et al., 2010). However, crosscutting relationships between the quartz sulphide veins and intrusive aplite dykes in the Navachab open pit indicate that magmatic activity overlapped with the mineralization (Wulff et al., 2010), and that regional plutonism was coeval with deformation (Kisters et al., 2004). The granite plutonism must have played a fundamental role for the hydraulic regime in the

southern Central Zone of the Damara belt, even though the geochemical, fluid inclusion, and stable isotope data do not provide direct evidence for the magmatic input to the mineralizing fluids (Dziggel et al., 2009). The most likely explanation is that the ore fluids originated from deep crustal equivalents of the metapelitic units of the Damara Supergroup and were released by dehydration reactions during prograde metamorphism at subsolidus conditions (Wulff et al., 2010). At the amphibolite-facies grades prevailing in the Damara belt and typical bulk compositions of the metapelites, biotite is the dominant hydrous mineral in the clastic metasedimentary rocks. Fluid released at higher metamorphic grades should, therefore, mainly be generated by the breakdown of biotite and the fluid is then focused into suitable pathways such as high-permeability shear zones (Wulff et al., 2010). The extremely high geothermal gradients in the mine area (80°C/km) are probably related to the advection of heat by melts generated at deeper crustal levels which ascended along the same ductile structures mentioned above (Wulff et al., 2010). Wulff et al. (2010) conclude that although the production and ascent of magmas into upper-crustal levels may have contributed in concentrating and transporting gold and other metals from the sites of fluid production to that of ore deposition, the currently available petrological and geochemical data are most consistent with metamorphic dehydration as the dominant process in extracting fluids and metals from midcrustal levels.

The zoo prospects occur within a radius of less than three kilometres from the gold mineralisation of the main Navachab open pit. Based on the quartz-vein inventory and the deformation of quartz veins, the relative timing of fluid-flow in the prospects coincides with the syn- to late- D_2 timing of mineralisation in the main open pit. Hence, the fluid system of the main open pit and that responsible for the mineralisation of the prospects formed, in all likelihood, part of the same, larger hydrothermal system. However, the style of mineralisation and alteration displays significant differences. The mineralisation in the zoo prospects is relatively poor in sulphides and the alteration is dominated by tremolite around the quartz veins. In contrast, the MC-type mineralisation in the main pit, in particular, is sulphide rich, with the occurrence of massive pyrrhotite pods. The alteration around both the MC-type mineralisation and the sheeted quartz veins is dominated by biotite-garnet-clinopyroxene assemblages (e.g. Nörtemann et al., 2000; Wulff et al., 2010). Questions then arise as to whether the hydrothermal systems were physically interconnected and what the

overall geometry of fluid-flow patterns was at the time of mineralisation. This assumes that mineralisation, alteration and quartz veins represent the vestiges of fluid channelways.

Several key observations can be made:

1. Fluid-flow is strictly fracture controlled. This is to be expected in the high-grade metamorphic sequence, but is probably even more so in the case of the marble-dominated succession, in which the pervasive dynamic recrystallization of the high-grade marbles during deformation will tend to close any grain-scale permeabilities. This is a peculiar feature of the Navachab-style mineralisation. Quartz veining is not necessarily associated with high-strain zones, as is the case with many shear-zone hosted lode-gold deposits. The ductility of the high-grade marbles prevented fracturing and veining, even in the presence of the most likely close-to-lithostatic fluid pressures. In order to develop fracture permeabilities and veins, additional lithological controls are required.
2. Fracturing occurs preferentially at lithological interfaces between rock types of different competencies and tensile strengths. This is the case for e.g. the MC-type mineralisation, the well-mineralized zones in the main Navachab Pit and at Anomaly 16, comprising the contact between Spes Bona Member schists and calc-silicate felses and Okawayo Member marbles. This is also the case for the zoo prospects that are centred around the dolomitic unit 5. Veining occurs where high-strains (steep, sheared F_2 limbs) coincide with this prominent rheological contact. Zones of higher, fracture-controlled fluid-flow will, thus, be stratabound, following rheological contacts and the geometry of the folded layers. Unless there is a structural connection between the stratigraphically controlled zones of increased permeability, fluid-flow will be largely confined to these layers, with no or only very limited connectivity. The NE-trending D_2 high-strain zones of more regional extent are developed in the lower formation of the Karibib Formation. Increased veining and potential mineralisation should be expected where the D_2 high-strain zones and e.g. unit 5 dolomitic marbles intersect. The closest situation to this scenario occurs on the western limb of the Dernberg anticlinorium, although D_2 strains are markedly lower and unit 5 is only sporadically preserved in synformal hinges.

3. Ore shoots in the Navachab mine show shallow plunges (e.g. Moore et al., 1999; Steven and Badenhorst, 2002; Wulff et al., 2010), either to the NNE or SSW and parallel to F_2 folds. These linear shoots lie in the plane of bedding, i.e. the contacts between rheologically favourable units. This highlights the control of fluid-flow by D_2 structures and the formation of directional permeability enhancement (zones or shoots of increased veining) parallel to D_2 structures. Regional-scale fluid-flow will be buoyancy controlled, so that the shallow-plunging shoots are at high angles to the mainly upward-directed flow. Shallowly-plunging fluid pathways may connect within the same layer and along the strike of the layer within which they are contained. This is likely to be the case between the Gecko, Grid A and Klipspringer prospects, although all prospects combine characteristics that are not or only partly realized in the other prospects (see chapter 5). A connectivity between different stratigraphic levels, e.g. the MC-type and zoo prospect mineralisation, is less likely. This is particularly so, given the presence of the largely impermeable lower units of the Karibib Formation that may, in fact, have acted as aquitards.

Chapter 8 Concluding Remarks

The regional structural and lithological mapping of the Navachab synform combined with the detailed mapping of the quartz veins in the zoo prospects has allowed for the identification of the controls of quartz veining in the Karibib Formation in the Navachab synform. From this study the main conclusions that can be drawn are:

The lithological mapping of the Karibib Formation in the Navachab synform has found that the Karibib Formation can be subdivided into six main units with the subdivision based on correlations between different sections traversed and lithological characteristics. This subdivision has led to a new geological map for the Navachab synform and allowed for the structural and stratigraphical position of each prospect to be determined. The study has found that the zoo prospects are situated within a thick, competent dolomitic marble horizon (unit 5) that is over- and underlain by thick, less competent calcareous marble horizons (unit 6 and unit 4 respectively). Furthermore this study has found that unit 5 can be further subdivided into five subunits (units 5a-e) each with different competencies. Lithological contrasts that exist between different units in the Karibib Formation of different competency exert a primary control on quartz veining. The greatest competency contrast and, hence, the larger zone of mineralisation exists between massive dolomitic marble (unit 5e) and calcareous marble (unit 6). A smaller zone of mineralisation is located at the contact of massive dolomitic marble (unit 5c and 5e) and dolomitic breccia (unit 5d). The massive dolomitic marble is the more competent rock in both cases and has a lower tensile strength than the incompetent rock and will fracture earlier in order to accommodate the strain rate of the surrounding incompetent rock. This factor is similar to the MC-type mineralisation at the contact of the Spes Bona Member and Okawayo Member in the main pit at Navachab Gold Mine and Anomaly 16 in the Usakos dome. The veining and mineralization is restricted to the higher strained, steeper beds of fourth- and fifth order folds in the tighter NE parts of the Navachab synform away from the SW hinge zone.

Through the correlation of units throughout the Navachab synform, it has been demonstrated that (1) parts of the carbonate units are structurally highly attenuated and significantly reduced in thickness. This occurs in S_2 -parallel high-strain zones, developed on

the steep- to overturned limbs of the first-order F_2 folds of the Karibib and Usakos domes and bounding the Navachab synform; and (2) a significant section of the lower 3 units has been completely excised from the Karibib Formation along the steep limb shared between the Navachab synform and adjacent Karibib dome.

The steep strata observed in the north of the Navachab synform resulted in geometric hardening of the Karibib Formation and lead to the formation of five distinct veins sets which developed in response to different accommodation of folding mechanisms, i.e. flexural-slip is succeeded by internal shortening and extension. Vertical and horizontal extension leads to fracturing of competent horizons and veining. Again this is similar to the main pit, but is not realized at Anomaly 16. However, a major difference exists between the main pit and the Navachab synform in that the horizontal extension is more prominent in the former, i.e. there is no ac veins in the main pit but are abundant in the synform.

High-strain and structural complexities are observed in the north of the Navachab synform. Internal shortening resulting from the tightening of the Navachab syncline lead to high-strain and the development of anastomosing S_2 . Depending on the geometry and relationship to structures (contacts, parasitic folds etc.) dilational sites resulted and acted as fluid sinks. A similar relationship is observed in boudin necks where higher finite strains and resulting necking of rocks create dilation.

Lastly, the intersection of veins is of paramount importance as it is where veins of two or more sets intersect that the highest potential for mineralisation is realized. The intersection of veins is specifically noted along contacts or structural irregularities (detached folds, undulating contacts etc.).

Where all these factors are realized there is a good potential for mineralisation, and where one or more of these factors is missing there is a lower potential for mineralisation.

References

Ameglio, L., Page, P. and Jacob, R.E., (2000). 3D-geometry of the Mon Repos granodiorite (Goas dioritic suite, Damara Belt, Namibia) inferred from gravity data. *Journal of African Earth Science*, 31, p. 2.

Badenhorst, F.P., (1992). The Lithostratigraphy of area 2115B and D in the Central Zone of the Damara Orogen in Namibia: with emphasis on facies changes and correlation, unpublished MSc thesis. University of Port Elizabeth. P. 124

Blaine, J.L., (1977). Tectonic evolution of the Waldau Ridge structure and the Okahandja Lineament, South West Africa. *Precambrian Research Unit Bulletin*, 21, p. 99.

Brandt, R., (1985). Preliminary report on the stratigraphy of the Damara Sequence and the geology and geochemistry of the Damaran granites in an area between Walvis Bay and Karibib. *Communications of the Geological Society of Namibia*, 1, 31-43.

Card, K.D., (1992). A review of the Superior Province of the Canadian Shield, a product of Archean accretion. *Precambrian Research Unit*, 48, 99-156.

Cassidy, K.F.D., Groves, D.I. and Mcnaughton, N.J., (1998). Late-Archean granitoid-hosted lode gold deposits, Yilgarn Craton, Western Australia: Deposit characteristic, crustal architecture, and implications for ore genesis. *Ore Geology Reviews*, 13, 65-102.

Corner, B., (1983). An interpretation of the aeromagnetic data covering the western portion of the Damara Orogen in South West Africa/Namibia. In: Miller, R. McG. (Ed.), *Evolution of the Damara Orogen of South West Africa/Namibia*. *Geol. Soc. S. Afr. Special Publication*, vol. 11, pp. 339-354.

Coward, M.P., (1983). The tectonic history of the Damara Belt. In: Miller, R. McG. (Ed.), *Evolution of the Damara Orogen in South West Africa/Namibia*. *Geol. Soc. S. Afr. Special Publication*, vol.11, pp. 409-421.

Cox, S.F., Sun, S.S., Etheridge, M.A. and Potter, T.F., (1995). Structural and geochemical controls on the development of turbidite-hosted gold quartz vein deposits, Wattle Gully mine, central Victoria, Australia. *Economic Geology*, 90, 1722-1746.

de Kock, G.S., (1992). Forearc basin evolution in the Pan-Africa Damara Belt, central Namibia: the Hureeb Formation of the Khomas Zone. *Precambrian Research Unit*, 57, 169-194.

Downing, K.N., (1982). Evolution of the Okahandja lineament and its significance in Damaran Tectonics (Namibia), unpublished Ph.D. thesis. University of Leeds, 242 pp.

Dziggel, A., Wulff, K., Kolb, J. and Meyer, F.M., (2009). Processes of high-T fluid-rock interaction during gold mineralization in carbonate-bearing metasediments: the Navachab gold deposits, Namibia. *Mineralium Deposita*, v. 44, 665-687.

Etheridge, M.A., Wall, V.J. and Vernon, R.H., (1983). The role of fluid phase during regional metamorphism and deformation. *Journal of Metamorphic Geology*, 1, 205-226.

Ferry, J.M., (1994). A historical review of metamorphic fluid flow. *Journal of Geophysical Research*, 99, 15487-15498.

Frimmel, H.E., (2009). Configuration of Pan-African Orogenic Belts in Southwestern Africa. In: Gaucher, A.N., Sial, A.N., Halverson, G.P., and Frimmel, H.E, Neoproterozoic-Cambrian tectonics, global change and evolution: A focus on Southwestern Gondwana. *Developments in Precambrian Geology*, 16, 145-151.

Goldfarb, R.J., Groves, D.I. and Gardoll, S., (2001). Orogenic gold and geologic time: a global synthesis. *Ore Geology Reviews*, 18, 1-75.

Goldfarb, R.J., Phillips, G.N. and Nokleberg, W.J., (1998). Tectonic setting of synorogenic gold deposits of the Pacific Rim. *Ore Geology Reviews*, 13, 185-218.

Goscombe, B., Gray, D., Armstrong, R., Foster, D.A. and Vogl, J., (2005). Event geochronology of the Pan-African Kaoka Belt, Namibia. *Precambrian Research Unit*, 140, 103.e1-103.e41.

Gray, D.R., Foster, D.A., Goscombe, B., Passchier, C.W. and Trouw, R.A.J., (2006). Ar/Ar thermochronology of the Pan-African Damara Orogen, Namibia, with implications for tectonothermal and geodynamic evolution. *Precambrian Research Unit*, 150, 49-72.

Groves, D.I., (1993). The crustal continuum model for late Archean lode gold deposits of the Yilgarn Block, Western Australia. *Mineral Deposita*, 28, 366-374.

Groves, D.I., Goldfarb, R.J., Robert, F. and Hart, C.J.R., (2003). Gold deposits in metamorphic belts: overview of current understanding, outstanding problems, future research and exploration significance. *Economic Geology*, 98, 1-29.

Groves, D.I., Goldfarb, R.J., Gebre-Mariam, M., Hagemann, S.G. and Robert, F., (1998). Orogenic gold deposits: A proposed classification in the context of their crustal distribution and relationship to other gold deposit types. *Ore Geology Reviews*, 13, 7-27.

Hodgson, C.J., (1989). The structure of shear-related, vein-type gold deposits: a review. *Ore Geology Reviews*, 4, 231-273.

Hoffmann, K.H., Condon, D.J., Bowring, S.A. and Crowley, J.L., (2004). U-Pb zircon date from the Neoproterozoic Ghaub Formation, Namibia: Constraints on Marinoan glaciations. *Geology*, 32, 817-820.

Jacob, R.E., (1974). Geology and metamorphic petrology of part of the Damara Orogen along the Lower swakop River, South West Africa. *Precambrian Research Unit*, vol. 17, 185 pp.

Jacob, R.E., Moore, J.M. and Armstrong, R.A., (2000). Zircon and titanite age determinations from igneous rocks in the Karibib district, Namibia: implications for Navachab vein-style gold mineralization. *Communication Geological Survey of Namibia*, 12, 157-166.

Johnson, S.D., (2005). Structural geology of the Usakos dome, Damara Belt, central Namibia, unpublished MSc thesis. University of Stellenbosch, 159 pp.

Jung, S. and Mezger, K., (2003). Petrology of basement-dominated terranes: I regional metamorphic T-t path from U-Pb monazite and Sm-Nd garnet geochronology (Central Damara Orogen, Namibia). *Chemical Geology*, 198, 223-247.

Jung, S., Hoffer, E. and Hoernes, S., (2007). Neo-proterozoic rift-related syneites (Northern Damara Belt, Namibia): Geochemical and Nd-Sr-Pb-O isotope constraints for mantle sources and petrogenesis. *Lithos*, 96, 415-435.

Junqueira, P.A., Lobato, L.M., Ladeira, E.A. and Simoes, E.J.M., (2007). Structural control and hydrothermal alteration at the BIF-hosted Raposos lode-gold deposit, Quadrilátero Ferrífero, Brazil. *Ore Geology Reviews*, 32, 629-650.

Kasch, K.W., (1983a). Folding and thrust tectonics in the south-eastern portion of the Damara Orogen around Omitara, Namibia. In: Miller, R. McG. (Ed.), *Evolution of the Damara Orogen of South West Africa/Namibia*. Geol. Soc. S. Afr. Special Publication, vol.11, 175-184.

Kasch, K.W., (1983b). Continental collision, suture progradation and thermal relaxation: A plate tectonic model for the Damara Orogen in central Namibia. In: Miller, R. McG. (Ed.), *Evolution of the Damara Orogen of South West Africa/Namibia*. Geol. Soc. S. Afr. Special Publication, vol.11, 423-429.

Kisters, A.F.M., (2005). Controls of gold-quartz vein formation during regional folding in amphibolites-facies, marble-dominated metasediments of the Navachab Gold Mine in the Pan-African damara Belt, Namibia. *South African Journal of Geology*, 108, 283-303.

Kisters, A.F.M., Jordaan, L.S. and Neumaier, K., (2004). Thrust-related dome structures in the Karibib district and the origin of orthogonal fabric domains in the South Central Zone of the Pan-African Belt, Namibia. *Precambrian Research Unit*, 133, 283-303

Kitt, S.L., (2008). Structural controls of auriferous quartz veins in the Karibib Area, Southern Central Zone of the Pan-African Damara Belt, Namibia, MSc thesis. University of Stellenbosch, 147 pp.

Kroner, A., (1984). Dome structures and basement reactivation in the Pan-African Damara Belt of Namibia (South West Africa). In: Kroner, A. and Greiling, R.O. (Eds.), *Precambrian Tectonics Illustrated*, 191-206.

Kukla, P.A. and Stanistreet, I.G., (1991). Record of the Damaran Khomas Hochland Accretionary Prism in central Namibia: Refutation of an "ensialic" origin of a late Proterozoic Orogenic Belt. *Geology*, 19, 473-476.

Masberg, H.P., (2000). Garnet growth in the medium pressure granulite-facies metapelites from the central Damara Orogen: igneous versus metamorphic history. *Communications of the Geological Survey of Namibia*, 12, 115-124.

McCuaig, T.C. and Kerrich, R., (1998). P-T-t-deformation-fluid characteristics of lode gold deposits: Evidence from alteration systematic. *Ore Geology Review*, 12, 381-453.

Miller, R.M., (1983). The Pan-African Damara orogen of South West Africa/Namibia. In: Miller, R.M. (Ed.), *Evolution of the Damara Orogen of South West Africa/Namibia*. Geol. Soc. S. Afr. Special Publication, vol.11, 431-515.

Miller, R.M., (2008). *The Geology of Namibia*. Ministry of Mines and energy Geological Society.

Miller, R.M., Frimmel, H.E. and Will, T.M., (2009). Geodynamic synthesis of the Damara Orogen Sensu Lato. In: Gaucher, C., Sial, A.N., Halverson, G.P. and Frimmel, H.E. (Eds.), *Neoproterozoic-cambrian tectonics, global change and evolution: a focus on southwestern Gondwana*, 16, 231-235.

Moore, J.M. and Jacob, R.E., (1998). The Navachab sheeted vein/skarn Au deposit, Namibia: a meothermal sheeted-vein/skarn system related to the Pan-African Damara Orogen. *Journal of African Earth Sciences*, 50-51.

Nörtemann, M.F.J., Mucke, A., Weber, K. and Meinert, L.J., (2000). Mineralogy of the Navachab skarn deposit, Namibia: an unusual Au-bearing skarn in high-grade metamorphic rocks. *Communications of the Geological Survey of Namibia*, 149-156.

Oliver, G.J.H., (1994). Mid-crustal detachment and domes in the central zone of the Damara Orogen, Namibia. *Journal of African Earth Sciences*, 19, 331-344.

Oliver, N.H.S., (1996). Review and classification of structural controls on fluid flow during regional metamorphism. *Journal of Metamorphic Geology*, 477-492.

Owen, G., (2010). *Geology of the Kranzberg Syncline and emplacement controls of the Usakos pegmatite fluid, Damara Belt, central Namibia*, unpublished MSc thesis. University of Stellenbosch.

Peschler, A.P., Benn, K. and Roest, W.R., (2006). Gold-bearing fault zones related to Late Archean orogenic folding of upper and middle crust in the Abitibi granite-greenstone belt, Ontario. *Precambrian Research Unit*, 151, 143-159.

Phillips, N.G. and Powell, R., (2009). Formation of gold deposits: Review and evaluation of the continuum model. *Earth-Science Reviews*, 94, 1-21.

Poli, L.C. and Oliver, G.J., (2001). Constrictional deformation in the Central Zone of the Damara Orogen, Namibia. *Journal of African Earth Sciences*, 33, 303-321.

Porada, H., (1985). Stratigraphy and facies in the upper Proterozoic Damara Orogen, Namibia, based on a geodynamic model. *Precambrian Research*, 29, 235-264.

Porada, H., (1989). Pan-African rifting and orogenesis in southern to equatorial Africa and eastern Brazil. *Precambrian Research Unit*, 44, 103-136.

Prave, A.R., (1996). Tale of three cratons: Tectonostratigraphic anatomy of the Damara Orogen in northwestern Namibia and the assembly of Gondwana. *Geology*, 24, 1115-1118.

Ridley, J., (1993). The relations between mean rock stress and fluid flow in the crust: With reference to vein- and lode-style gold deposits. *Ore Geology Reviews*, 8, 23-37.

Robert, F. and Poulsen, K.H. (2001). Vein Formation and deformation in greenstone gold deposits. *Reviews in Economic Geology*, 14, 111-155.

Sawyer, E.W., (1981). Damaran structural and metamorphic geology of an area south-east of Walvis Bay, South West Africa/Namibia. *Geological Survey of South West Africa/Namibia*, 7, 94 pp.

Sibson, R.H., Robert, F. and Poulsen, K.H. (1988). High-angle reverse faults, fluid pressure cycling and mesothermal gold-quartz deposits. *Geology*, 16, 551-555.

Stanistreet, I.G., Kukla, P.A. and Henry, G., (1991). Sedimentary basinal responses to a late Precambrian Wilson Cycle: the Damara orogen and Nama Foreland, Namibia. *Journal of African Earth Sciences*, 13, 141-156.

Steven, N.M. (1993). A study of epigenetic mineralization in the Central Zone of the Damara Orogen, Namibia, with special reference to gold, tungsten, tin and rare earth elements. *Memoirs of the Geological Survey of Namibia*, 16, 166 pp.

Steven, N.M. and Badenhorst, F. (2002). Mesothermal gold deposits of the Damara Orogen. Excursion guidebook, 11th Quadrennial IAGOD Symposium and Geocongress, Windhoek, 225 pp.

Steven, N.M., Badenhorst, F.P., Kitt, S. and Wulff, K. (2008). The Navachab gold deposit, Namibia: the largest non-Witwatersrand-type gold deposit in southern Africa. Extended Abstracts. SEG-GSSA Conference, Misty Hills, South Africa.

Tack, L. and Bowden, P. (1999). Post-collisional granite magmatism in the central Damaran (Pan-African) orogenic belt, western Namibia. *Journal of African Earth Science*, 28, 653-674.

Tanner, P.W.G. (1989). The flexural-slip mechanism. *Journal of Structural Geology*, 11, 635-655.

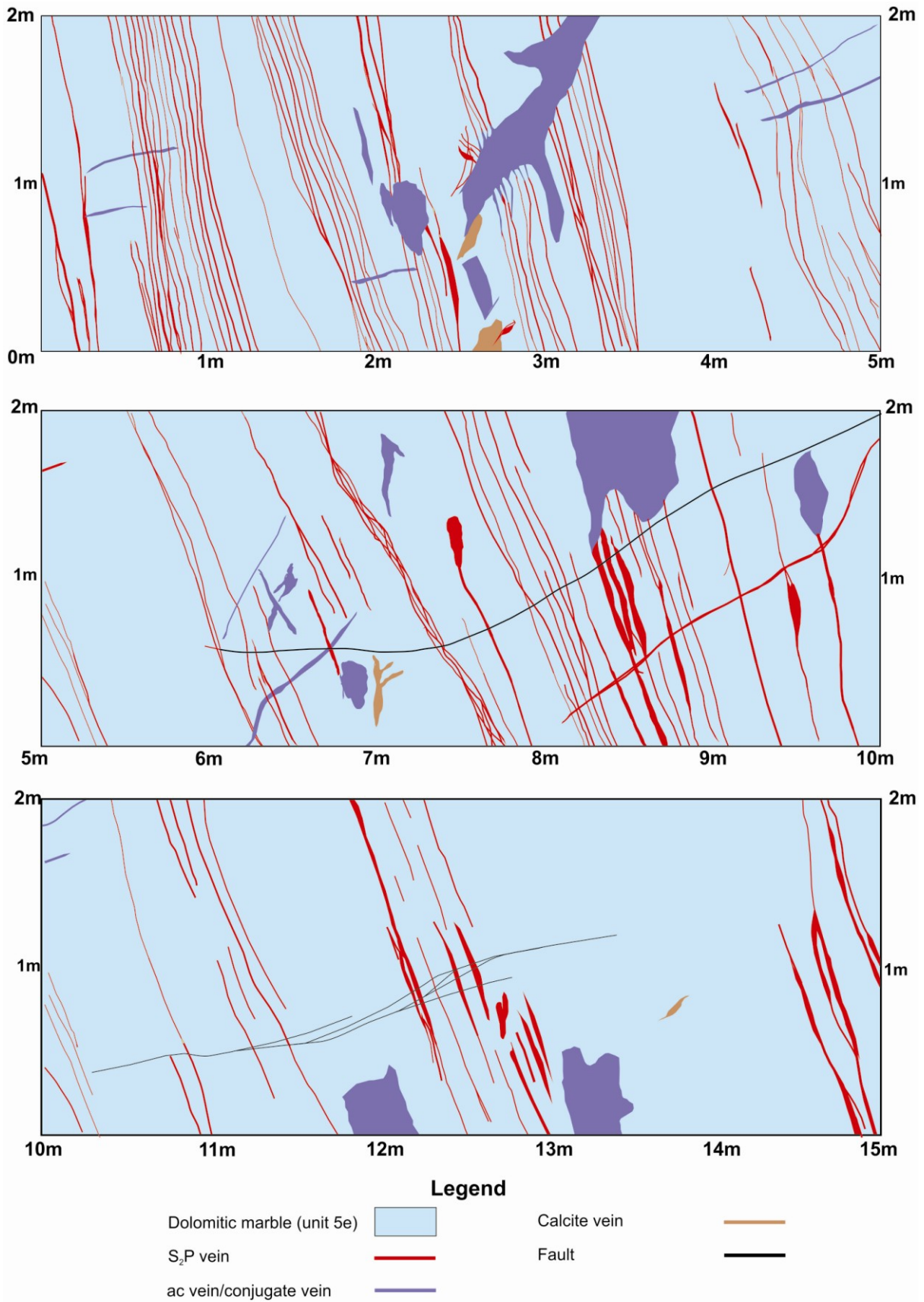
Vearncombe, J.R. (1998). Shear zones, fault networks, and Archean gold. *Geology*, 26, 855-858.

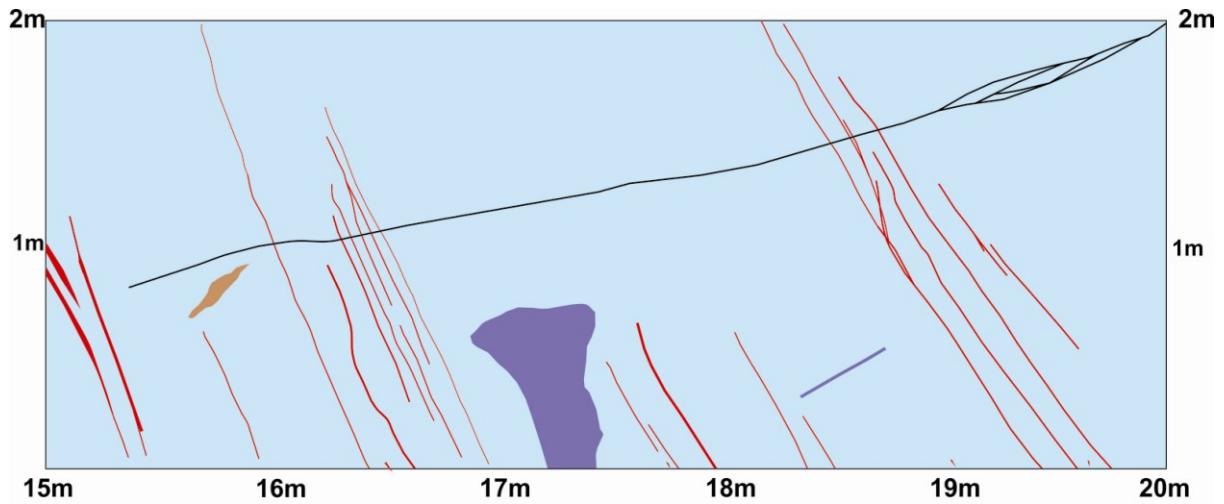
Vielreicher, R.M., Groves, D.I., Ridley, J.R. and McNaughton, N.J. (1994). A replacement origin for the BIF-hosted gold deposit at Mt. Morgans, Yilgarn Block, W.A. *Ore Geology Reviews*, 9, 352-347.

Ward, R.G., Stevens, G. and Kisters, A.F.M. (2008). Fluid and deformation induced partial melting and melt volumes in low-temperature granulite-facies metasediments, Damara Belt, Namibia. *Lithos*, 105, 253-271.

Wulff, K., Dziggel, A., Kolb, J., Vennemann, T., Böttcher, M.E. and Meyer, F.M. (2010). Origin of mineralizing fluids of the sediment-hosted Navachab Gold Mine, Namibia: constraints from stable (O, H, C, S) isotopes. *Economic Geology*, 105, 285-302.

Appendix IIa: Gecko Pit 1 Panel 1; Cross-section

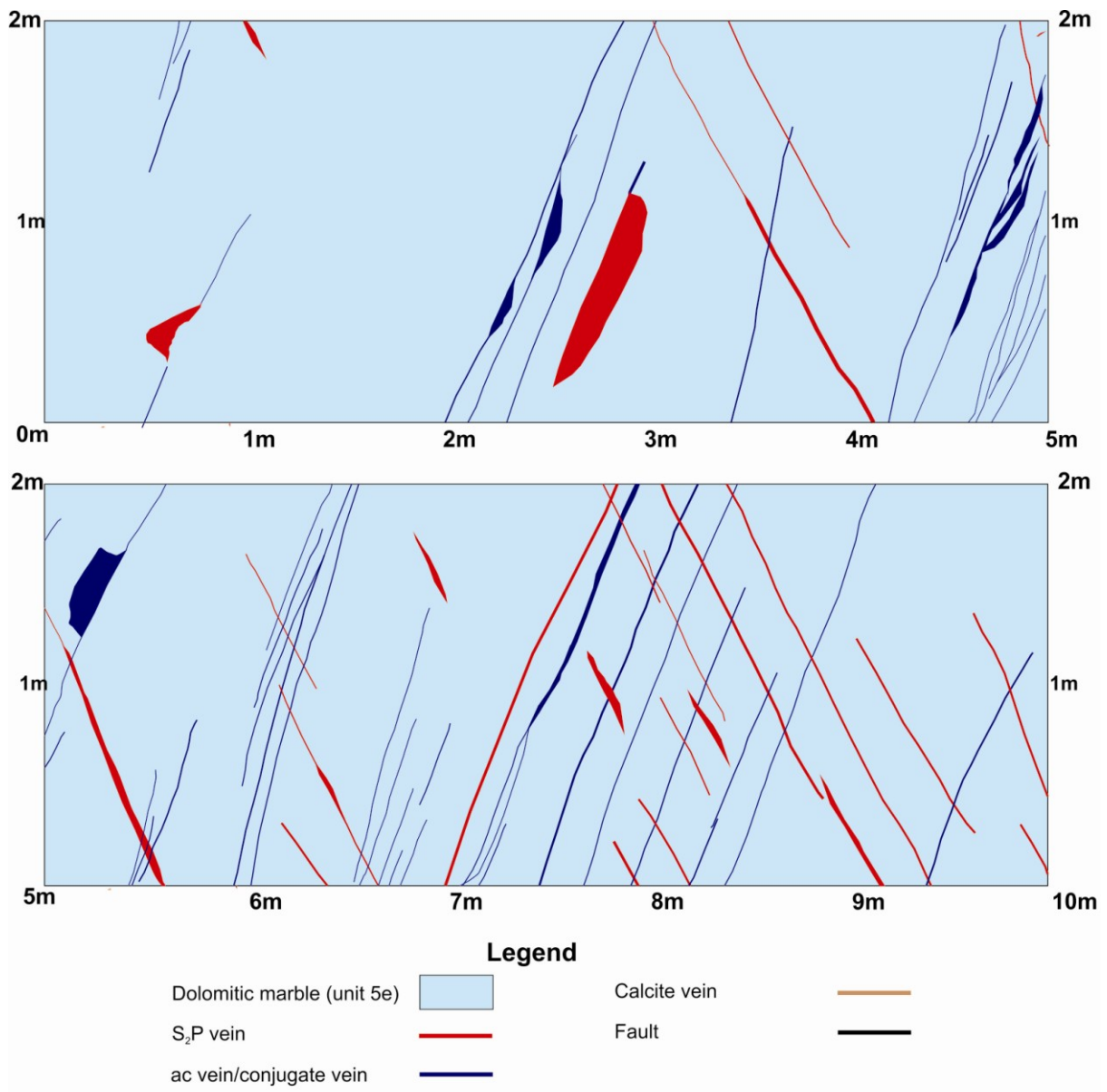


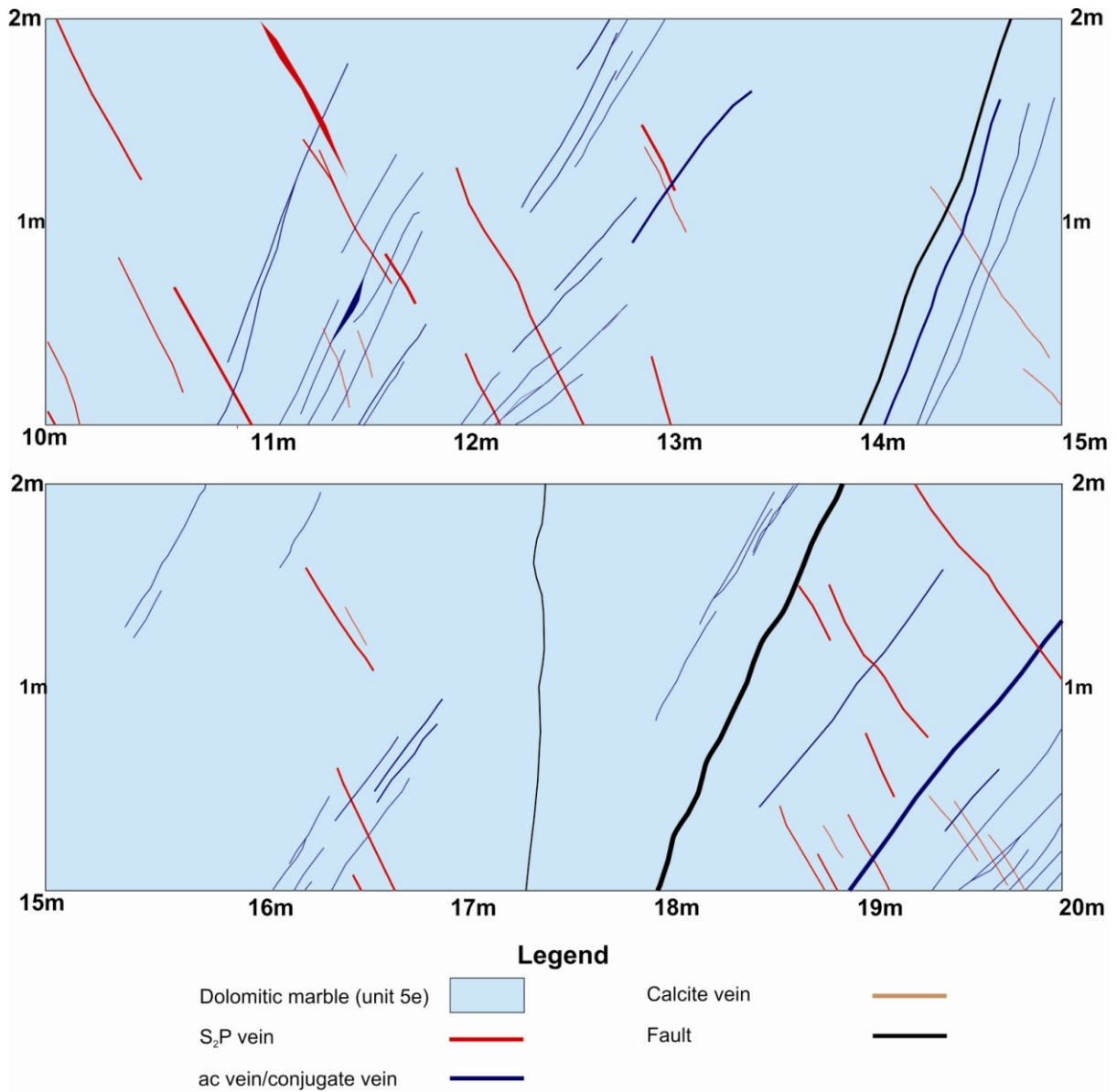


Gecko Pit 1 Panel 1 (Cross-section; 20m)					
Sample No	At (m)	Thickness (mm)	Spacing (m)	Vein Orientation	
				Dip Direction	Dip
1	0.08	3	0.6	280	70
2	0.58	2	16.2	281	78
3	0.77	3	1.1	279	75
4	1.8	4	15	280	79
5	1.95	110	3.4	278	82
6	3.45	2	1.3	284	78
7	3.46	2	1.3	284	78
8	3.48	2.5	13	284	78
9	3.61	4	8.4	278	84
10	6.63	2	3.4	273	76
11	7.3	6	2	294	75
12	7.45	4	14.8	21	74
13	7.83	2	0.8	283	76
14	7.84	3	1.1	283	76
15	7.89	2	0.7	283	76
16	7.9	2.5	0.7	283	76
17	7.91	2	0.25	278	77
18	9.22	3	3.8	280	80
19	9.28	2	5.5	282	80
20	9.61	4	14.5	288	84
21	10.96	5	2.8	296	81
22	11.24	4	4	290	76
23	11.28	2	1.8	279	73
24	11.29	3	1.5	279	73
25	11.3	4	1.8	279	73
26	12.1	8	0.7	272	68
27	12.11	9	4.8	272	68
28	12.16	3	6.8	272	68

29	12.23	5	5	272	68
30	12.23	2.5	4.5	286	84
31	12.27	2	0.9	284	79
32	12.28	6	6.4	284	79
33	13.09	5	19.6	289	81
34	14.71	4	1.2	277	81
35	14.72	4	0.5	277	81
36	14.72	4	4.8	277	81
37	14.77	2.5	17.5	276	79
38	14.88	3	3.6	268	85
39	16.45	3	4.3	264	76
40	16.49	3	1.8	264	76

Appendix IIb: Pit 1 Panel 2; Longitudinal section

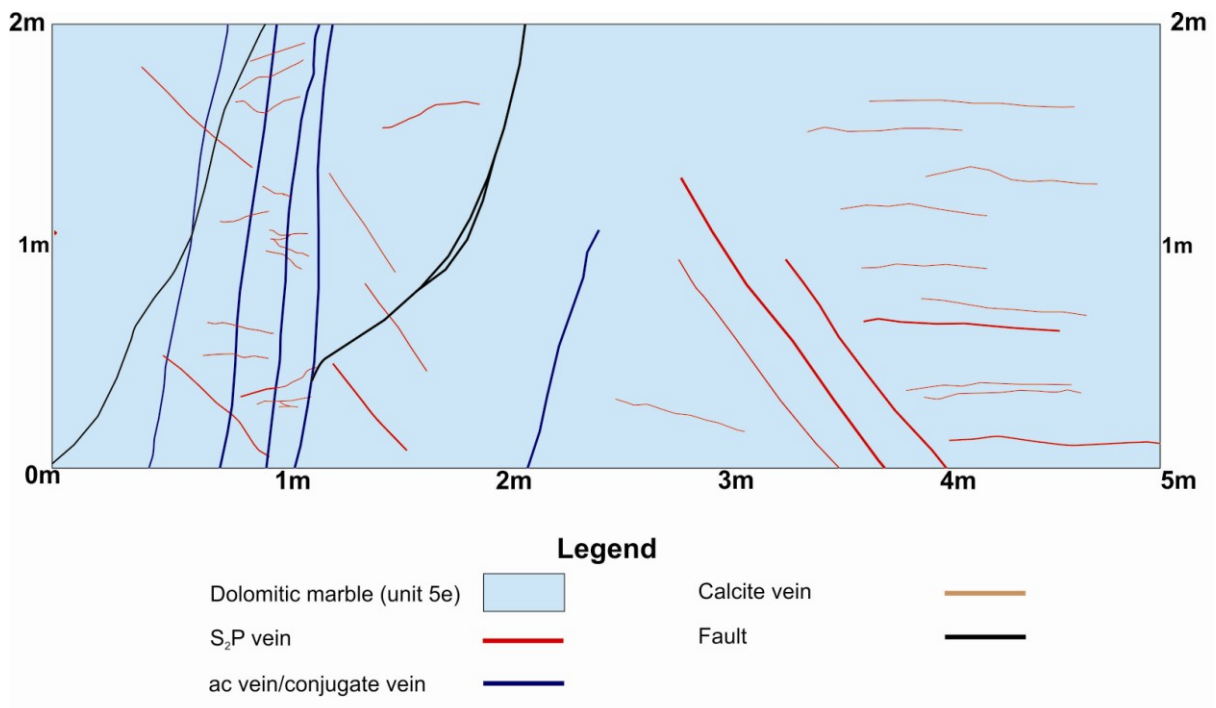


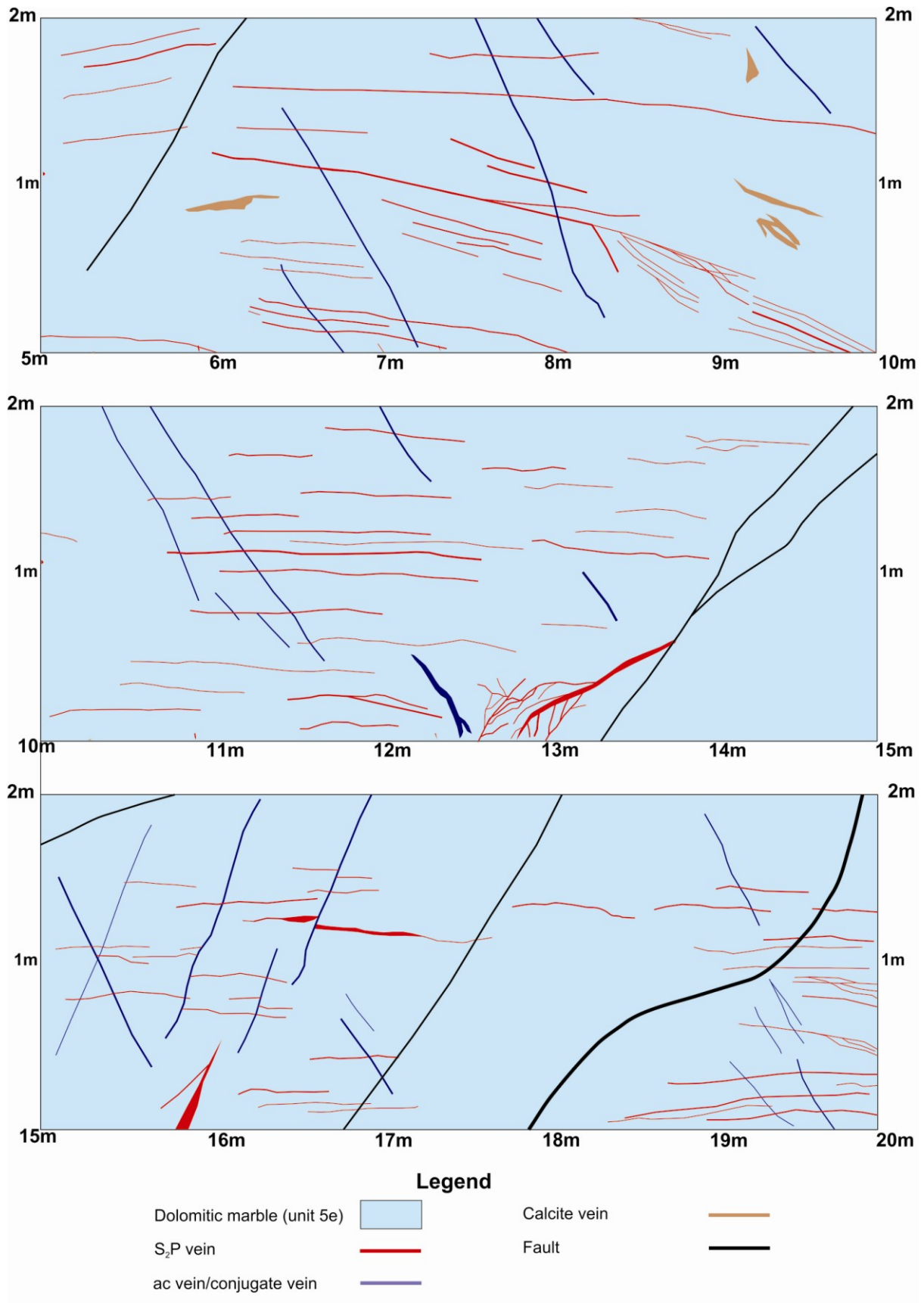


Gecko Pit 1 Panel 2 (Longitudinal section 20m)					
Sample No	At (m)	Thickness (mm)	Spacing (m)	Vein Orientation	
				Dip Direction	Dip
1	2.23	4.5	1.49	277	81
2	3.72	2	1.04	19	71
3	4.76	2	0.03	274	79
4	4.79	2	0.28	276	74
5	5.07	3	0.11	276	74
6	5.18	2.5	0.07	282	66
7	5.25	6	1.55	3	75
8	6.8	2	0.09	277	75
9	6.89	2.5	0.36	273	81
10	7.25	3	0.02	270	80
11	7.27	9	0.04	268	84

12	7.31	2	0.4	270	80
13	7.71	3	0.17	273	79
14	7.88	5	0.6	280	76
15	8.48	4.5	0.13	12	75
16	8.61	2	0.28	267	65
17	8.89	3.5	0.59	29	72
18	9.48	4	0.33	32	77
19	9.81	4	0.14	11	66
20	9.95	2	1.01	278	74
21	10.96	2	0.92	268	79
22	11.88	6.5	0.34	32	77
23	12.22	3	1.93	25	81
24	14.15	10	0.08	269	85
25	14.23	2	0.02	270	82
26	14.25	3	0.01	270	79
27	14.26	2.5	4.43	17	65
28	18.69	3	0.09	278	74
29	18.78	2	0.53	283	79
30	19.31	3		284	69

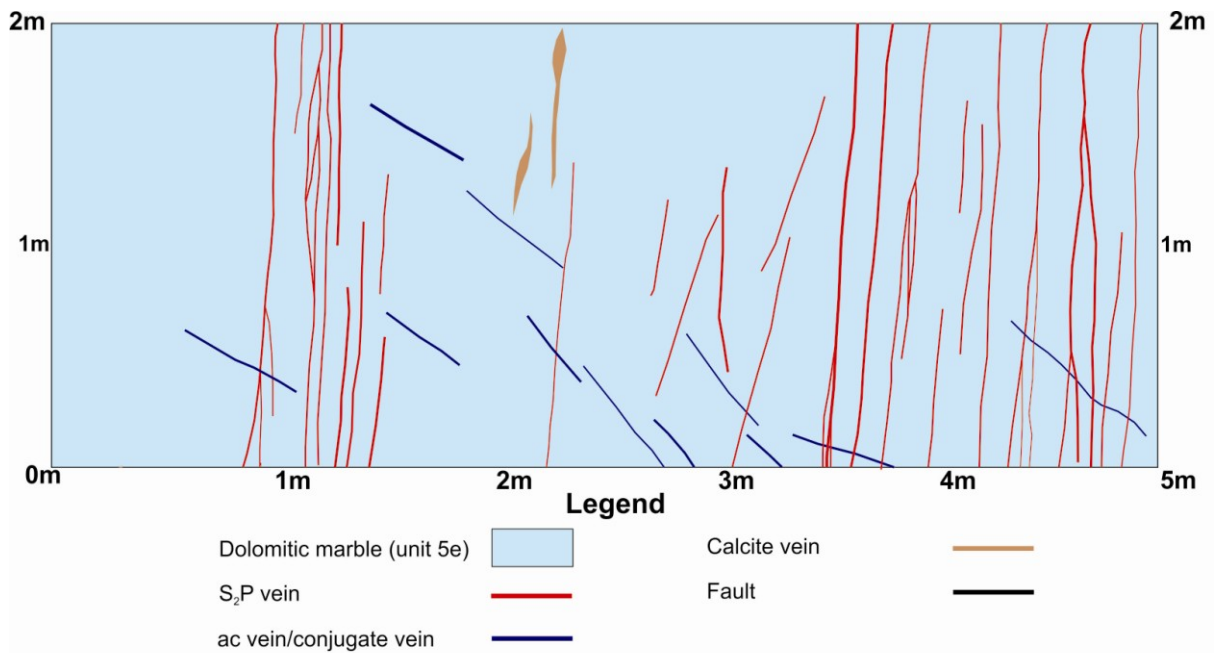
Appendix IIc: Pit 2 Panel 1; Longitudinal section

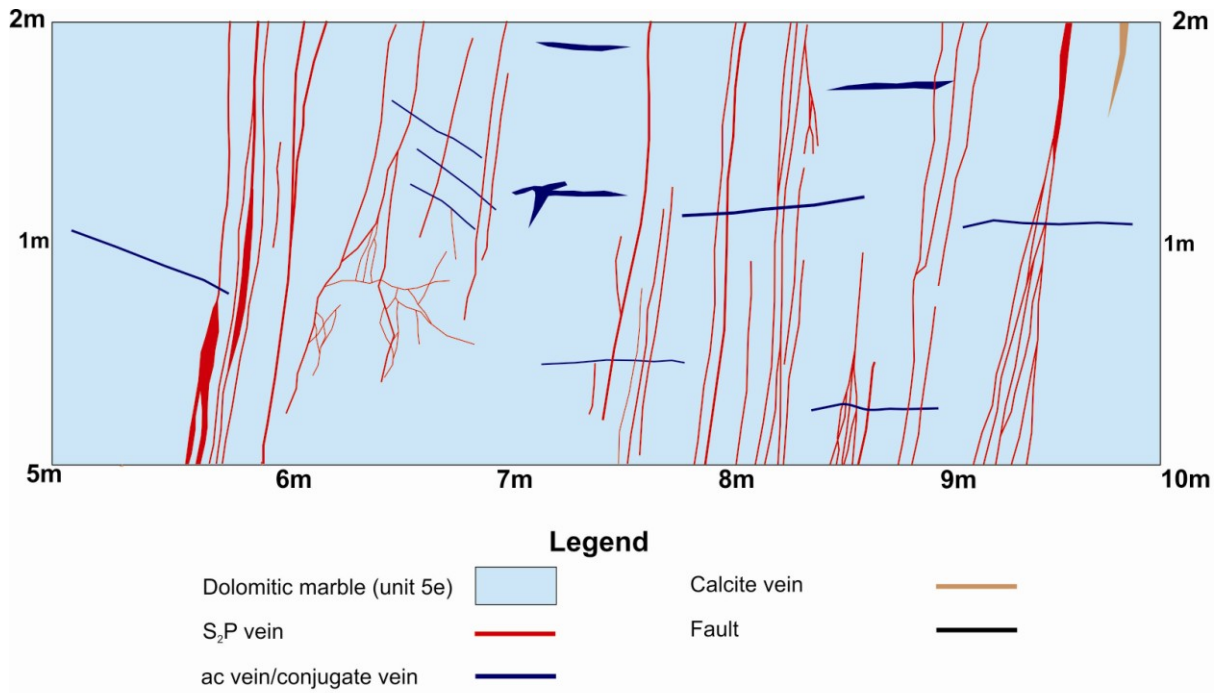




Gecko Pit 2 Panel 1 (Longitudinal section; 20m)					
Sample No	At (m)	Thickness (mm)	Spacing (m)	Vein Orientation	
				Dip Direction	Dip
1	0.72	2	0.1	272	88
2	0.82	2	0.22	273	84
3	1.04	2.5	0.35	275	67
4	1.39	2	1.97	27	81
5	3.36	2	2.73	34	67
6	6.09	2.5	0.61	315	74
7	6.7	3	0.98	21	71
8	7.68	2	0.17	323	66
9	7.85	3	1.25	10	80
10	9.1	2.5	1.91	327	78
11	11.01	2.5	0.52	23	69
12	11.53	3	1.13	318	70
13	12.66	2.5	1.13	318	79
14	13.79	2.5	1.47	321	76
15	15.26	3	0.84	16	80
16	16.1	2	3.6	294	79
17	19.7	3	0.15	308	61
18	19.85	3.5		38	69

Appendix IId: Pit 2 Panel 2; Cross-section





Gecko Pit 2 Panel 2 (Cross-section; 10m)					
Sample No	At (m)	Thickness (mm)	Spacing (m)	Vein Orientation	
				Dip Direction	Dip
1	1.08	3	1.05	302	84
2	2.13	5	0.92	43	60
3	3.05	2	0.4	303	78
4	3.45	4.5	0.22	295	79
5	3.67	5.5	0.22	301	81
6	3.89	3	0.78	303	83
7	4.67	2.5	0.61	293	86
8	5.28	7.5	0.14	307	78
9	5.42	17	0.27	306	75
10	5.69	2	0.54	306	75
11	6.23	2	0.23	311	76
12	6.46	2.5	0.09	305	74
13	6.55	2	0	309	84
14	6.55	6	0.71	35	71
15	7.26	2	0.26	306	84
16	7.52	6	0.37	308	83
17	7.89	2.5	0.12	294	86
18	8.01	7	0.16	311	84
19	8.17	15	0.34	24	63
20	8.51	3	0.52	308	88
21	9.03	2	0.41	306	85
22	9.44	3		311	80

Appendix IIe

Borehole AWD-3			
Sample No	At (m)	Vein Thickness (mm)	Alteration
1	81.23	2.1	Contact zone. Light brown wall rock alteration
2	81.45	3.2	
3	81.65	4.5	
4	81.79	2.4	
5	83.53	5	
6	84.90	42	
7	84.95	2	
	85.65		
	86.52		
8	90.60	2.2	First zone of mineralisation at contact of unit 5e and unit 6
9	95.99	51	
10	99.95	2.1	
11	103.57	2	
12	103.59	7	
13	107.59	4	
14	108.48	7	
15	109.13	10	
16	109.36	2	
17	112.54	2.5	
18	114.10	2	Predominantly barren dolomitic marble. Has a few pods of alteration that do not exceed 5 m in width.
	115.18		
19	117.33	2.2	
20	117.51	4.1	
21	118.77	4.3	
22	126.56	18	Second zone of mineralisation at contact of unit 5d and unit 5c
23	126.78	2.2	
	138.49		Barren dolomitic marble
	151.15		
	175.42		
	186.74		
	192.21		

Appendix II f

Borehole AWD-4			
Sample No	At (m)	Vein Thickness (mm)	Alteration
1	162.59	11	Contact zone. Light brown alteration with tremolite needles
2	162.63	36	
3	163.07	47	
	165.09		First zone of mineralisation at contact of unit 5e and unit 6.
4	173	9	
	178.696		
5	181.616	76	Predominantly barren dolomitic marble. Has a few pods of alteration.
6	181.92	46	
7	183.176	20	
9	188.788	2	
10	188.922	3	
11	191.564	3	
12	191.81	3	
13	191.838	4	
14	191.884	2	
15	201.878	4	
	202.95		Second zone of mineralisation at contact of unit 5d and unit 5c.
	229.994		

Appendix II g

Borehole AD-128				
Sample No	At (m)	Thickness (mm)	Spacing (m)	Alteration
1	0.02	2	0.4954	
2	0.52	3.1	1.443	
3	1.96	7.2	0.3732	
4	2.33	3.2	0.7208	
5	3.05	4.2	0.0636	
6	3.12	4.1	0.3404	
7	3.46	2.2	0.5255	
8	3.98	2.3	0.1169	

9	4.10	2.6	0.5029	
10	4.60	2.3	0.2298	
11	4.83	3.4	0.7003	
12	5.53	2.8	0.0785	
13	5.61	3.2	0.866	
14	6.48	5.3	0.1432	
15	6.62	4.8	1.1907	Wallrock alteration.
16	7.81	3.4	0.776	
17	8.59	2.3	1.4214	
18	10.01	5.3	0.0583	
19	10.07	8.2	0.2656	
20	10.33	4.7	1.6654	
21	12.00	9.7	0.5058	Wall-rock alteration
22	12.50	6.2	0.0621	
23	12.57	9.1	1.0245	
24	13.59	4.3	0.1047	
25	13.70	8.7	0.0343	
26	13.73	3.4	2.319	
27	16.05	3.1	0.3563	Wall-rock alteration
28	16.40	4.9	1.2758	
29	17.68	2	0.9166	
30	18.60	3.1	0.24	
31	18.84	2.2	0.2478	
32	19.09	7.3	0.299	
33	19.38	3.7	0.2208	
34	19.60	4.2	0.4889	
35	20.09	3.3	1.6808	Wall-rock alteration with oxides with sulphides
36	21.77	3.7	0.1801	
37	21.95	4.1	1.2817	
38	23.24	7.8	0.5522	
39	23.79	7.4	0.4587	
40	24.25	6	2.4322	
41	26.68	2.4	0.3563	
42	27.04	9.7	0.542	
43	27.58	10.2	0.9065	
44	28.48	3.8	0.886	
45	29.37	3.1	1.4017	
46	30.77	3.4	0.4823	Alteration with viz. Au and numerous veinlets
47	31.25	3.2	0.1978	
48	31.45	2.7	1.4661	
49	32.92	2.9	0.2153	
50	33.13	2.3	0.7185	

51	33.85	4.1	0.2308
52	34.08	3.2	

Appendix IIh

Borehole AD-129				
Sample No	At (m)	Thickness (mm)	Spacing (m)	Alteration
1	1.10	5	0.07	
2	1.17	4	0.43	
3	1.60	2	0.60	
4	2.20	2.4	0.04	
5	2.24	4	0.89	
6	3.13	2.6	0.13	
7	3.26	21	0.07	
8	3.34	4	0.06	
9	3.40	7	0.05	
10	3.45	4	0.24	
11	3.69	2.1	0.18	
12	3.87	3.2	0.01	
13	3.87	2	0.37	
14	4.24	3.2	0.15	
15	4.39	3.2	0.26	
16	4.65	3.8	0.17	
17	4.81	4.2	0.22	
18	5.03	3.4	0.15	
19	5.18	3.1	0.71	
20	5.89	2	0.84	
21	6.73	2.2	0.22	
22	6.94	2.1	0.01	
23	6.95	3	0.36	
24	7.31	2.6	0.05	
25	7.37	2.1	0.10	
26	7.47	3	0.08	
27	7.55	11	2.73	
28	10.29	3	0.20	
29	10.49	11	1.08	
30	11.57	5.1	0.20	
31	11.77	2.1	0.07	
32	11.84	2	0.97	

33	12.80	2.2	0.42	
34	13.22	20	0.50	
	13.72		0.08	
35	13.81	3.2	0.07	
36	13.88	2.4	0.11	
37	13.99	3	0.49	
	14.48		0.90	
38	15.39	2.1	0.24	Stockwork for 98cm
39	15.63	2	0.73	
	16.35		0.06	
40	16.42	3.2	0.43	Stockwork for 42cm
41	16.85	2.1	0.25	
	17.09		0.44	Stockwork for 20cm
42	17.54	2.6	0.15	
43	17.68	3.3	0.18	
44	17.86	12.2	0.20	
45	18.06	9.2	0.14	
	18.20		0.63	Stockwork for 40mm with visible gold
46	18.83	2	0.70	
47	19.53	2.2	1.19	
48	20.72	5.5	0.01	
	20.73		0.32	Stockwork for 21cm
49	21.05	2	0.28	
50	21.32	9.6	0.71	
51	22.03	2.1	0.23	
52	22.27	2	0.28	
53	22.55	2.4	0.42	
	22.96		0.78	Stockwork for 53cm
54	23.75	2	0.19	
55	23.94	3	0.11	
56	24.04	2.9	0.05	
57	24.09	2	0.08	
58	24.17	2	0.43	
59	24.60	2.2	0.61	
60	25.21	3.4	0.53	
61	25.74	3	1.69	
	27.43		1.01	Stockwork for 25cm
62	28.45	4	1.08	
63	29.53	3.4	0.41	
64	29.94	2	0.45	
65	30.39	3.2	0.92	
66	31.31	2.1	0.01	

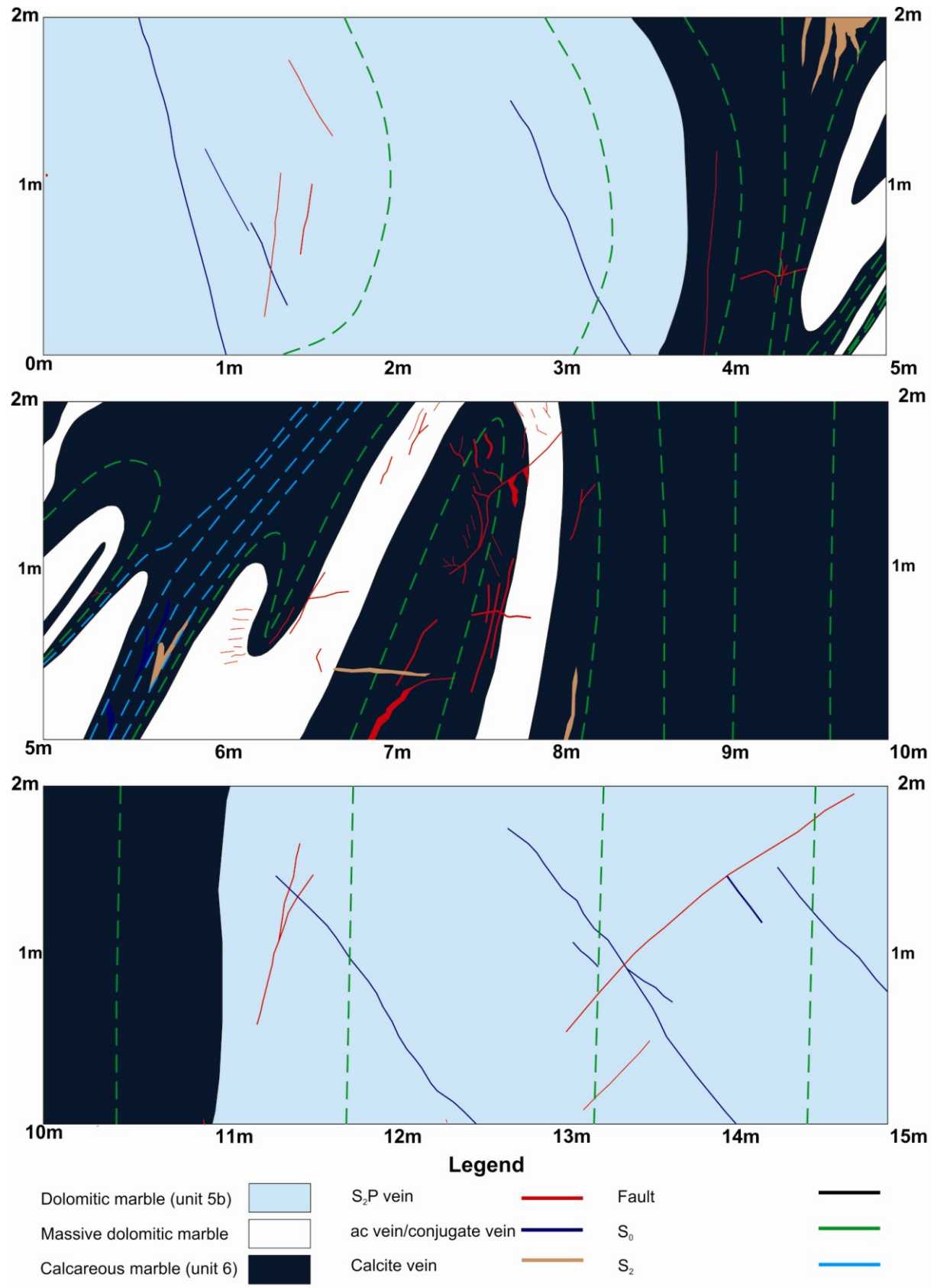
67	31.32	5.5	1.05	
68	32.37	2.1	0.53	
69	32.91	10	0.06	
70	32.96	2	1.45	
	34.41		3.02	Stockwork for 28cm
71	37.43	6.2	0.21	
72	37.64	3.4	3.50	
73	41.14	5.4	0.44	
74	41.58	4.8	2.20	
75	43.78	8.8	1.25	
76	45.03	2	0.12	
	45.15		0.81	Stockwork for 32cm
77	45.96	2.1	2.87	
78	48.83	2.3	3.07	
79	51.90	7.1	2.27	
80	54.17	2.1	1.32	
81	55.49	2.8	8.40	
82	63.89	4.8	2.87	
83	66.76	3	0.27	
84	67.02	3	1.16	
85	68.18	2	0.95	
	69.13		1.62	Stockwork for 51cm
86	70.75	2	5.71	
87	76.46	7	0.37	
88	76.82	3.4	1.22	
89	78.04	4.1	2.32	
90	80.36	3.2		

Appendix III

Borehole AD-130			
Sample No	At (m)	Thickness (mm)	Spacing (m)
1	0.02	10.5	0.03
2	0.04	4.1	0.10
3	0.15	2	0.06
4	0.20	8.7	0.12
5	0.32	3.6	1.36
6	1.68	7.3	0.02
7	1.70	5.2	0.60
8	2.30	2.7	0.54
9	2.84	3.2	0.18

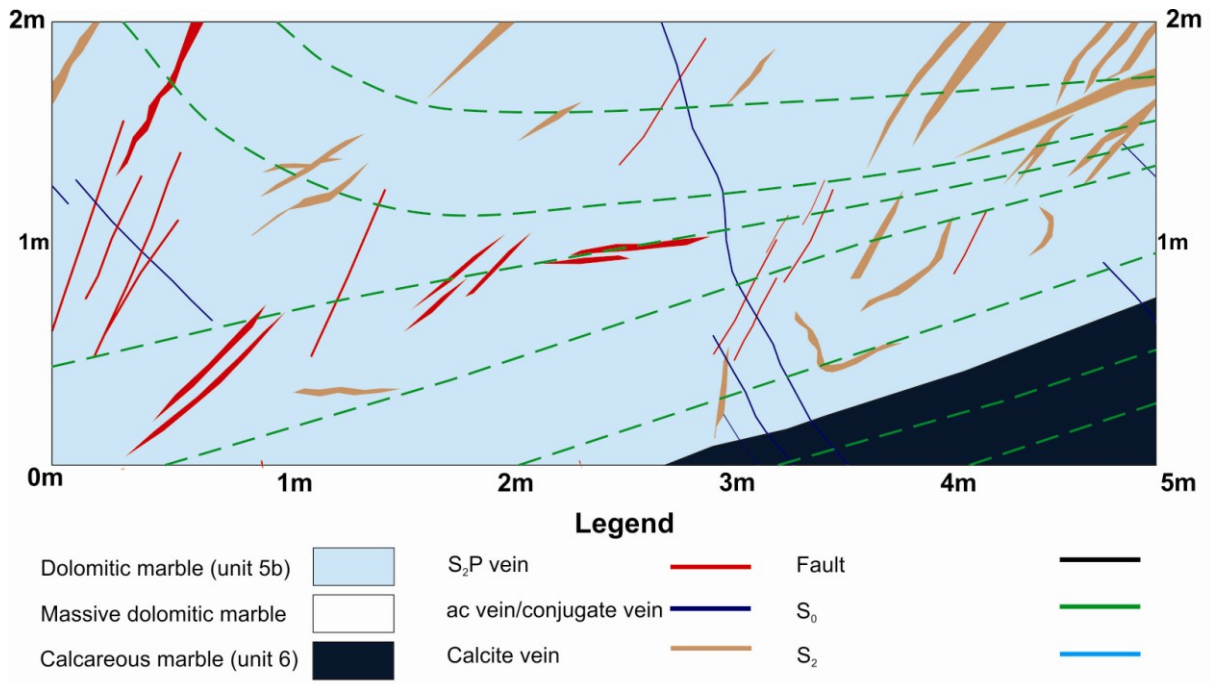
10	3.02	3.7	0.00
11	3.03	3	0.30
12	3.33	2.8	0.66
13	3.99	2.4	0.04
14	4.03	2.1	1.05
15	5.08	2.3	0.21
16	5.29	10.4	0.09
17	5.38	12.3	0.01
18	5.39	3	0.09
19	5.48	19	0.28
20	5.76	3.1	0.75
21	6.51	2.1	0.10
22	6.61	2.3	0.65
23	7.26	7.4	0.01
24	7.27	4.3	0.18
25	7.45	5.8	0.12
26	7.57	4.3	0.00
27	7.57	2.7	0.38
28	7.95	2.4	0.24
29	8.19	2.3	0.24
30	8.43	2.7	0.16
31	8.60	4.9	0.15
32	8.74	5.2	0.23
33	8.97	3.9	0.35
34	9.32	2.2	0.84
35	10.15	3.1	0.02
36	10.17	2.1	0.29
37	10.46	3.3	1.46
38	11.92	3.7	0.04
39	11.95	2.7	0.22
40	12.17	3	0.57
41	12.74	2.3	0.29
42	13.03	2.5	0.20
43	13.23	2.2	0.26
44	13.49	3.1	0.11
45	13.60	4.4	0.05
46	13.65	2.3	0.67
47	14.32	3.2	0.33
48	14.65	4	0.68
49	15.33	3.7	

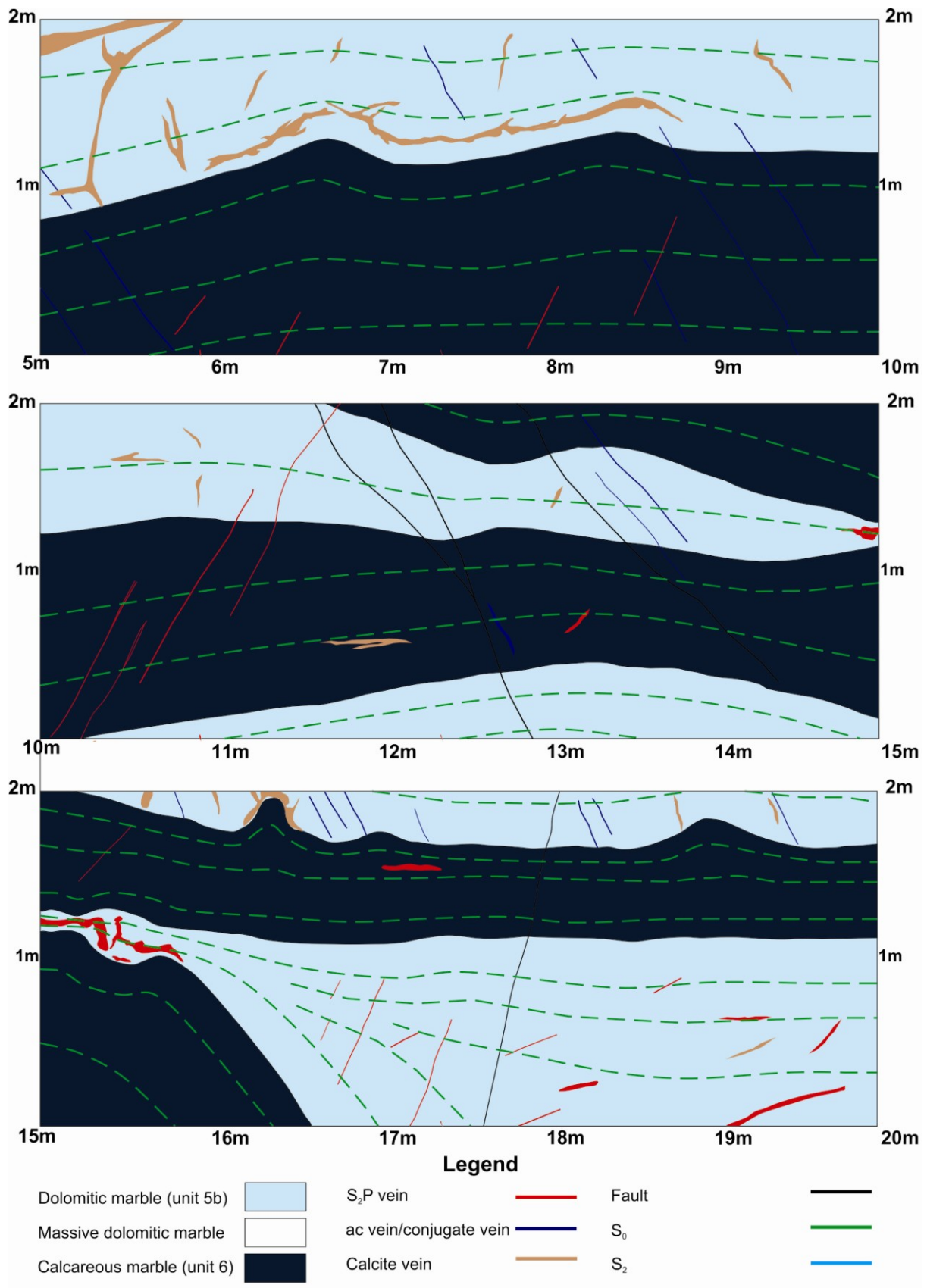
Appendix IIIa: Mid level Panel 1; Cross-section

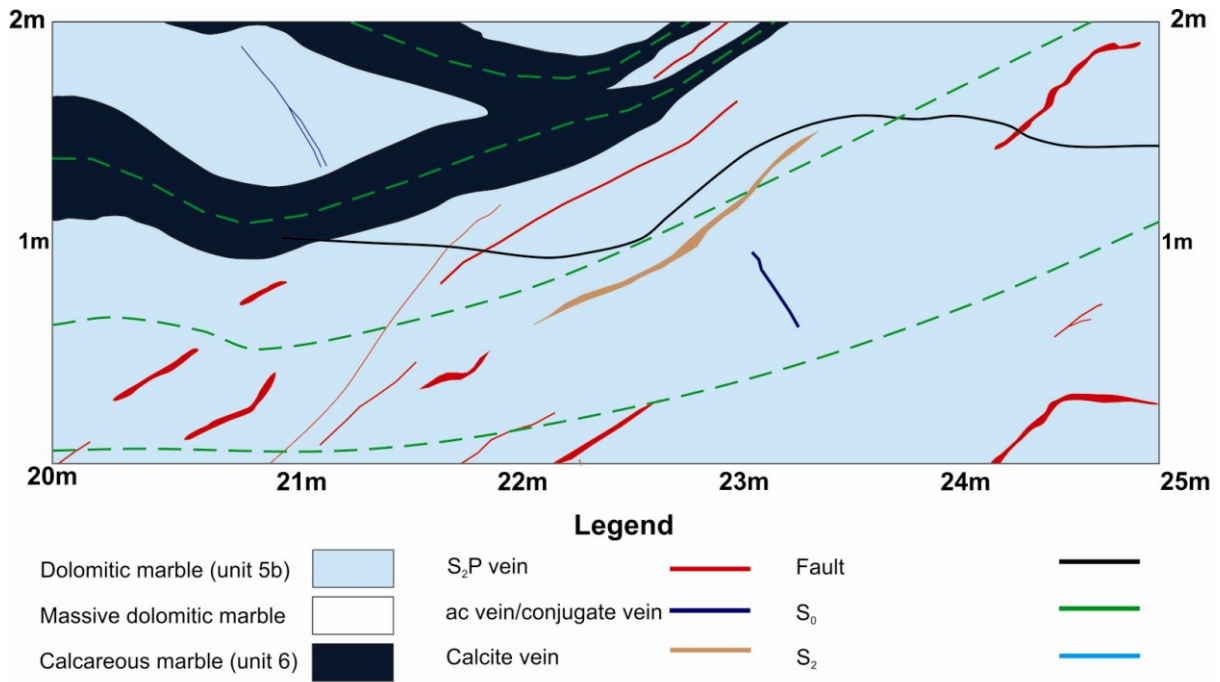


Grid A ML Panel 1 (Cross-section; 15m)					
Sample No	At (m)	Thickness (mm)	Spacing (m)	Vein Orientation	
				Dip Direction	Dip
1	0.87	2	2.2	37	67
2	3.07	3	3.5	18	79
3	6.57	3	1.17	293	84
4	7.74	4	0.1	294	86
5	7.84	3	3.7	296	85
6	11.54	2	1.04	295	79
7	12.58	3	1.18	53	72
8	13.76	4	0.06	55	84
9	13.82	2.5	0.89	308	70
10	14.71	2		12	74

Appendix IIIb: Mid level Panel 2; Cross-section



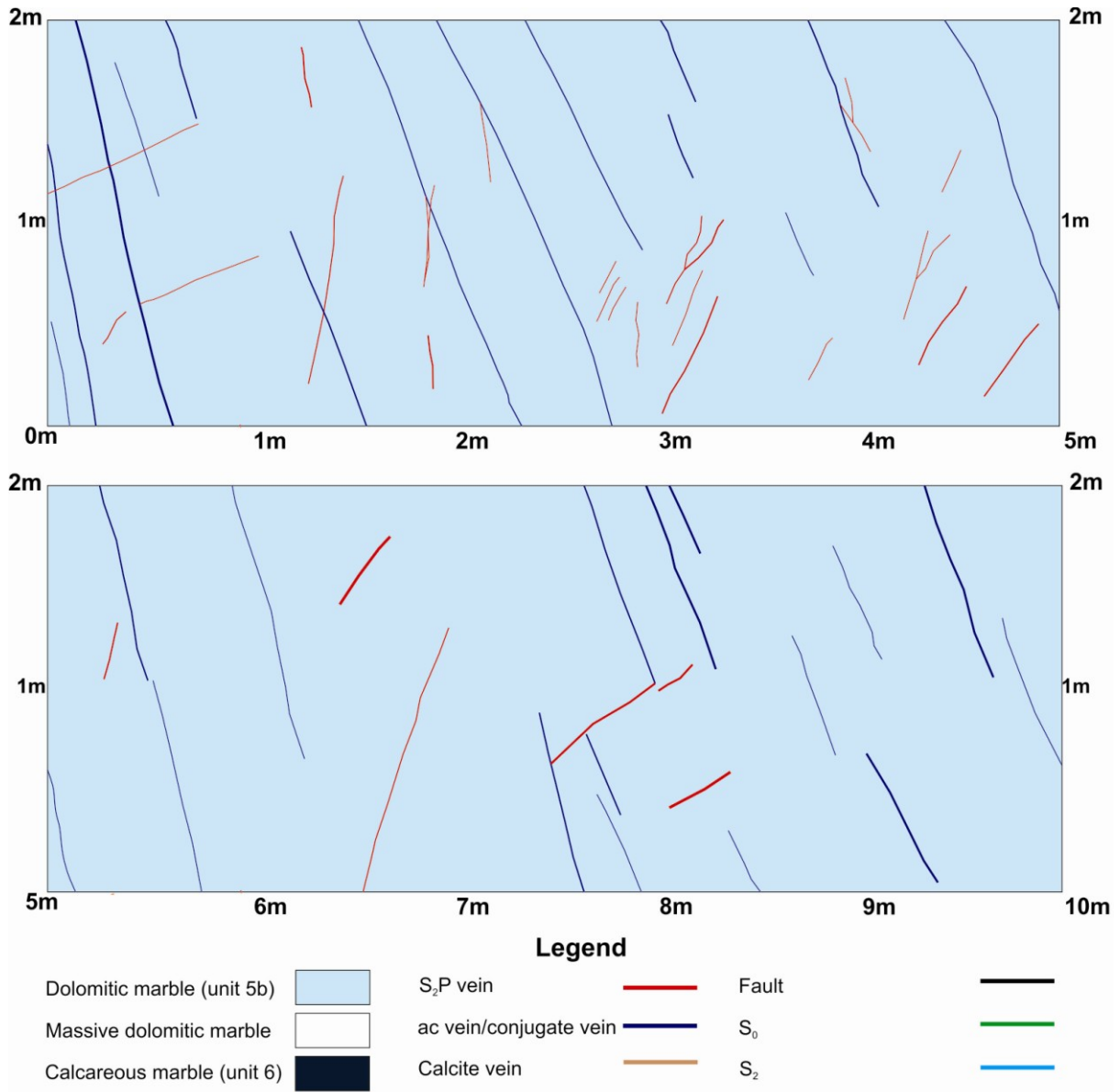




Grid A ML Panel 2 (Cross-section; 25m)					
Sample No	At (m)	Thickness (mm)	Spacing (m)	Vein Orientation	
				Dip Direction	Dip
1	0.03	8	0	268	76
2	0.03	4	0.16	280	69
3	0.19	4	0	276	76
4	0.19	2	0.05	5	66
5	0.24	4	0.95	280	66
6	1.19	11	0.28	292	75
7	1.47	3	0.47	298	69
8	1.94	10	0.11	277	70
9	2.05	4	0.6	282	67
10	2.65	12	0.56	356	40
11	3.21	2	0.17	34	75
12	3.38	2.5	0.08	33	70
13	3.46	2	0.09	279	75
14	3.55	5	0.31	275	75
15	3.86	5	1.21	281	74
16	5.07	3	4.07	37	71
17	9.14	3	0.31	28	66
18	9.45	2.5	1.41	33	70
19	10.86	2	0.34	269	67
20	11.2	2	2.53	273	78
21	13.73	3	7.81	36	73

22	21.54	2	0.62	283	65
23	22.16	3		300	68

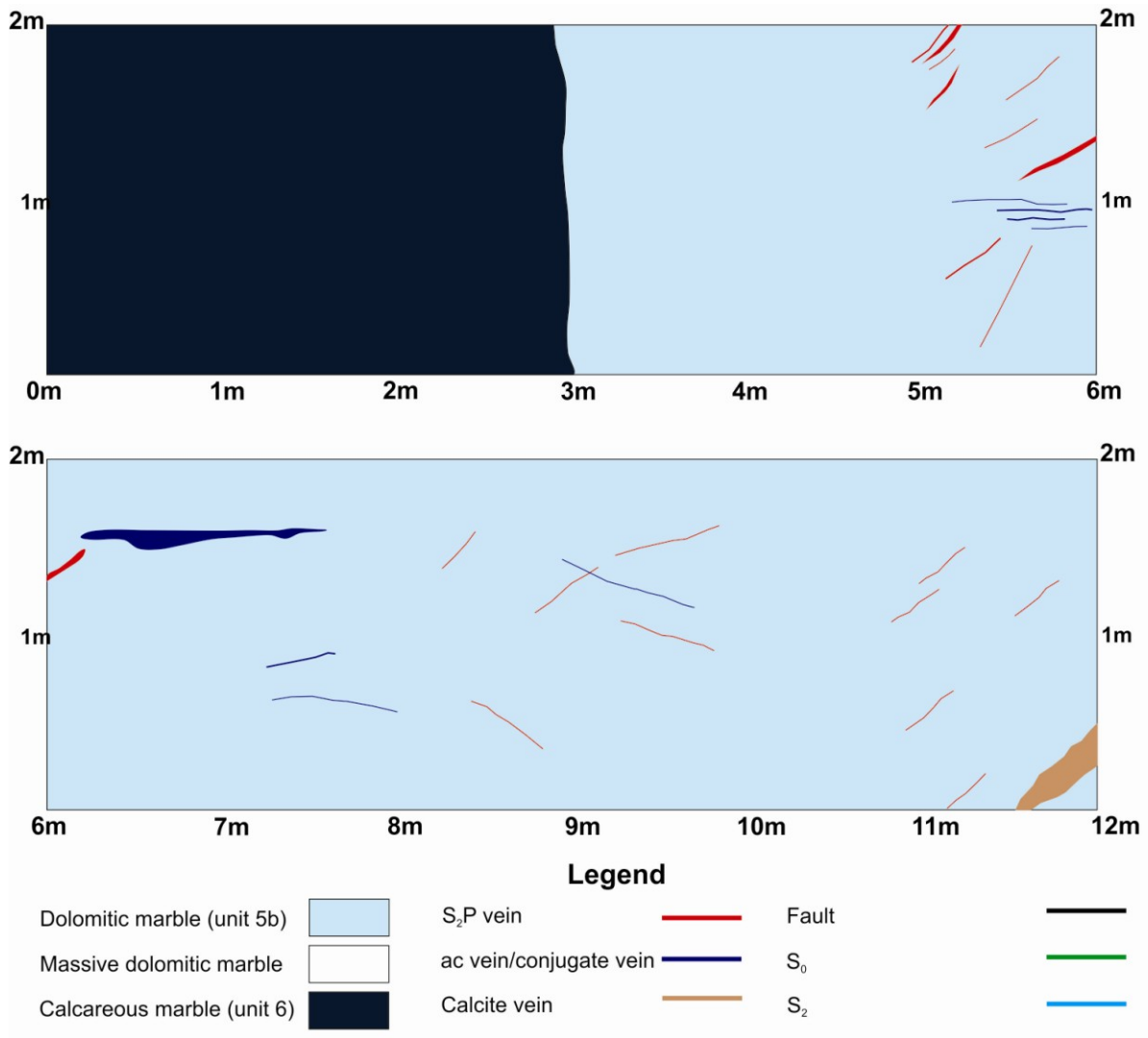
Appendix IIIc: Mid level Panel 3; Longitudinal section

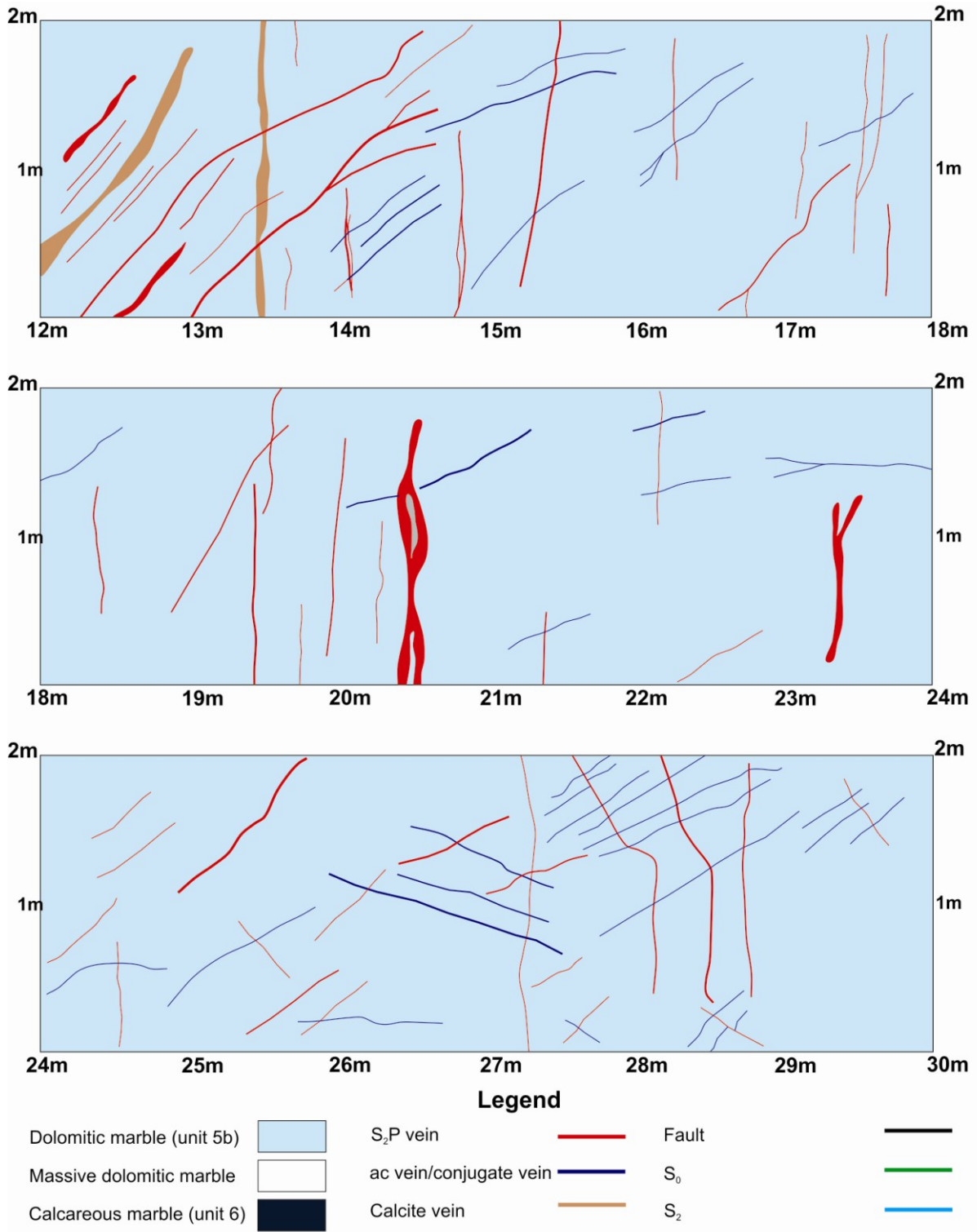


Grid A ML Panel 3 (Longitudinal section; 10m)					
Sample No	At (m)	Thickness (mm)	Spacing (m)	Vein Orientation	
				Dip Direction	Dip
1	0.04	8	0.29	23	74
2	0.33	4	1.27	42	74
3	1.6	2	0.53	252	79
4	2.13	5	0.31	38	73

5	2.44	8	0.38	40	78
6	2.82	2.5	0.28	36	83
7	3.1	7	0.15	260	69
8	3.25	4	1.53	39	75
9	4.78	2.5	0.7	43	70
10	5.48	3	0.88	38	74
11	6.36	2	1.39	43	72
12	7.75	3	0.26	249	77
13	8.01	10	0.87	42	84
14	8.88	10	0.95	32	73
15	9.83	7		38	76

Appendix III d: Upper level Panel 1; Cross-section

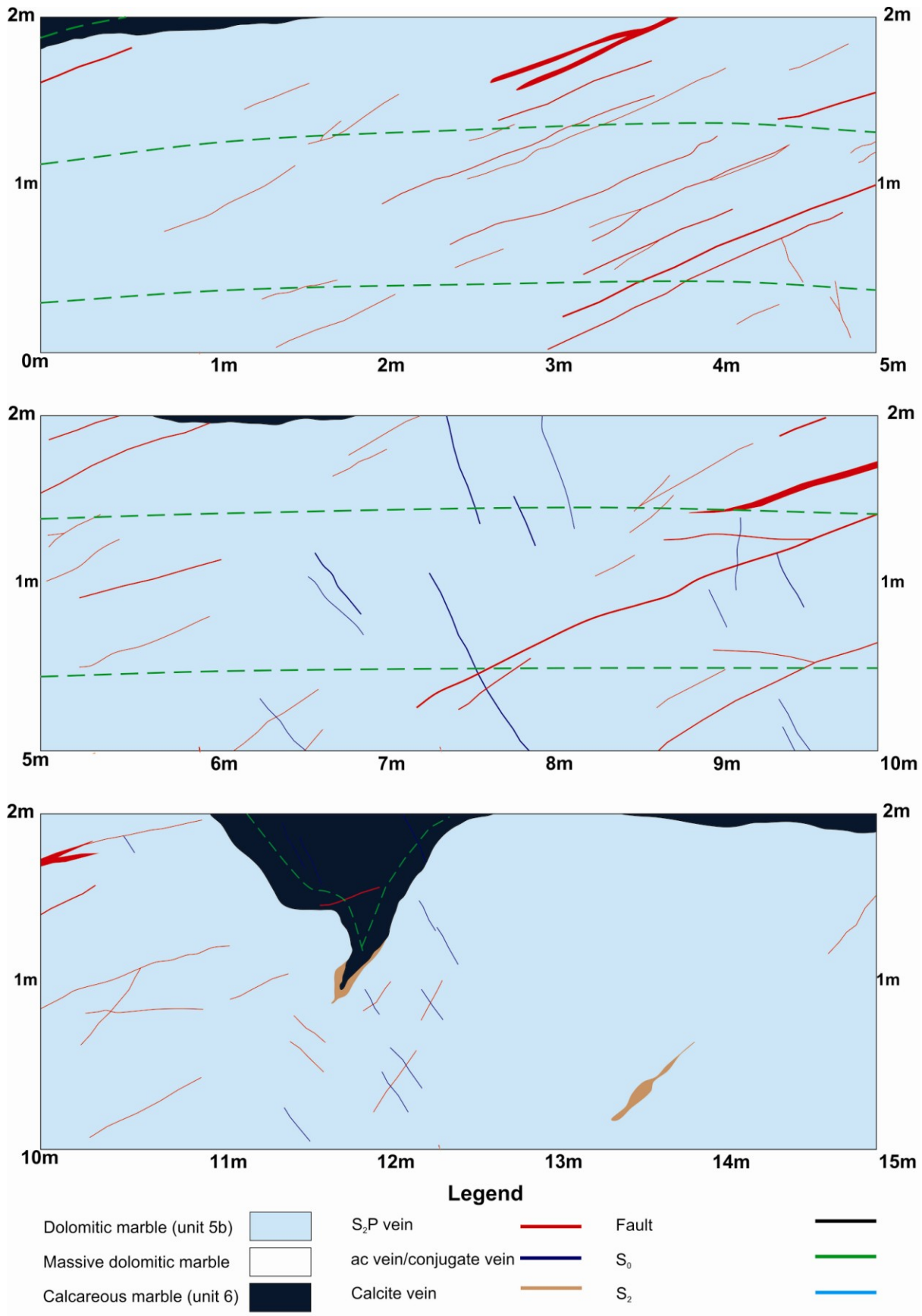


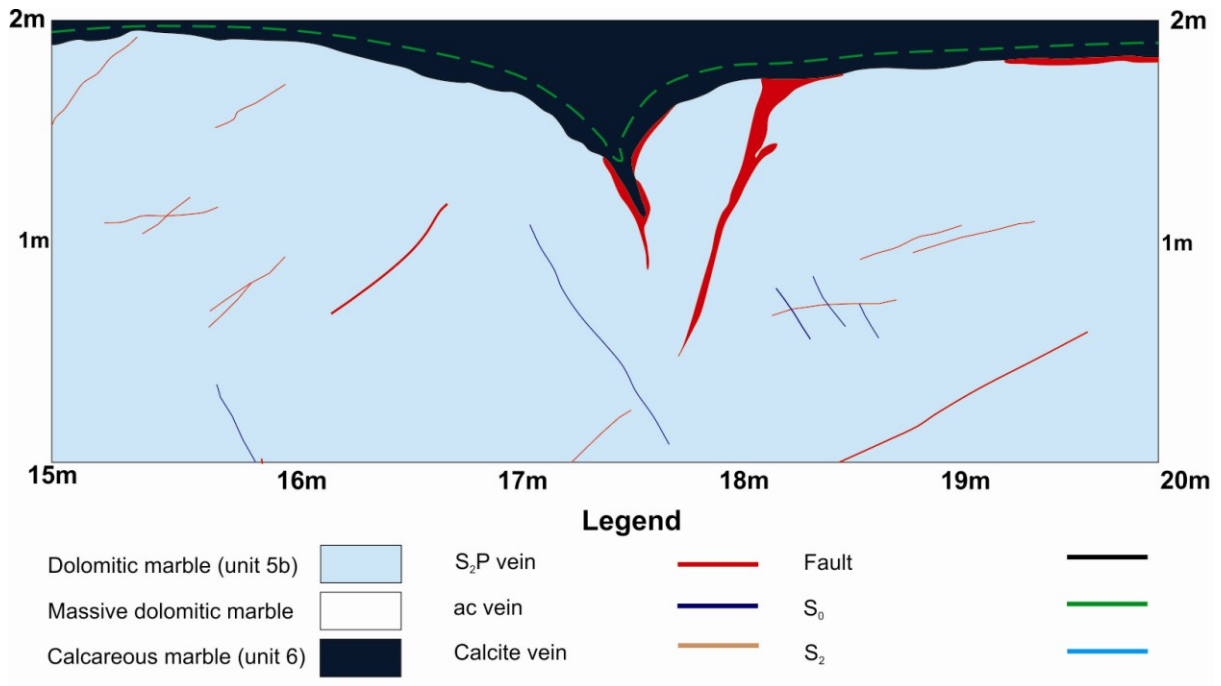


Grid A UL Panel 1 (Cross-section; 30m)					
Sample No	At (m)	Thickness (mm)	Spacing (m)	Vein Orientation	
				Dip Direction	Dip
1	5.66	4	3.15	329	59
2	8.81	4	0.84	1	56
3	9.65	5	2.66	22	52

4	12.31	2	0.01	328	55
5	12.32	2	0.24	324	60
6	12.56	4	0.35	337	57
7	12.91	6	0.12	263	51
8	13.03	2	0.49	312	65
10	13.52	4	0.1	326	55
11	13.62	13	0.6	310	48
12	14.22	3	0.06	314	44
13	14.28	30	0.08	305	41
14	14.36	3	0.21	327	49
15	14.57	2	0.90	314	50
16	15.47	4	1.60	327	45
17	17.07	6	0.22	266	65
18	17.29	2	0.10	338	47
19	17.39	4	0.03	294	86
20	17.42	7	0.06	296	84
21	17.48	15	0.11	289	80
22	17.59	4	0.19	344	55
23	17.78	20	0.55	344	50
24	18.33	2	0.12	334	49
25	18.45	3	1.20	346	47
27	19.65	30	0.39	280	83
29	20.04	5	0.18	292	80
30	20.22	46	0.61	287	89
31	20.83	2.5	5.47	340	49
34	26.3	15	0.73	224	74
35	27.03	7	1.56	223	84
37	28.59	16	0.43	222	74
38	29.02	18	0.25	228	80
39	29.27	6		226	81

Appendix IIIe: Upper level Panel 2; Longitudinal section





Grid A UL Panel 2 (Longitudinal section; 20m)					
Sample No	At (m)	Thickness (mm)	Spacing (m)	Vein Orientation	
				Dip Direction	Dip
1	1.15	8	0.77	271	56
2	1.92	6	1.38	302	57
3	3.3	5	0.48	278	52
4	3.78	9	0.95	301	54
5	4.73	6	0.75	298	64
6	5.48	3	1.09	283	65
7	6.57	4	0.95	356	78
8	7.52	3	0.59	5	82
9	8.11	3	0.41	294	67
10	8.52	6	1.12	288	60
11	9.64	3	0.53	17	62
12	10.17	2	0.22	287	66
13	10.39	4	2.00	275	80
14	12.39	2.5	0.29	11	72
15	12.68	3	0.10	24	68
16	12.78	2	0.36	283	60
17	13.14	3	1.70	27	80
18	14.84	3	0.47	284	57
19	15.31	2	0.95	304	68
20	16.26	3	1.27	296	57
21	17.53	6	2.02	25	85

22	19.55	3	0.10	292	67
23	19.65	3	0.23	292	77
24	19.88	4		295	63

Appendix IIIf

Borehole AD-122			
Sample No	At (m)	Vein Thickness (mm)	Spacing (m)
1	0.68	3.1	0.03
2	0.71	7.8	0.75
3	1.46	14.5	0.22
4	1.68	4.6	0.38
5	2.06	4	0.26
6	2.32	2.1	0.56
7	2.88	2.3	0.06
8	2.94	2.7	0.04
9	2.98	19.3	0.13
10	3.12	2.8	0.69
11	3.80	8	0.03
12	3.84	3.2	0.54
13	4.38	3.9	0.08
14	4.46	2	0.09
15	4.55	2.4	0.13
16	4.68	2.1	0.12
17	4.80	10	0.16
18	4.96	11.8	0.14
19	5.10	3.2	0.20
20	5.30	4.7	0.54
21	5.84	6.2	0.33
22	6.17	2.8	1.21
23	7.38	5.2	0.45
24	7.83	2.3	0.96
25	8.78	17.3	0.13
26	8.92	3	0.08
27	8.99	10.2	0.40
28	9.40	2.4	0.30
29	9.70	13.1	0.17
30	9.87	3.1	0.11
31	9.98	2.9	0.23

32	10.21	3.1	0.39
33	10.59	4	0.07
34	10.67	10.8	0.16
35	10.83	6.5	0.09
36	10.92	2.3	0.23
37	11.15	4	0.07
38	11.22	4	0.06
39	11.28	3.7	0.15
40	11.42	7	1.08
41	12.50	18.2	1.01
42	13.51	5.3	0.16
43	13.67	2.4	0.95
44	14.62	11.4	0.35
45	14.97	4	0.06
46	15.03	6.2	1.43
47	16.46	3.4	1.21
48	17.67	5.4	0.08
49	17.75	5.9	0.14
50	17.89	3.7	1.63
51	19.52	3.4	0.59
52	20.11	4.2	0.99
53	21.10	3	0.05
54	21.15	6.2	0.46
55	21.61	3.1	

Appendix IIIg

Borehole AD-123			
Sample No	At (m)	Vein Thickness (mm)	Spacing (m)
1	0.22	2	0.15
2	0.37	4	1.49
3	1.86	2	0.57
4	2.43	22	0.18
5	2.62	9	0.26
6	2.88	2	0.12
7	3.00	5	1.12
8	4.12	4	0.80
9	4.92	4	0.74
10	5.66	3	0.07

11	5.73	4	0.70
12	6.43	7	1.83
13	8.26	5	0.23
14	8.50	4	0.22
15	8.71	10	0.43
16	9.14	2	0.85
17	9.99	3	0.86
18	10.85	3	0.04
19	10.90	2	0.35
20	11.25	14	0.43
21	11.67	11	0.09
22	11.76	2	0.98
23	12.74	9	0.33
24	13.07	9	1.10
25	14.17	8	1.66
26	15.83	3	0.07
27	15.90	4	0.90
28	16.80	3	1.98
29	18.78	3	0.07
30	18.85	2	0.57
31	19.42	4	1.64
32	21.06	5	0.56
33	21.62	4	1.02
34	22.65	6	0.06
35	22.71	2	0.28
36	22.98	3	0.44
37	23.42	2	0.28
38	23.70	11	0.40
39	24.11	6	0.09
40	24.19	4	0.12
41	24.31	4	0.94
42	25.24	2	1.42
43	26.67	2	0.32
44	26.99	2	0.18
45	27.17	2	1.67
46	28.84	2	0.07
47	28.91	3	1.34
48	30.25	3	0.13
49	30.38	4	0.01
50	30.39	3	4.00
51	34.38	3	1.60
52	35.99	19	0.49

53	36.48	5	0.85
54	37.32	10	0.20
55	37.53	2	1.68
56	39.21	4	0.42
57	39.63	3	1.16
58	40.79	2	0.54
59	41.32	15	0.32
60	41.65	3	0.01
61	41.65	3	0.03
62	41.69	4	1.31
63	42.99	2	0.12
64	43.11	5	0.21
65	43.32	4	0.02
66	43.34	3	0.17
67	43.51	3	0.17
68	43.68	6	0.91
69	44.59	2	0.18
70	44.77	3	0.44
71	45.21	4	1.81
72	47.02	3	1.07
73	48.10	8	1.09
74	49.19	4	0.17
75	49.36	3	0.39
76	49.75	3	1.28
77	51.03	5	0.80
78	51.82	3	0.56
79	52.39	11	0.39
80	52.78	3	0.66
81	53.43	3	1.20
82	54.64	3	0.58
83	55.21	2	0.53
84	55.74	5	0.12
85	55.87	2	0.11
86	55.97	8	0.37
87	56.34	14	0.50
88	56.84	3	1.54
89	58.37	4	0.23
90	58.60	2	2.13
91	60.73	10	0.12
92	60.85	4	0.95
93	61.80	2	

Appendix IV

Klipspringer (300 m road cut)				
Sample No	At (m)	Thickness (mm)	Vein Orientation	
			Dip Direction	Dip
1	0.04	3	27	66
2	0.21	4	35	72
3	11.24	4	29	73
4	11.48	3	264	32
5	11.79	4	243	39
6	12.87	3	54	76
7	13.74	4	228	33
8	14.29	5	31	76
9	14.83	35	14	70
10	15.59	27	37	66
11	16.17	2	77	74
12	16.47	13	57	68
13	16.59	3	307	74
14	18.66	9	271	49
15	18.85	19	34	76
16	19.71	4	292	69
17	21.29	4	67	61
18	22.98	4	58	73
19	34.04	6	78	34
20	40.54	4	58	74
21	40.93	3	249	50
22	43.79	5	23	74
23	45.17	40	11	83
24	47.51	3	304	80
25	47.64	9	297	66
26	48.04	7	72	86
27	52.52	4	56	71
28	53.59	5	41	76
29	53.92	3	41	71
30	82.36	3	48	77
31	83.14	4	68	76
32	85	3	52	70
33	85.61	5	43	67
34	86.01	4	60	68
35	87.4	5	54	71
36	87.47	4	303	65

37	91.64	6	51	60
38	110.37	3	86	85
39	115.43	7	54	74
40	115.69	3	313	86
41	126.94	7	60	67
42	130.82	9	59	68
43	130.88	5	52	64
44	131.2	5	98	66
45	131.23	4	160	83
46	182.51	12	242	76
47	187.92	9	40	49
48	183.24	4	37	71
49	183.43	3	63	47
50	197.78	7	61	50
51	223.97	13	42	71
52	224.19	3	54	72
53	225.29	4	59	49
54	273.99	36	48	60
55	283.53	4	67	71
56	287.03	6	72	75
57	295.56	13	326	86

Appendix V

Klipspringer (300 m road cut)				
Sample No	At (m)	Thickness (mm)	Vein Orientation	
			Dip Direction	Dip
1	5.07	4	70	68
2	11.77	3	110	69
3	11.79	2	64	58
4	31.29	5	111	60
5	13.42	4.5	71	34
6	35.72	24	208	61
7	36.13	35	82	50
8	36.53	16	87	61
9	37.71	4.5	88	55
10	42.83	2	193	76
11	42.91	7	74	45
12	44.21	2	205	57
13	46.51	2.5	20	69

14	55.31	9	189	72
15	56.28	4	74	56
16	61.39	3.5	196	88
17	74.76	3	182	71
18	93.23	4	189	65
19	117.83	2	93	53
20	119.84	6	179	60
21	136.12	3	174	63
22	138.25	3	198	81